Seismic Performance of Eccentrically Braced Frames Designed According to Canadian Seismic Provisions

Mona Rais Esmaili

A Thesis in

The Department of

Building, Civil and Enviornmental Engineering

Presented in Partial Fullfillment of the Requirements

for the Degree of Master of Applied Science (Civil Engineering)

at Concordia University, Montreal, Quebec, Canada

May 2015

CONCORDIA UNIVERSITY
School of Graduate Studies

This is to certify that the thesis prepared

By: Mona Rais Esmaili

Entitled: Seismic Performance of Eccentrically Braced Frames Designed According to Canadian Seismic Provisions

and submitted in partial fulfillment of the requirements for the degree of

Master of Applied Science (Civil Engineering)

complies with the regulations of the University and meets the accepted standards with respect to originality and quality.

Signed by the final examining committee:

Dr. Adel M. Hanna Chair

Dr. Ashutosh Bagchi Examiner

Dr. Mohammad Mannan Examiner

Dr. Anjan Bhowmick Supervisor

Approved by _____
Chair of Department or Graduate Program Director

_____
Dean of Faculty

Date _____

ABSTRACT

Seismic Performance of Eccentrically Braced Frames Designed According to Canadian Seismic Provisions

Mona Rais Esmaili

Eccentrically braced frames (EBFs) are very effective lateral load resisting systems against earthquakes because of their hybrid behavior that includes great stiffness corresponding to the bracing actions, and considerable ductility owing to the inelastic activity of a small part of the floor beam called link. Current capacity design approach of EBFs is to confine the inelastic behavior of the frame primarily to the link such that other members remain essentially in elastic range. Limited research works are available in the literature studying the behavior of multi-storey EBFs designed according to the current Canadian seismic provisions. This thesis was aimed to study seismic performance of EBFs through nonlinear time history analysis (NLTHA) of three 4-, 8- and 14-storey chevron eccentrically braced frames. The selected EBFs were subjected to real and artificial ground motion records scaled to match the response spectrum of Vancouver. All the EBFs, designed according to current capacity design provisions, exhibited excellent seismic performance in terms of stiffness, strength, and ductility. It was observed that the inelastic link rotations of all EBFs were lower than the design limit of 0.08 rad, except for the two upper floors in 14-storey EBF where the link rotation slightly exceeded the limit. Seismic analysis also showed that maximum inelastic link shear forces exceeded the values recommended in design for many earthquake records.

Although NLTHA can precisely estimate structural seismic responses, it requires high computational demands making it impractical for engineering design offices. On the other hand, the conventional pushover analysis does not consider contributions of higher modes to the structural responses and thus it often does not provide good estimation of seismic responses for taller buildings. Capacity-Spectrum Method (CSM) and modal pushover analysis (MPA) are two simple nonlinear static methods that have been proposed and recently used for seismic performance evaluation of few lateral load-resisting systems. This research further studies the application of CSM and MPA as alternatives for rigorous NLTHA to estimate seismic performance parameters of EBFs. The three selected EBFs were analyzed using MPA and CSM and the results were compared with nonlinear seismic analysis results. It was observed that both CSM and MPA predicted the peak top displacements of EBFs with sufficient accuracy.

To my husband and my best friend, Shahram,

For his beautiful insight about life which always encouraged me to fulfill my dreams

To my dearest mother,

For her endless teachings, supports, love and prayers

ACKWNOWLEDGMENTS

Taking the steps to accomplish a master degree in civil engineering was so challenging yet rewarding for me. In the course of this process, many people have contributed to my academic achievements. Special thanks are owed to my supervisor, Dr. Anjan Bhowmick, for providing helpful research guidance in pursuit of my graduate studies. His strong encouragement helped me remain focused and motivated throughout my research work. I would like to express my sincere gratitude to Dr. Kinh Ha who introduced me to the world of civil engineering and finite element modeling concept by instructing his invaluable courses

I also would like to acknowledge the Faculty of Engineering and Computer Science, Concordia University, Montreal, Canada and the Natural Sciences and Engineering Research Council of Canada for their support and providing funding to this project.

I wish to appreciate all technical supports and inspirations I have received from my dear friends and colleges particularly, Moon Moon Dhar, Sandip Dey, and Arghya Chatterjee. Wish you a happy life and all the best in your future professional careers. Finally, I would like to express my deepest appreciation to my husband and my family because of their endless supports during my studies.

TABLE OF CONTENTS

List of Figures

List of Tables

List of Symbols

A	Gross link cross sectional area
A_w	Web cross sectional area
b_f	Width of link flange
C_f	Compressive force in a member
C	Damping matrix
d	Depth of the link section
D_{nx}	Dimension of the building plan at level x normal to the direction of seismic loading
D_n	Deformation of n^{th} mode SDOF system
D_t^*	Displacement of SDOF system
D_y^*	Yield displacement of SDOF system
D_t	Displacement of MDOF system
e	Length of the link
F_{brace}	Brace axial force
F_y^*	Yield strength of SDOF system
F_y	Yield strength
F_t	Additional lateral force concentrated at the top of structure
F_x	F_x is the lateral load force at each level
F_{sn}	Lateral force related to n^{th} mode of SDOF system
F_n	Notional load

h_s	Storey height
h_x	Height of the structure above the level x
I_E	Earthquake importance factor
k	Lateral stiffness matrix
L_n	Mass of n^{th} mode SDOF system
m^*	Mass of n^{th} mode SDOF system
m	mass matrix
M_P	Plastic moment resistance
M_r	Factored moment resistance
$M_P^{'}$	Plastic moment resistance of the link reduced due to axial load
M_v	Factor considering higher modes effects on base shear
M_f	Bending moment in a member
M_n	Effective modal mass of the n^{th} vibration mode
$P_{eff}(t)$	Effective lateral earthquake force
p_i	Lateral force at any storey i
P_f	Axial force in the link
R_d	Ductility related force reduction factor for ductility
R_μ	Ductility related force reduction factor for ductility
R_o	Overstrength related force modification factor
R_y	Factor of the probable yield stress
S_n^*	Effective lateral force of the n^{th} vibration mode
S_{ae}	Elastic spectral acceleration

S_{de}	Elastic spectral displacement
S_d	Inelastic spectral displacement
$S(T_a)$	Spectral acceleration for period of the building
S_a	Inelastic spectral acceleration
T_c	Characteristics period
T_a	Fundamental lateral period of the building based on NBCC 2010
T_o	Transition period
U_2	Amplication factor should be used to account for the p-delta effects
u	Vector of n lateral floor displacements relative to ground
$\ddot{u}_g(t)$	Earthquake ground motion
u_{rno}	Maximum roof displacement of MDOF system related to n^{th} mode
V_{link}	Link shear force
V_{cum}	Cumulated lateral shear force
V_{min}	Minimum base shear of the structure
V_{max}	Maximum base shear of the structure
V_u	Ultimate link shear force
V	Design Base Shear
V_d	Dynamic Base Shear
V_P	Plastic shear resistance
V_P'	Plastic shear resistance of the link reduced due to axial load
V_{Beam}	Shear force in the beam

V_{bno}	Ultimate base shear at U_{rno}
V_{bny}	Yield base shear at U_{rny}
W	Total seismic weight resisted by the frame
W_x	Portion of the weight of structure at level x
Z_x	Plastic section modulus of steel sections
α_o	Link strength factor
α_n	Strain hardening of pushover curve of n^{th} mode
Δ_f	Inter-storey displacement at each level
Δ_{in}	Inelastic drift
Δ_{el}	Elastic drift
φ	Resistance factor
ϕ_n	Elastic mode shape of n^{th} mode
Γ_n	Modal participation factor
ι	Displacements of masses resulting from static application of a unit ground displacement
ω	Circular frequency
ξ	Damping ratio
μ	Ductility factor
γ	Total link rotation
θ	Total storey drift angle

List of Abbreviations

ADRS	Acceleration Displacement Response Spectrum
AISE	American Institute Of Steel Construction
ASCE	American Society Of Civil Engineers
CSA	Canadian Standards Association
CSM	Capacity Spectrum Method
EBF	Eccentrically Braced Frames
FE	Finite Element
FEMA	Federal Emergency Management Agency
MDOF	Multi Degrees Of Freedom System
MPA	Modal Pushover Analysis
NBCC	National Building Code Of Canada
NLTHA	Non-Linear Time History Analysis
PBSD	Performance Based Design
PEER	Pacific Earthquake Engineering Research
SDOF	Single Degree Of Freedom

Chapter 1. Introduction

1.2. General

Eccentrically braced frames (EBFs) have been recognized as effective lateral load resisting systems providing large ductility comparable to moment resisting frames (MRFs) and excellent stiffness similar to concentric braced frames (CBFs). The high stiffness of EBFs stems from the existence of the braces, and their superior ductility is due to the inelastic activity of a section called link. The link is a part of the floor beam located between the ends of the braces or between the brace end and the column flange. The links are the most important members of EBFs dissipating large amount of energy through their plastic behavior, and influencing the strength, stiffness and ductility of the frame. Figure 1.1 illustrates some usual configuration of eccentric braced frames. Among different configuration of EBFs, the eccentric chevron braced frame is preferable since it prevents the link to column connection which is recommended to be avoided in the literature (Engelhardt and Popov 1989).

The underlying concept of EBFs is restricting all inelastic actions into the links so that other members act elastically under severe earthquake loadings. Therefore, the link is the key member from which the design of eccentrically braced frame initiates; while other members are designed to withstand the maximum forces developed by the fully yielded link. The link behavior is primarily affected by its length. Short links, also called shear links, mainly yield in shear whereas long links yield in flexure. Generally, the short links are recommended for designing EBFs (Engelhardt and Popov 1989) because in this case the plastic shear strains are uniformly distributed along the web of the links, allowing for large inelastic rotation of the link without any

excessive local strains. For long links high bending moments are required at the end of the link in order to produce large inelastic rotations. The high bending moments create high local plastic deformations preventing the desired inelastic rotations of the link. The reported maximum link rotation by the experimental research is about 0.1 radian for shear links (Whittaker et al. 1987) and about which 0.02 radian for long links (Engelhardt and Popov 1989).

Current Canadian design provisions (CSA 2009, NBCC 2010) require that EBFs be designed according to capacity design approach. In this approach, the links are sized for the seismic forces specified by NBCC 2010 and other frame members should be designed for the forces developed by the fully yielded and strain-hardened link. Limited studies are available in the literature that focused seismic performance of EBFs designed according to current Canadian seismic provisions. In this research, seismic performances of 4-, 8-, and 14-storey EBFs are studied. A detailed finite element model that can accurately simulate monotonic and dynamic behavior of EBFs is developed. The finite element model included both material and geometric non-linearities. The reliability of FE model was first validated by comparing FE results with the experimental ones. The FE models were used to study seismic performance of EBFs through non-linear dynamic analysis. Although this method is known as the most accurate method in determining seismic responses, it is not very useful at the design level due to its high computational demands. The precise prediction of strength and deflection is very important at the design phase, since it can assure the desired level of performance.

In recent years, the performance-based seismic design (PBSD) is employed as a more reliable method for designing structures using accurate prediction of seismic demands at the design level. This demonstrates the need for efficient and precise seismic evaluation tools for every structural

system. Pushover analysis has been introduced by current guidelines (FEMA-273 1997, FEMA-356 2000) as a practical non-linear static procedure to estimate seismic responses. However, since this method just considers the effect of the first fundamental mode to the response, it is not useful for the structures in which higher mode effects are considerable. To overcome the mentioned limitation, modal pushover analysis (MPA) was introduced by Chopra and Goel (2001) as an alternative method to improve the pushover procedure by including higher mode contributions to seismic demands. The accuracy of this method has previously been studied on moment resisting frames (Chintanapakdee and Chopra 2003, Goel and Chopra 2004); however, no significant research has been yet conducted on the application of modal pushover on EBFs. Another simplified method that has been proposed to estimate seismic performance parameters of structure is Capacity-spectrum method (CSM). To date, no research has examined the applicability of CSM method for estimating seismic demands of EBFs. This thesis is evaluating the accuracy of modal pushover analysis and capacity spectrum methods in estimating seismic demands of EBFs by comparing results from MPA and CSM with the accurate results of rigorous nonlinear dynamic analysis.

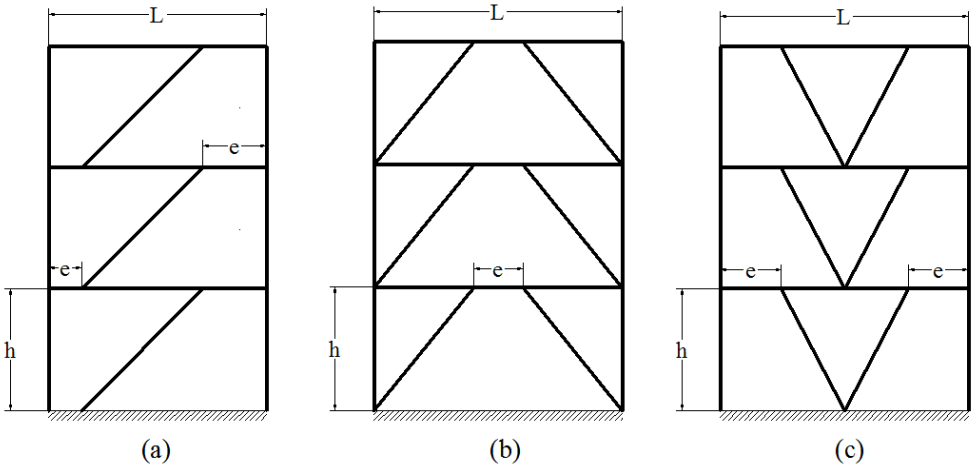

Figure 1.1. a) Eccentric D-braced frame, b) Eccentric chevron-braced frame, c) Eccentric V-braced frame

1.3. Objectives and Scope

The main objectives of this research are as follows:

1. Develop a detailed finite element model to study the seismic performance of EBFs designed according to Canadian design requirements. The finite element model, which considers both material and geometric non-linearities, is validated with an available experimental study to verify its ability in precise determining the responses of EBFs.
2. Perform non-linear seismic analyses on eccentrically braced frames, using detailed finite element models, to evaluate the important response parameters of EBFs precisely. The results of these analyses are employed to investigate differences between the seismic responses and the design predictions.
3. Investigate the capability of modal pushover method in predicting seismic demands of EBFs through comparing different response parameters such as storey displacements, inter-storey drifts, and base shear obtained from MPA with the accurate results of non-linear time history analyses.
4. Investigate the applicability of capacity-spectrum method for estimating seismic demand parameters. Roof displacement and structural ductility demand are estimated as the performance parameters. If the applicability of MPA and CSM on EBFs is justified, it can be employed as an efficient alternative of rigorous non-linear time history analysis at the design phase

1.4. Methodology

To achieve the presented objectives, three eccentrically braced frames with 4, 8 and 14 storeys were designed and analyzed for Vancouver representing a high seismic zone in Canada. The following methodology was used to fulfill the mentioned objectives:

Three eccentric braced frames with 4-, 8- and 14-storeys were designed according to current Canadian design provisions (NBCC 2010, CSA 2009). The designed EBFs were precisely modeled using ABAQUS, powerful finite element software capable of solving problems with significant non-linearities. In order to have a reliable FE model, the finite element modeling technique was firstly validated by modeling an experimental full-scale EBF and comparing its results with the corresponding experimental results.

A set of eight real and artificial ground motion records were selected and scaled for the Vancouver region and employed for non-linear seismic analyses of the three mentioned EBFs to obtain and study the important seismic responses of EBF such as storey displacements, inter-storey drifts, link rotations, and link shear forces.

The applicability of modal pushover method to estimate EBFs seismic demands was investigated. To perform modal pushover procedure, the frequency analyses were conducted on the three designed EBFs to find the fundamental mode shapes and periods of each frame. Then a series of non-linear pushover analyses were conducted on the designed EBFs subjected to the forces related to each mode. The results of these analyses were employed to identify the properties of the single degree of freedom system corresponding to each mode leading into determination of different response parameters of EBFs such as storey displacements and inter-

storey drifts. The steps are explained in detail in chapter 5. These results were compared with the results of non-linear seismic analysis.

In the Capacity spectrum method, the capacities of the designed EBFs were determined from pushover analysis and were combined with design response spectrum of Vancouver to estimate the peak roof displacement and ductility demand of EBFs. The method is formulated in acceleration-displacement format and inelastic spectra, rather than elastic spectra are used.

1.5. Thesis Outline

This thesis includes seven chapters. The first chapter presents a brief discussion of the existing problems corresponding to seismic performance evaluation of eccentrically braced frames. Then the objectives and the methodology used for this study are introduced. The second chapter provides a review of some important experimental, analytical and numerical research works previously done on eccentrically braced frames. Also, some previous studies on modal pushover analysis are discussed. Chapter 3 describes the modeling technique, details and specifications of the finite element model developed in ABAQUS to study the performance of EBFs. The validation of the finite element model is also provided in this chapter. Besides, the capacity design approach suggested by CSA\CAN S16-09 used for designing three 4-, 8- and 14-storey EBFs is presented. The created finite element models of the designed frames are also provided in this chapter. Chapter 4 presents the process of selecting ground motion records for non-linear time history analysis. Important response parameters of the designed eccentrically braced frames subjected to the selected earthquakes are also demonstrated and discussed. Chapter 5 describes the modal pushover analysis method to estimate seismic demands and performance of eccentrically braced frames. The responses obtained from MPA method are compared with the

results of non-linear time history analysis. Chapter 6 presents the application of Capacity Spectrum method to estimate seismic demands of three selected EBFs. Results from CSM are compared with those from nonlinear dynamic analysis. Chapter 7 summarizes the conclusions of the studies and also provides the recommendations for future research.

Chapter 2. Literature Review

2.1. General

With the advent of eccentrically braced frames in the mid-1970s, extensive studies were initiated to investigate the behavior of EBFs under cyclic and seismic loadings. This chapter introduces the experimental, analytical and finite element studies have been conducted on EBFs; as well as, the main findings of these studies. Also, the first proposed capacity design method for EBFs is explained in detail. This chapter also describes the background of modal pushover analysis which is used for seismic performance evaluation of eccentrically braced frames.

2.2. Past Studies on EBFs

A vast number of studies have been conducted on EBFs over the past 40 years. They can be classified into three major categories. The first category includes the experimental studies, having been performed on full scale models or on isolated members of EBFs. The first experimental study on eccentrically braced frames consists of a series of quasi-static tests which have been done in 1970s at the University of California, Berkeley (Roder and Popov 1977). In the study, firstly the behavior of short links under cyclic loading was studied. The results showed that links which yield in shear have the best energy dissipation mechanism due to their great stability during large cyclic deflection. They also reported extensive strain hardening, observed in the shear links. Considering the results of their experiments, they suggested an analytical model based on sandwich beam theory. Two one-third scale three storey EBFs were modeled and their results were compared with the responses of analytical model. The results of these experiments confirmed high strength, stiffness and energy dissipation of EBFs.

The first dynamic experiment on eccentric braced frames was a shaking table study on a one third scale five storey EBF with eccentric x-bracing (Yang 1982). The objective of this study was to evaluate the seismic resistant efficiency of x-braced EBFs. Based on the dynamic results, it was reported that damages were limited to buckling and fracture of the shear link. Also, it was demonstrated that weaker links dissipated more energy and produced smaller forces. It was concluded that the dynamic response of EBF was governed by strength of shear link.

Later, in 1987, an earthquake simulation test was accomplished on a 0.3-scale model of a six-story chevron braced frame (Whittaker et al. 1987). Also, a seismic testing was performed on a full scale 6 storey EBF with eccentric k-braces under 1952 Taft record. In this study, yielding and buckling of gusset plates were observed at some levels, leading into reducing the strength and energy absorbing capability of the corresponding floors. However, the overall performance of EBF was excellent (Roeder et al. 1987).

Popov et al. (1992) investigated the effect of maintaining uniform link strength factor along the height of frame by evaluating previous full scale experiments on EBFs (Roeder et al. 1987), and a 13 storey EBF designed by Martini et al. (1990). Neither of cases considered a uniform link strength factor during design phase which resulted into soft storey mechanism in the first experiment and using vertical ties in the latter one. They concluded that keeping the link strength factor uniform along the height of EBF prevents excessive link inelastic rotations in some levels, and avoids soft storey mechanism in lower storeys.

More recent experiments were also carried out on full scale models. These studies include full scale testing of one-storey chevron type EBF with replaceable shear link under cyclic loading, performed by Mansour (2010). He used two types of replaceable links including W sections with

end plate connections and back to back channels with web connections. In the experimental work, seven shear links were used in a full scale EBF with 7.5 m wide and 4.5 meter height under AISC (2005) loading protocol, to investigate the local response of replaceable links and the global behavior of the frame. From his experiments, it was concluded that the removable link meets the performance criteria of Canadian standard (CSA 2009) without any failure or sever strength degradation. The results of his study showed that EBFs with ductile replaceable links provide improved ductility comparing to the conventional EBFs.

Another full-scale experiment was a pseudo-dynamic test of a dual EBF with removable link (Dubina 2014). In the study, he combined eccentrically braced frames with replaceable links to a moment resisting frames in order to have a dual structure. A reinforced concrete slab was considered at each floor. The aim of this study was to assess the overall seismic performance of the dual EBF, and study the link removal technology. He concluded that the structure indicated an excellent seismic performance. Permanent drifts were resolved by removing bolted links. He suggested unbolting for removing the links with small plastic deformation, for large deformation case, flame cutting of the links were suggested.

There are also a large number of experiments which studied isolated members, specially the links' behavior. In 1983, cyclic behavior of link beams was investigated by some experimental studies. Popov and his colleagues studied the behavior of shear links with w-shape sections, being employed in a sub-assemblage, reproducing the link behavior in a real EBF under cyclic displacements (Hjelmstad and Popov 1983, Kasai and Popov 1986).

Engelhardt and Popov (1989) investigated the behavior of long links by a total of 14 tests on 12 specimens with W sections and A36 steel material. These links were assumed to connect to the

columns. The results of their studies showed that short links which yield in shear are more efficient in dissipating energy than long links which primarily yield in flexure. Also, they found that web buckling which weakens the load carrying and energy dissipation capacity of the link can be resolved using evenly spaced web stiffeners. Moreover, because of poor behavior of link to column connections, they recommended to avoid this type of EBF. Current Canadian standard (CSA 2009) for designing EBFs permits using both short and long links; however, based on the aforementioned studies, they also recognized the shear links more preferable in terms of the design and behavior. Engelhardt and Popov recommended link overstrength factor of 1.5 which represent the maximum force that can be produced by yielded and strain hardened link.

The mentioned tests used ASTM A36 steel; however, with the spread of ASTM A992 steel in constructions, researchers started to investigate its applicability and effect on eccentrically braced frames performance. In 2005, a series of 23 cyclic tests were performed to evaluate the overstrength factor of w shape links made of A992 (OkazakiArce et al. 2005). The results of their study showed that the ASTM A992 w shape links showed the maximum overstrength of 1.47 for shear links. They concluded that the overstrength factor of 1.5 which is recommended by AISC is applicable for new steel under study. Another study was carried out on 37 link specimen to extend the results of previous experiment (Okazaki and Engelhardt 2007). In this study, the maximum overstrength factor of 1.62 was observed for ASTM A992 steel. They explained that sections with high ratios of flange to web area showed lower overstrength factors. They concluded that the performance of EBF links made of ASTM A992 was well and it could meet the performance criteria suggested by 2005 AISC Seismic Provisions.

Parallel to the experimental researches, some analytical studies have been also done on EBFs. The aim of these studies was proposing models which can predict the inelastic behavior of EBFs. One of the early models for link was proposed by Roeder and Popov (1977). In this model, the shear forces and moments were assumed to be resisted by web and flanges respectively. The model considered combined isotropic and kinematic hardening. This model was designed to represent links yielded in shear and with small moments at the ends which is not the case for all the links.

To overcome the shortages of previous model, Ricles and Popov (1987, 1994) developed another element which was able to predict the shear and flexural yielding of links successfully. The element was modeled as a linear beam element with plastic end hinges, representing all inelastic deformation of the link. The elastic beam limited the axial deformations through itself. Shear and flexural yielding and combined kinematic and isotropic hardening were considered in this model. Based on the approach of Ricles and Popov (1987), another analytical model, aimed to be used in computer codes, was developed by Ramadan and Ghobarah (1995). They intention was to develop a more simple model comparing to the one suggested by Ricles and Popov, which can be easily used in the computer codes. This model was employed in DRAIN-2DX (Parkash et al. 1992).

Along with the analytical and experimental studies, the finite element techniques were also employed to study the behavior of eccentrically braced frames. For finite element modeling of full scale EBFs or link member, some of the analytical models described above were employed to investigate their seismic responses. The shear link developed by Ricles and Popov (1987, 1994) was included in ANSR-1 program (Mondkar and Powell 1975) to study seismic behavior

of EBFs and to improve their design approach (Koboevic 2000). ANSR-1 is a finite element program for nonlinear time history analysis (NLTHA).

In 1987, the behavior of EBFs under pseudo dynamic test was investigated by finite element analysis (Balendra et al. 1987). In the study, the frame was discretized into five elements including brace, which was modeled by truss element; beam and two columns, being modeled by beam elements with a bilinear moment curvature relation; and the link, being modeled with the shear link element yielding under pure kinematic hardening. Also, a finite element model was employed to study the effect of axial forces in the links on EBFs' performance (Ghobarah and Ramadan 1990). In modeling of the link, 4 node shell elements, working based on the incremental Lagrangian continuum mechanics equation, were used. They considered material nonlinearity by taking into account the actual stress-strain relationship. For geometric nonlinearity, large displacements and rotations were allowed by updating node coordinates and normal vectors. This finite element model was used to study seismic performance of links with various lengths. The advantages of the short links in maximum deformation angle and ductility were confirmed (Ghobarah and Ramadan 1991). David (2009) used ANSR-1 to perform nonlinear time history analysis on high-rise eccentrically braced frames. Nonlinear beam column elements were employed to model the outer beam, braces and the columns. The link was modeled by the shear link element proposed by Ricles and Popov (1994).

An extensive finite element study was carried out in the University of California, San Diego to study the effect of the loading protocol on short link rotation capacity (Richards 2004). In this study, 112 finite element link models ranging from short to long links with different flange to thickness ratios were analyzed under cyclic loading. They concluded that the flange width-

thickness ratio did not influence the plastic link rotation capacity directly. The design rotations for intermediate links were not conservative. Also they compared the results of A992 with A36 steel material. They found that using ASTM A992 steel for wide flange shapes has not considerable effect on links overstrength. They also recommended to consider shear forces in the flanges of the link for determining ultimate strength of the links. They also developed nine models of 3 and 10 storey EBFs with short, intermediate and long links in Ruaumoko, which is a finite element application for 2D and 3D nonlinear time history analysis (Karr 2002), to study the overall frame behavior and different member forces. In these models panel zones were not modeled and their deformations were neglected. Beams, outer beams, braces, and columns were modeled as beam-column. Shear links were modeled using a method similar to that proposed by Ramadan and Ghobarah (1995) with modifications in elastic stiffness of the links.

In 2013, European researchers (Della Corte et al. 2013) performed analytical and numerical study on shear links made of European shapes HE and IPE, to verify the link plastic overstrength factor. They proposed a simple analytical model based on the results of finite element model, validated by some experimental tests. The shear links were developed in ABAQUS, using four nodes shell elements. Based on their FE model and comparing its results with the available experimental data, they concluded that for very short links with compact cross section, the shear strength equal to 2 can be achieved. For compact built-up links with very short length even larger values of shear strength can be obtained. Also, a finite element study was conducted to optimize link member of EBFs for maximum energy dissipation (Ohsaki and Nakajima 2012). The objective function was the plastic dissipated energy before failure. Based on the results of their study, they concluded that the energy dissipation of the links is greatly affected by optimizing the locations and thickness of stiffeners.

New Zealand Heavy Engineering Research Association (HERA) carried out an advanced finite element analysis on EBF with removable links to verify the performance of EBFs (Mago 2013). The FE model was developed in ABAQUS/CAE. The FEA model represents a one storey eccentrically braced frame. The results of the FEA showed that in the collector beam, insignificant plastic strains were observed, occurring close to the endplate under the highest cycles of loading. These plastic strains did not influence the structural performance. It was concluded that the welded web stiffener attracts significant local plastic strain.

Most of the finite element studies on EBFs didn't use detailed FE models which are able to capture the local behavior of the structure. To the author's knowledge, there are very limited detailed FE models available for multi-storey EBFs. Such a model can predict both local and global behavior of EBFs. Also, validated detailed FE models can be a good replacement for experimental ones for further investigations. Therefore, providing a full scale model that can predict all the behavior of full scale real structure is necessary to avoid the high costs and efforts made by real experiments. In this study, detailed continuous finite element models of short, medium and high-rise EBFs were created to study the local and global behavior of EBFs in response to seismic loading.

2.3. Capacity design methodology for EBFs

Some of the early experimental studies (Popov et al. 1987, Popov and Engelhardt 1988) are the basis of design recommendations that are currently used in Canadian standard for steel structures (CSA 2009). In 1988, based on the results of experimental works on three and six storey EBFs and on the links with equal and unequal end moments, Popov and Engelhardt proposed the capacity design principles for EBFs. In the capacity design procedure, some elements within the

structural system are designed to dissipate energy by their inelastic activity, while limiting the behavior of the other members within the elastic range. In EBFs, the links are designed for yielding and strain hardening, and the other elements are designed for the forces of fully yielded links. This assures that all the members of EBFs except for the links are strong enough to behave elastically. They suggested three considerations for designing EBFs. Firstly, the link sections should be selected and detailed to provide the required frame strength and ductility. Secondly, other members of EBFs should be chosen with stronger sections in order to allow developing the strength and ductility of the links. Finally, the ductility demand of the structure and the link should be estimated; and the links should be detailed to meet the rotation demand. To follow these considerations, the links must be designed for the code seismic forces, and all other members of the frame should be designed for the ultimate forces produced by the links. The following presents the suggested design guidelines by Popov and Engelhardt (1988) for EBFs.

Bracing arrangement

The first thing that should be decided in design of EBFs is the bracing arrangement to be used. To choose the bracing arrangements, they recommended avoiding configurations which requires link to column connections. To consider this recommendation, using a chevron EBF is a good choice. Moreover, they emphasized that the brace to the beam angle should be chosen more than 40 degrees in order to avoid high axial forces in the beams and links resulting in strength and stability problems.

Link length

Another important decision is choosing the link length at the preliminary stages. They suggested using short shear link because of its high energy dissipation capacity and ductility. To assure that the selected links is yielding in shear, they recommended using equation 2.1. Based on the previous experimental researches, they stated that considerable strain hardening could occur in shear links, resulting in ultimate shear forces of 1.4 to $1.5V_p$. For shear links, the link end moments are considerably greater than M_P, leading into flanges strains. In order to avoid excessive strain in flanges, they recommended limiting link end moments to $1.2M_P$. Assuming perfect plasticity and no M-V interaction, the link length was recognized to be equal to $2M_P / V_p$. Substituting V_p by $1.5V_p$ and M_P with $1.2M_P$, equation 2.1 can be derived.

$$e \leq 1.6M_P / V_p \qquad 2.1$$

They recommended this equation to guarantee shear yielding of the links. For preliminary decision making, using link length on the order of 1 to $1.3M_P / V_p$ was found effective.

Link size

The first section which should be chosen in EBFs corresponds to the links. The links must be sized for seismic level forces considering the free body diagram shown in Figure 2.1.

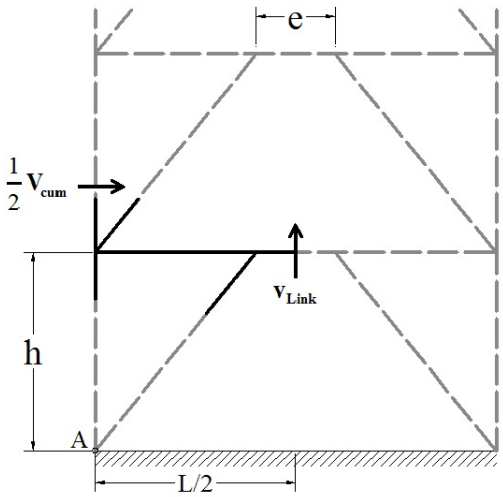

Figure 2.1. Simplified F.B.D of chevron EBF

The shear force in the link can be found by equation 2.2.

$$V_{link} = (h/L)V_{cum} \qquad 2.2$$

V_{cum} is the accumulated storey shear of top floors of EBF to the level under consideration. The selected link section should have a plastic shear resistance at least equal to V_{link} .

Selection of other EBF members

After selecting the link sections, they recommended to calculate the ultimate shear force of the link by equation 2.3. Other member should be sized for the forces calculated based on equation 2.3 for fully yielded links.

$$V_{ult} = 1.5V_p \qquad 2.3$$

Based on the previous experiments, they explained that sometimes the ultimate shear forces in the links were observed higher than $1.5V_p$. Therefore, they suggested to design the braces conservatively.

For the beam outside the link (outer beam), since it is subjected to a large axial force and larger bending moment, they suggested to design it as beam-column. They explained that larger angle between brace and beam could reduce the axial forces in the beams. To prevent instability in the beams because of the presence of the high axial forces, using lateral bracing was recommended by Popov and Engelhardt. Also, Columns should be designed to behave elastically under ultimate link forces and gravity load effects.

Link rotation demand

After selecting members sections, the rotation of the links should be checked to ensure that the frame required ductility is obtained. To determine the rotation of the link, they suggested using rigid-plastic mechanism shown in Figure 2.2, resulting in equation 2.4.

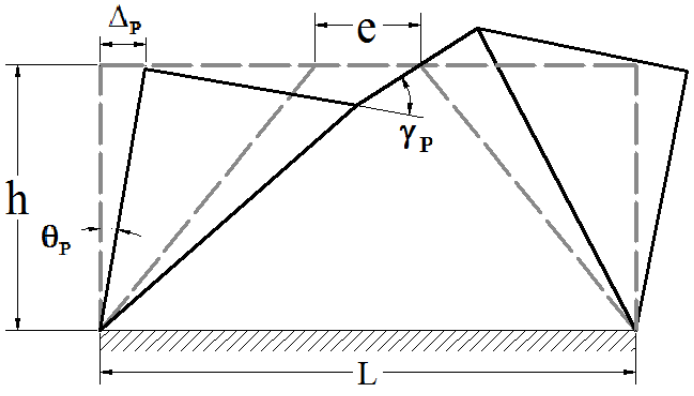

Figure 2.2. Rigid-Plastic mechanism of EBF

$$\gamma_p = \left(\frac{L}{e}\right)\theta_p \qquad 2.4$$

where θ is ultimate frame drift angle. The elastic drift can be calculated under code level forces and then multiplied by a factor to account for ultimate drift.

Link details

Accurate detailing of stiffeners and lateral bracing at the link ends lead into obtaining the full strength and rotation capacity of the shear links. They recommended using two sided, full depth stiffeners at the end of the link and intermediate stiffeners with equal spacing within the links. The intermediate stiffeners could be one sided for beams with depth less than 24 inches. These stiffeners were intended for strengthening the web and avoiding lateral-torsional buckling and flange buckling. Lateral bracing was aimed to prohibit out of plane deformation of the braces end, causing twisting of the beams and links.

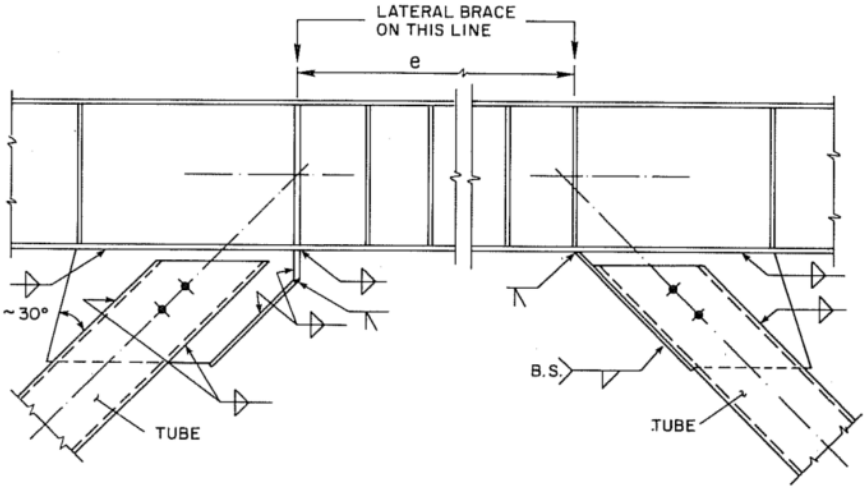

Figure 2.3. Typical detail for hollow section braces to beam connection (Popov and Engelhardt 1988)

Brace to link connection should be designed for compression strength of the brace and the moment developed in the brace ends. The brace should be positioned such that its centerline

meets the beam centerline at the end or inside the link. Stiffening the gusset plate ends close to the links are also recommended where the bending moments in the beam causes large stress along the edge of gusset plate.

For EBFs design, the same design philosophy and considerations is currently used in CSA (2009) with some modifications in the recommended values and factors for calculating member forces, link rotations, etc. The current Canadian standard (CSA 2009) criteria for designing eccentrically braced frames are discussed in detail in chapter 4.

2.4. Performance Evaluation of EBFs

Seismic performance evaluation of structures is an important part of the performance based design process which gives an estimation of the probable responses of the structure to earthquake hazards. Performance based design is a new design philosophy in which the design criteria are defined based on a specified level of performance under a particular level of seismic hazard. Then the performance of the designed structure should be assessed to determine the probable responses of the system in the case of extreme loading. If the designed structure doesn't meet the performance objective, it should be modified until the objectives are met. On the other hand, the typical design process suggested by the building codes is not performance based. In the typical design process, the members of the structure should be selected to satisfy some specific criteria suggested by the building codes. Some of these criteria were provided to satisfy some level of seismic performance; however, the real seismic performance of the structure is not evaluated at the design level. Therefore, providing simple methods to assess the performance of the structures accurately is advantageous for both performance-based and code-based design procedures. Also,

the application of the provided methods in accurate prediction of seismic responses should be evaluated for every new system.

In order to evaluate seismic performance of various types of structures, different analysis methods are suggested by the guidelines (FEMA-273 1997, FEMA-356 2000). These analysis procedures can be classified as linear analysis methods including response spectrum analysis and linear time history analysis; and non-linear analysis procedures consisting of non-linear static procedure (NSP) and non-linear time history analysis (NLTHA).

The response spectrum method is a linear dynamic analysis method which estimates the peak modal responses of a structure using the response spectrum of a selected ground motion. The peak modal responses should then be combined using a modal combination rule such as Complete Quadratic Combination (CQC) or Square Root of Sum of Squares (SRSS) to determine total response quantities. Linear time history analysis solves the equation of motion corresponding to a structure using an appropriate numerical method to estimate the seismic responses at each time step. However, these methods are limited to the structures in low to moderate seismic zones, where the responses of the structure are mainly elastic. For irregular structures, or for structures with highly non-linear responses, these procedures may lead into wrong results.

On the other hand, non-linear dynamic procedure can be used for any structure and it can provide the most accurate results. However, this method is complicated and it needs high computational demands. Therefore non-linear static procedure is suggested as a more simple method to predict seismic responses of the structure. Pushover analysis method is a non-linear static procedure offered by current guidelines (FEMA-273, FEMA-356) as a practical method to evaluate seismic

demands of structures. In this method, a predefined force distribution is applied to a multi-storey structure increasingly to reach a target displacement. This method is used to determine the force deformation relation of the structure; through which other performance parameters can be evaluated. The pushover method is defined based on two assumptions. Firstly, it assumes that the mode shape of the structure doesn't change even after yielding; secondly, it limits the response of the structure to its fundamental mode. Although both assumptions influence the results, several researches (Saiidi and Sozen 1981, Fajfar and Fischinger 1988, Krawinkler and Seneviratna 1998, Skokan and Hart 2000) indicated that the responses of the structure are still accurate. Krawinkler and Seneviratna (1998) confined the accuracy of NSP responses to low- to medium-rise structures, behavior of which are dominated by the first mode. However, this method is not very accurate in prediction of seismic responses of high-rise buildings whose responses are contributed by higher modes.

To overcome the latter limitation of pushover method, Chopra and Goel (2001) proposed an improved pushover analysis called modal pushover, in which the contributions of all important modes of vibration to the responses were combined. While keeping the simplicity of NSP, modal pushover method provides more accurate results through considering higher mode contributions to seismic responses of structures. In this method, the lateral distributed forces of each mode should be firstly determined. Applying these forces to the multi-storey structure, provides the base shear-roof displacement curve; idealizing which, results into the force-deformation relation of a single degree of freedom (SDOF) system corresponding to each mode. Solving the equations of motion of SDOF systems gives the peak deformation which can be converted to the peak roof displacement of MDOF structure. This peak roof displacement can be finally used to determine other response parameters of interest using the provided pushover curves of MDOF system. The

total responses can be obtained by preferred modal combination rules. The results of proposed modal pushover analysis can be improved by including the p-delta effects due to gravity loads in all considered modes (Goel and Chopra 2004). The accuracy of MPA were examined by applying to the SAC buildings (Goel and Chopra 2004), and to sixty regular and forty eight irregular frames, concluding the superior accuracy of MPA Comparing to the conventional pushover procedure (Chintanapakdee and Chopra 2003). Although, MPA method was reported as a good estimation of seismic demands for studied structures; it still needs to be examined for every new system, especially when the nonlinearity matters. Because in this case, there would be some errors arising from the underlying assumptions of MPA, including neglecting the coupling of modal coordinates $q_n(t)$ for nonlinear systems, and assuming the force deformation relation of the SDOF systems as bilinear curves (Chopra and Goel 2001). To the author's knowledge, no research has been conducted on the application of modal pushover analysis on EBFs to date. In this research, the accuracy of modal pushover analysis method on predicting seismic demand of EBFs is evaluated by comparing MPA results with the results of nonlinear time-history analysis for short, medium and high-rise EBFs.

Chapter 3. Finite Element Modeling of Eccentrically Braced Frames

3.1. Introduction

The main objective of this chapter is to develop a reliable finite element model that can simulate the behavior of ductile eccentric braced frame. To study the behavior of eccentrically braced frame, a 3D nonlinear finite element model was developed in ABAQUS (Hibbitt and Sorensen 2011). ABAQUS is a general purpose finite element software solving different static, quasi-static, and dynamic problems. ABAQUS/CAE offers a user-friendly modeling and visualization environment with advanced meshing capability. ABAQUS has also extensive element and material libraries, making it appropriate to solve problems involving material and geometry non-linearities. This chapter describes the details of the development of the finite element model. Several key features of finite element model, such as selection of analysis procedure, element definition, and material properties definitions are discussed first. The validity of the finite element model is examined using available experimental results. The validated model is then used for FE modeling of three multi-storey EBFs designed based on the capacity design approach suggested by CSA S16-09 (CSA 2009). The capacity design procedure for EBFs is also explained in detail and the final selected sections are presented.

3.2. Selection of Finite Element Analysis Procedures

There are different dynamic analysis options to solve both linear and non-linear problems in ABAQUS. For severe nonlinear dynamic problems, ABAQUS suggests direct time integration of all degrees of freedom of the FE model. ABAQUS classifies the dynamic integration operators into two main categories of implicit and explicit. In the explicit approach, the values of dynamic

responses at a time instant ($t + \Delta t$) can be determined based on the values at the previous instant (t). Thus, there is no need to form and invert the global mass and stiffness matrices. This makes the solution of each time step inexpensive. However, this approach is conditionally stable, meaning that the time increment should be small in compare to the time increment in the implicit, to provide a stable and an accurate solution. This smaller time step largely increases the computational demands. ABAQUS/Standard employs the Hilber-Hughes-Taylor time integration method which is an implicit operator. In the implicit dynamic, the values of responses at time $t + \Delta t$ are determined based on the values at both instants t and $t + \Delta t$, so the unknown quantities exist in both sides of the equations. Therefore, a set of nonlinear equilibrium equations must be solved at each time increment simultaneously. Since this operator is unconditionally stable, the size increment can be relatively large. The implicit approach was used for all the analyses in this thesis. This method is preferred because it is using relatively large time increment sizes while it assures the stability of the system.

3.3. Finite Element Model Specifications

3.3.1. Geometry and mesh

For finite element modeling of EBFs, efforts were made to create a FE model which precisely represents the similar experimental models. For all the selected EBFs, the dimensions of the frame geometry and the section were accurately extracted from the available data and were used for the finite element modeling. The details of the test specimen and designed multi-storey EBFs are presented in the sections 3.5 and 3.7 respectively.

One of the important factors in finite element modeling is selection of the appropriate mesh size for the FE model, because it directly influences the accuracy of the results and the computational demands. Using a coarse mesh may result into imprecise solution; on the other hand, employing a finer mesh may increase the accuracy of the results; but it also increases the computation time. Therefore, it is important to perform the mesh convergence study to find the optimum mesh sizes. For the experimental specimen, since it is a one-storey EBF on which the pushover analysis was conducted, using a fine mesh was not computationally expensive. However, for the designed multi-storey EBFs which should be employed for nonlinear time history analysis, finding the optimum mesh size is very important. To investigate the optimal mesh size, four different mesh sizes, varied from 4500 to 45000 elements, were selected for the designed 4-storey EBF. For each selected mesh, the top storey displacement and the maximum von Mises stress under equivalent lateral forces were extracted as the convergence criteria. Figure 3.1 shows the results and their variation with respect to the fine mesh for different mesh sizes. Since obtaining the stresses convergence is usually more difficult than the displacements, their results variations are also more considerable, with the maximum variation of %15 for the coarser mesh and minimum difference of %0.41 for the normal mesh. These variations are less significant for the displacement, with the maximum of %3.1 for the coarser mesh and the minimum of 0.2% for the normal mesh. As it can be seen from the Figure 3.1, the normal mesh with 13737 elements is the optimal mesh size for this structure; because, it not only represents a much higher accuracy comparing to the coarser meshes, but also it decreases the computational demands significantly comparing to the finer mesh with 45256 elements which raises the precision of the results only 0.4%. The results of this mesh study were used for judgment of the mesh sizes for the 8 and 14-storey EBFs.

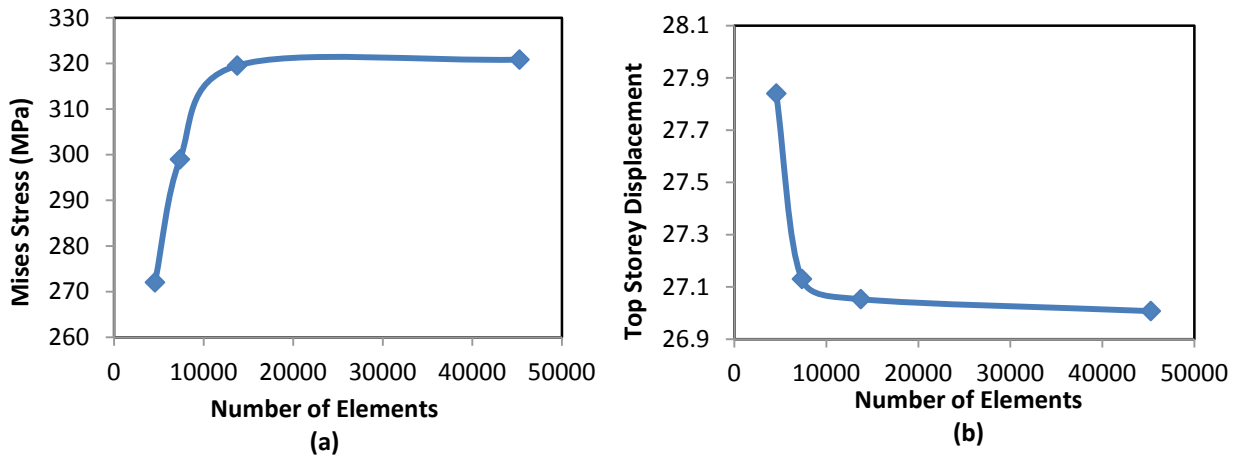

Figure 3.1. Mesh convergence study for 4-storey EBF a) Maximum von Mises stress vs. mesh refinement, b) Top storey displacement vs. mesh refinement

3.3.2. Element Type

ABAQUS provides an extensive library of different types of elements. In this study, the element S4R, a 4 node reduced integration shell element was used for all the EBFs. In general, shell elements may be employed when the in-plane dimensions of the elements are much higher than its thickness. Shell elements are advantageous because they reduce the computational demands significantly. Also they are easy to mesh, and they lead to a robust solution. The element S4R has six degrees of freedom at each node, three translations and three rotations defined in a global coordinate system. S4R is under the category of general purpose conventional shell element, which is able to model either thin or thick shell behavior when the thickness decreases or increases. This element is famous for robust and accurate solution in all loading conditions. It may account for transverse shear deformation, becoming very small when the shell thickness reduces. This element is appropriate for large-strain analysis because it consider finite membrane strains and large rotations. This reduced integration element is suitable for calculating the strains

and stresses in the points with optimal accuracy. Also reducing the number of integration points leads into reduction of CPU usage and storage space.

3.3.3. Material Properties

The comprehensive material library available in ABAQUS offers various material properties to be able to represent the real material behavior closely. The material properties can be found from the available stress vs. strain data of steel obtained from tension coupon tests. For finite element validation, tension coupon test was not provided for the end plate connected link (Figure 3.2) as the original researcher reported (Mansour 2010). However, Mansour suggested employing the material model calibrated by Korzekwa and Tremblay (2009) for finite element modeling. This material model was developed for steel plates made of G40.21-350WT steel with nominal yield strength 350 MPa and tensile strength 450 MPa. For seismic analysis, the non-linear material behavior was modeled using an elasto-plastic stress-strain curve with the strain hardening of 2% of the elastic stiffness, and by considering the kinematic hardening rule and von Mises yield criteria. A 5% proportional damping ratio was used in all seismic analyses. For all pushover analyses, the non-linear isotropic hardening was employed.

3.3.4. Boundary Conditions

In the FE modeling, it was attempted to have similar boundary conditions (BCs) to the corresponding experiment. The columns were modeled to have pin support condition at the base. Connection between the link and the floor beam was defined by common nodes to be able to transfer the forces and moments created by the strain-hardened link. Also the connection between the braces and the beam are moment connections. All other connections were considered as pin connections. Lateral supports were also provided to restrain the out of plane

movement of the EBF. Lateral bracing was employed at the top and bottom flanges of the floor beams at two ends of the links. To account for the lateral bracings in FE model, the out of plane displacements of the nodes were restrained. The same modeling technique and boundary conditions were used for modeling of 4-, 8- and 14-storey chevron braced frames.

3.4. Types of Analyses

Three types of analyses were performed on the finite element models presented in this thesis, consisting of pushover, frequency and seismic analyses. To perform non-linear pushover analysis on the FE model of the selected test specimen, displacement-controlled procedure was employed, in which the displacement was applied to the center of the floor beam increasingly, to reach the target displacement. The results of this analysis are presented in section 3.6 for validation of the FE model. A series of frequency analyses were performed on the designed multi-storey EBFs to obtain the fundamental periods and the primary mode shapes of the frames. The results of frequency analyses were utilized to calculate the damping coefficients required for the seismic analyses. The fundamental periods of EBFs were also used for scaling of the Earthquake records used in seismic analysis. The mode shapes were employed for the modal pushover analysis explained in chapter 5. Non-linear seismic analyses were also performed on the designed EBFs to study the seismic performance of these frames. For seismic analysis, eight ground motions were selected and scaled to match the design spectrum of Vancouver. To use these scaled ground motions in FE simulations, the support conditions were modified to allow movement in the direction of the ground motion. Detailed explanation of seismic analyses and results are presented in chapter 4.

3.5. Description of Selected Experimental Model

To study the responses of a structure using finite element modeling, it is reasonable to create a FE model based on data of an experimental specimen, and to validate the FE results with the experimental responses. The experimental case used in this study is a full scale model of a one-storey eccentrically braced frame with replaceable shear link, designed and tested by Nabil Mansour (2010). Different types of shear links including C sections with bolted or welded web connections, and W sections with end plate connections were employed for the experimental study. The experiments were conducted on both full scale one-storey EBF and individual links under cyclic loading. The results were employed to study the global response; as well as, the local behavior of the members and their connections.

For the validation part of this thesis, the one-storey EBF with link specimen 11A with end plate connection was modeled in ABAQUS. The frame was assumed to be representative of the second level of a five-storey eccentric braced frame designed based on CAN/CSA S16-09 (CSA 2009) and NBCC (NBCC 2005) for high seismic zone in British Columbia, Canada. To connect the link specimen 11A to the outer beam, Mansour used two end plates, one welded to the end of the floor beam and the other welded to the end of the link. The two plates were bolted together to attach the link to the outer beam (Figure 3.2). Figure 3.3 presents the overall configuration of the experimental model created by Mansour. In the experimental model, the width and height of the frame were considered 7.5 and 4.58 meter respectively. The link length was equal to 800 mm.
The summary of sections and dimensions used in the experimental study is shown in Table 3.1.

Table 3.1 Summary of 1-storey eccentrically braced frame (Mansour 2010)

Bay width (mm)	Link length (mm)	Intermediate stiffeners	Link Beam	Beam outside the link	Brace	Column
L=7500	e=800	3 at 200 mm	W360×72	W530×196	HSS254×254×13	W360×347

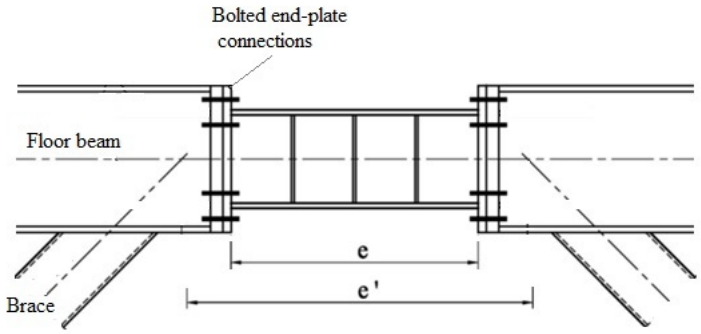

Figure 3.2. Link specimen 11A (Mansour 2010)

Figure 3.3. One-storey EBF with Link specimen 11A (Mansour 2010)

3.6. Validation of Finite Element Model

The results of the finite element model were validated using the results of the one-storey EBF with end plate connected link conducted by Nabil Mansour (2010). Displacement controlled analysis was used for validation of the experimental model. Based on the reported results of experimental work, the maximum total frame drift was reported equal to 1.7% corresponding to the link rotation of γ=0.11 rad. Using equation 3.1, the lateral frame displacement was found around 78 mm. This displacement was applied to the center of the floor beam, and the structure was pushed increasingly to reach the target displacement obtained from the experimental test.

$$\theta = \frac{D_{12}}{h} \qquad 3.1$$

where θ is total storey drift, D_{12} is lateral frame displacement, and h is height of the frame.

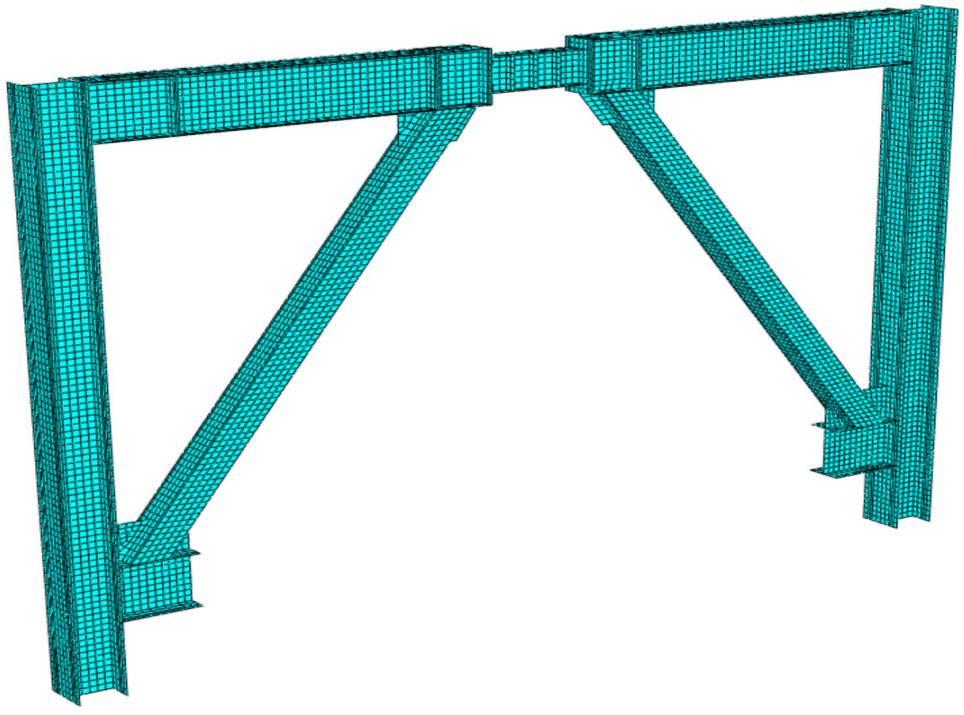

Figure 3.4. FE Model of 1-storey specimen tested by Mansour (2010)

The experimental curve presented in Figure 3.5 is the envelope of the hysteresis curve presented by Mansour (2010) for the one storey EBF with link specimen 11A. As it can be seen from Figure 3.5, the finite element results well match the experimental results. A small Error of 3% may be due to the difference between the way of applying load in the real experiment and in the finite element model and also the limitations of finite element modeling.

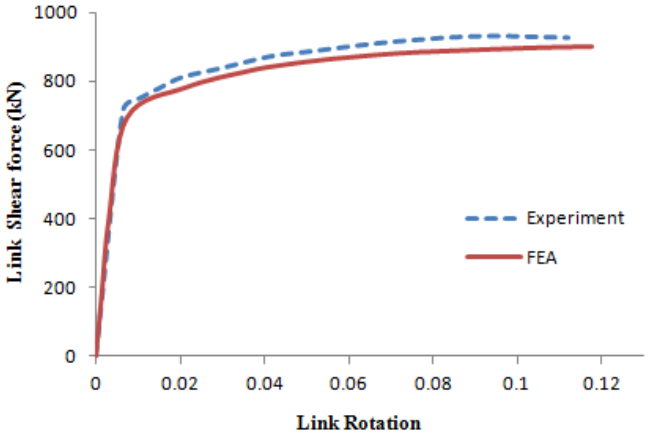

Figure 3.5. validation curve of 1-storey specimen by Mansour (2010)

3.7. Design of Multi-Storey EBFs

3.7.1. Building Geometry and Loading description

To evaluate the performance of eccentrically braced frames, a set of three office buildings with 4, 8 and 14 storeys, were designed according to the provisions of the national building code of Canada (NBCC, 2010) and the limit states design of steel structures described in CAN/CSA 16-09 (CSA, 2009). The office building, located in Vancouver, has a symmetrical plan with a total area of 1400 meter square. It is located in the site class C. Two identical chevron type EBFs were used symmetrically in N-S and E-W directions to resist lateral forces. Thus, each EBF can resist half of the design seismic loads. Since there is no eccentricity in the

building, the effect of accidental torsion was only considered in the design. It was calculated using equation $(\pm 0.10 D_{nx}) F_x$, where F_x is the lateral load force at each level and D_{nx} is the plan dimension of the building at level x perpendicular to the direction of seismic loading (NBCC, 2010). Based on the calculations, a 5% increase in the lateral loads may account for the accidental torsion for the current building. Notional lateral loads equal to 0.5% of the factored gravity loads, were also applied at each storey to consider the initial imperfections and partial yielding in the column (CSA, 2009). The typical floor plan and elevations used for this study are shown in Figure 3.6 and Figure 3.7 All the frames have equal bay width and storey height of 8 and 3.8 meter respectively. The dead load and live load of the floors were taken 4.2 kPa and 2.4 kPa. The roof dead load was considered as 1.5kPa and the snow load, calculated based on NBCC 2010 was equal to 1.82 kPa. The load combinations 1D+0.5L+E and 1D+0.25S+E were selected for the floors and the roof in compliance with NBCC 2010. The nominal yield strength of 350 MPa and modulus of elasticity of 200,000 MPa were considered for all the members.

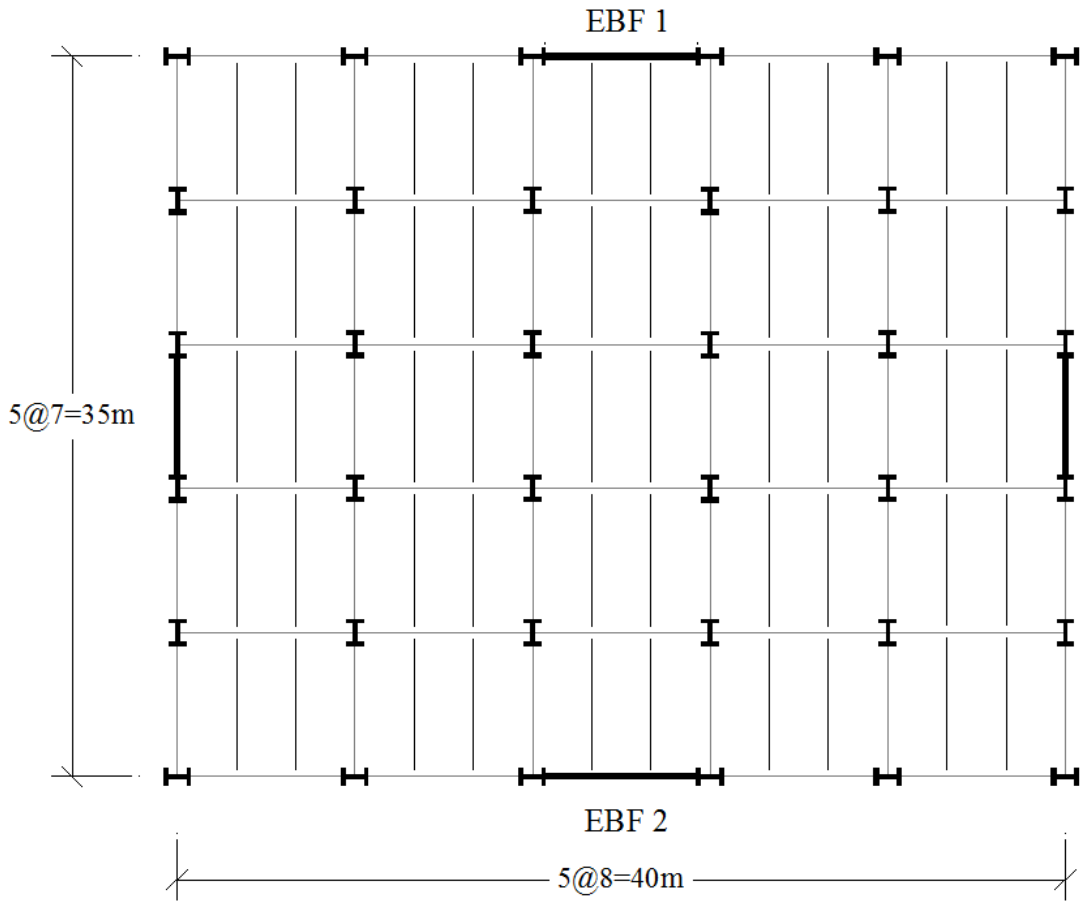

Figure 3.6. Typical floor plan of office building

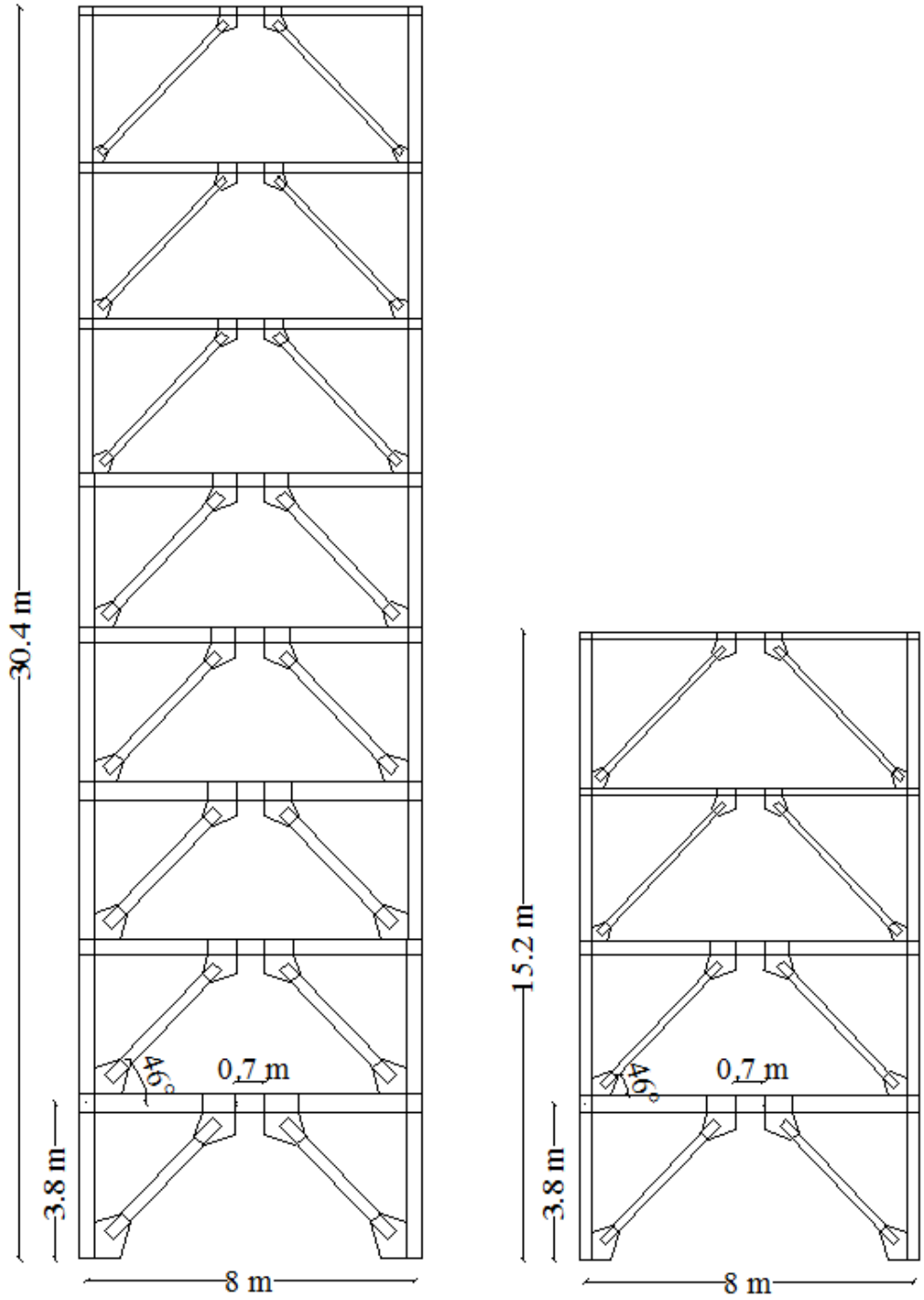

Figure 3.7. EBFs Elevations

3.7.2. Design procedure

The eccentrically braced frame, presented in this research were designed based on the capacity design approach for EBFs (CSA, 2009). In the capacity design of EBFs, the link is considered as the most ductile component to which all the inelastic behavior should be confined; therefore, only the links are sized for the code level seismic forces and all other members are sized for the forces generated by the fully yielded and strain hardened link in order to behave elastically. However, since the end of the outer beam (immediately after the link end) is under high axial force and bending moment, its yielding at the link connection is acceptable provided that enough lateral supports are supplied. (Engelhardt and Popov 1989)

In design of EBFs, the required strength, stiffness and ductility of the frame should be provided. This can be achieved by choosing appropriate bracing arrangement, link length and link section. The links should be sized and detailed such that they can provide the necessary lateral strength and ductility to the frame. The ductility of a link is usually defined as its plastic rotation capacity. The ratio of e/L significantly influences on the stiffness and strength of EBFs. Keeping the length of the link short results in higher frame stiffness a as shown in Figure 3.8.

The bracing arrangement is also important in EBFs configuration. The angle between brace and beam should be within 40 to 60 degree to avoid large axial force component in floor beams resulting from small angles. Large angles may result into strength and stability problems (Popov and Engelhardt, Seismic Eccentrically Braced Frames 1988).

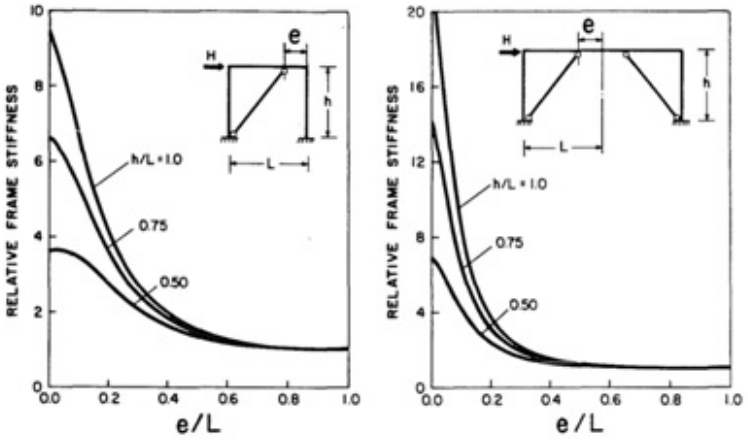

Figure 3.8. Variation of elastic lateral stiffness with e/L for EBFs (Popov and Engelhardt 1988)

In the preliminary design of EBFs, the sections of the links were selected to resist forces caused by the NBCC seismic loads. All other elements were designed for the forces created in yielded and strain hardened link. The design procedures can be summarized as follows:

Step 1. Calculate the design base shear

Distribute the design base shear vertically

Add the effects of notional load, accidental torsion and amplification factor U_2 to obtain the final lateral forces per frame

Step 2. Design the link

Choose the link length

Select the link section for the shear forces induced by NBCC seismic loads

Step 3. Design the outer beam (the beam outside the link) as beam-column for the loads coming from the strained-hardened link and the gravity loads

Step 4. Design the Brace as beam-column for the strained hardened link forces and gravity loads

Step 5. Design the Columns for the strained hardened link forces and gravity loads

Step 6. Calculate the drift and checking the drift requirement

Step 7. Determine the link rotation and checking link rotation requirement

Step 8. Modify the sections if required, to satisfy the requirements of step 6, 7 and 9

In the design process, the storey drift did not govern the design; however, some columns and braces sections were modified to control the link rotation to be less than the code limit of 0.08.

3.7.2.1 Calculate the Design Base Shear:

In order to find the design base shear, the equivalent static force procedure introduced in NBCC 2010 was used for 4 and 8 storey EBFs. At first, the fundamental period of the EBFs shall be obtained by equation 3.2.

$$T_a = 0.025h_n \qquad 3.2$$

where h_n is the height of the structure in meter. However, because the actual period of EBFs is much larger than the empirical period suggested by NBCC (Koboevic et al. 2012, Mansour 2010), the maximum allowable period provided by NBCC 2010 which is equal to two times the period of the code ($T_d = 2T_a$) was used. This assumption was checked and proved by the periods obtained from frequency analysis, performed on each EBF. Table 3.2 indicates that the periods determined by frequency analysis are larger than 2 times the periods suggested by NBCC 2010.

Table 3.2 comparison between fundamental period obtained from frequency analysis and $2T_a$

EBFs	Design Period $2T_a$	Frequency Analysis Period
4 Storey EBF	0.76	0.99
8 Storey EBF	1.52	1.773
14 Storey EBF	2.66	3.325

For 4 and 8 storey frames, the design base shear can be calculated by equation 3.3, while the minimum and maximum conditions should be considered.

$$V_{min} = \frac{S(2)M_v I_E W}{R_d R_o} \le V = \frac{S(T_a)M_v I_E W}{R_d R_o} \le V_{max} = \frac{2}{3}\left(\frac{S(0.2)I_E W}{R_d R_o}\right) \qquad 3.3$$

Where T_a is the empirical period, $S(T_a)$ is the spectral acceleration, M_v is the factor considering higher modes effects on increasing base shear, I_E is the importance factor, R_d is force reduction factor for ductility, R_o is force reduction factor for overstrength, and W is the total seismic weight resisted by the frame.

According to NBCC 2010, this method is applicable for regular structures less than 60 meter in height and with the fundamental period of 2 seconds or less. Since, for 14-storey structure, the period is more than 2 seconds; the preliminary sections were selected based on V_{min} corresponding to the spectral acceleration for the period of 2 seconds. Then, a modal response spectrum analysis was implemented to obtain the elastic base shear (V_e). This value should be multiplied by the importance factor I_E and divided by $R_d R_o$ to find the dynamic base shear V_d. As it can be seen in Table 3.3, the obtained value of V_d was compared to 80% of design base shear calculated by equivalent static force procedure. Since it was less than 0.8V, final V_{Design} was taken as 0.8V for 14-storey EBF as it was suggested by NBCC 2010.

Table 3.3 14-Storey EBF Design Base Shear

V (kN)	0.8V (kN)	Spectrum analysis V_e (kN)	$V_d = V_e / R_o R_d$ (kN)	Final V_{Design} (kN)
1914.84	1531.87	6497.5	1083	1531.87

Distribution of Lateral Forces

The calculated base shear can be distributed over the height of the structure using equation 3.4.

$$F_x = (V - F_t) W_x h_x / \left(\sum_{i=1}^{n} W_i h_i \right) \qquad 3.4$$

Where F_t is an additional lateral force concentrated at the top of the structure equal to $0.07 T_a V$ for the structures with the periods larger than 0.7 sec. The value of F_t should be less than or equal to $0.25V$. h_x represents the height of the structure above the level x and W_x is the portion of the weight of structure at level x.

According to S16-09, for sizing energy dissipating elements, the effects of notional loads and p-delta effects should be considered. The notional loads can be calculated by equation 3.5.

$$F_n = 0.005(1W_{DL} + 0.5W_{LL} + 0.25W_{SL}) \qquad 3.5$$

The factor U_2 is the implication factor should be used to account for the p-delta effects.

$$U_2 = 1 + \frac{\sum C_f R_d \Delta_f}{h_s \sum V_f} \leq 1.4 \qquad 3.6$$

Where: Δ_f : is the first order inter-storey displacement at each level

$\sum C_f$: is the sum of the column axial loads acting at the storey that is considered

$\sum V_f$: is the total storey shear

The final distributed lateral forces for three EBFs are presented in Table 3.4 to Table 3.6.

3.7.2.2 Link design

CSA S16-09 Requirements for links

There are some requirements for the links in CSA S16-09 clause 27.7. According to these requirements, the link sections should be class 1. For shear links, where the link length is smaller than $1.6M_p / V_p$, sections with class 2 flanges and class 1 webs may be used. For link with wide flange cross sections which were used in this study, V_p is equal to $0.55wdF_y$. The shear resistance of the link should be considered as the minimum of $\varphi V_P^{'}$, and $2\varphi M_P^{'} / e$.

Where $$V_P^{'} = V_P\sqrt{1-\left(\frac{P_f}{AF_y}\right)^2} \quad , V_P = 0.55wdF_y \qquad 3.7$$

and $$M_P^{'} = 1.18M_P\sqrt{1-\frac{P_f}{AF_Y}} \le M_P \quad , M_p = Z_xF_y \qquad 3.8$$

P_f is the axial force in the link and A is the gross area of the link.

For selecting the link length the CSA standard emphasizes that it should be greater than the depth of the link beam. It also requires limitation for the link rotation, which is the inelastic component of the rotation of the link with respect to the rest of the beam. For shear links the link rotation must not exceed 0.08 rad.

The web of the link should be uniform with no attachments other than the link stiffeners. At the end of the links, full depth web stiffeners must be used on either sides of the web. Their minimum thickness should be taken as 0.75w and the combined width must be greater than $b_f - 2w$. For shear links, when the link rotation is equal to 0.08 rad, the intermediate web

stiffeners intervals should be less than $30w - 0.2d$, and when the rotation angle is 0.02 rad, their gap should be smaller than $52w - 0.2d$. For other values of link rotation, the interpolation is required to find the proper stiffeners intervals.

Link Length calculation

For designing the link, firstly the link length was selected based on the following criteria:

- For shear links $e \le 1.6M_P / V_p$
- For yielding in shear $\varphi V_P^{'} < 2\varphi M_P^{'} / e \Rightarrow e < 2M_P^{'} / V_P^{'} \Rightarrow e < \dfrac{2Z_x F_y}{0.55A_w F_y} \Rightarrow \boxed{e < \dfrac{3.6Z_x}{A_w}}$
- The link length shall not be less than the depth of the link beam. $e \ge d$

Checking these requirements, the link length was selected as e=700 mm.

Link section selection

The sections of the links should be chosen to have the shear strength (V_p) very close to the shear forces in the link created by NBCC factored seismic loading. Therefore, the minimum web area can be calculated by equation 2.1.

$$\varphi V_P = 0.9\left(0.55dwF_y\right) \Rightarrow \min dw = \frac{V_{link}}{0.9\left(0.55Fy\right)} \qquad 3.9$$

where V_{link} may be obtained by approximating the shear force in the link, using the free body diagram for each floor.

$$\frac{V}{2}.\,h = V_{link}.\frac{L}{2} \Rightarrow V_{link} = \frac{\sum Vh}{L} \qquad 3.10$$

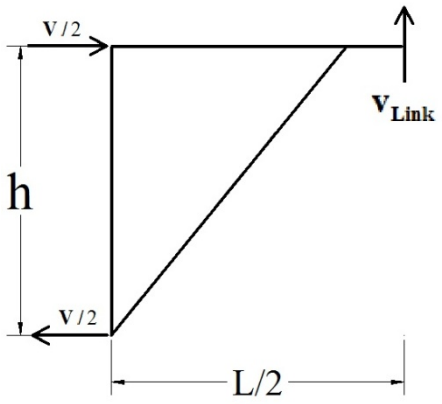

Figure 3.9. Free-Body diagram of EBF

The other important aspect in shear link design, is the link strength factor $\alpha = \frac{V_P}{V_{Link}} \geq 1$. (Popov et al., Methodology for optimum EBF link design 1992) Maintaining α uniform throughout the height of the EBF results in simultaneous yielding of all links against increasing lateral forces and avoids from excessive concentration of link deformations in some storeys (Popov, et al., 1992). For the current designed EBFs, uniform alpha were achieved in all but top storeys where shear forces in the links were small, but stronger sections were essential to meet the shear link and class 1 requirements.

After selecting the link sections, all the mentioned provisions of CSA S16-09 for shear links were checked.

3.7.2.3 Designing the outer Beam

According to CSA S16-09, section of the outer beam should be class 1 or 2. It should be designed to resist forces fully yielded and strain hardened links. This force can be calculated as

$V_u = 1.3R_y V_p$ where 1.3 is the factor corresponding to the increase above the yield value because of strain hardening, and R_y accounts for the factor of the probable yield stress.

In this research, it is considered that the exterior beam and link have the same section, and their connection is moment resisting connection. The beam should resist the moments transferred from the strain hardened link and the axial forces; therefore, is must be designed as a beam-column.

3.7.2.4 Designing the Brace

CSA S16-09, clause 27.7.10 introduces class 1 or 2 section for the diagonal braces. Each brace and its end connection should resist the axial force and moments of the strain hardened link; and of the gravity load 1D+0.5L+0.25S. The forces in the link are considered as $1.3R_y$ times the nominal strength of the link for links with wide-flange cross sections. The intersection of the brace and the beam centerlines must be at the end or within the link. Moment resistant connections may be used for the braces designed to resist a portion of the link end moment. The braces should be configured such that their angles with the floor beam remain between 40 and 60 degree as mentioned earlier. The resulting forces of strain hardened link in the braces can be obtained by equation 3.11

$$F_{brace} = \frac{V_u \times L}{(L - e)\sin\alpha} \qquad 3.11$$

The forces due to the gravity loads were also calculated and considered in the design. Because of the presence of the axial forces and bending moments together in the brace, they were also considered as the beam-column and were check for the requirements of beam-columns.

3.7.2.5 Designing the Column

According to CSA S16-09, the column section should be class 1 or 2. The columns should be designed to resist the cumulative effect of yielding links and gravity loads. The amplification factor accounting for strain hardening shall be taken as $1.15\,R_y$ for all the floors except for the top two storeys where $1.3R_y$ must be used. They should meet the requirements of clause 13.8 considering axial compression and bending together. The additional bending moment due to column continuity and relative storey drift should be considered in the interaction equation as $0.4ZF_y$ for the top two storeys and $0.2ZF_y$ for the other levels. Z is plastic section modulus of steel sections.

In the design process, the column axial forces due to yielded link were calculated by finding $V_{rlink} = (1.15 \text{or} 1.3) R_y F_y V_P$, then the forces in the braces were calculated and finally the column axial forces were obtained by equation 3.12.

$$F_{Col}^{i} = F_{Col}^{i+1} + F_{brace}^{i+1} \sin\beta \pm V_{Beam} \qquad 3.12$$

where F_{Col}^{i+1} and F_{brace}^{i+1} are the axial forces immediately above the column and brace; and V_{Beam} is the shear force in the beam.

The results were combined with the axial forces due to gravity load obtained from load combination 1D+0.5L+0.25S. Since the moments are minimal in the columns, the priliminary design was done for the calculated axial forces. The selected column sections were checked for interaction equation to ensure the capacity of the columns, considering the additional mentioned

bending moments specified in CSA S16-09 combined with the bending moments under gravity and lateral loads.

3.7.2.6 Drift Requirement

The largest storey drift allowed by the code for eccentrically braced frame is 0.025h where h is the storey height of the frame (NBCC, 2010). In the design phase, the lateral displacement can be determined from a linear analysis on EBFs subjected to seismic design forces. Clause 4.1.8.13 of NBCC 2010 states that the elastic displacement values should be multiplied by $R_d R_o / I_E$ to obtain inelastic displacements for the lateral load resisting system.

$$\Delta = \frac{R_d R_o}{I_E} \Delta_{el} \qquad 3.13$$

3.7.2.7 Link Rotation Requirement

According to CSA S16-09, the shear link rotation must not be more than 0.08 rad. To calculate the inelastic link rotation in the design phase, the elastic drift corresponding to factored seismic load should be calculated. Then the inelastic rotation angle can be determined by equation 2.4.

$$\theta = \frac{3\Delta_{el}}{h_s} \quad \Rightarrow \quad \gamma = \left(\frac{L}{e}\right)\theta \qquad 3.14$$

After selecting all the member sections, the maximum top storey drift and the maximum link rotations should be calculated and compared with the code limit, if they don't meet the requirements of the code, the sections should be modified. Table 3.4 to Table 3.6 present the summary of selected sections and inelastic link rotations for three EBFs.

Table 3.4 Selected Sections for 4-Storey EBF

Storey	Link length (mm)	Design Seismic forces	Beam	Brace	Column	Link rotation (rad)
4	700	261.88	W200x31	HSS152x152x8	W310x67	0.068
3	700	366.58	W200x71	HSS178x178x9.5	W310x67	0.067
2	700	258.03	W360x72	HSS203x203x9.5	W310x107	0.062
1	700	144.14	W410x67	HSS203x203x13	W310x107	0.056

Table 3.5 Selected Sections for 8-Storey EBF

Storey	Link length (mm)	Design Seismic forces	Beam	Brace	Column	Link rotation (rad)
8	700	240.28	W200x31	HSS178x178x8	W360x162	0.06
7	700	239.94	W250x58	HSS178x178x13	W360x162	0.06
6	700	215.04	W250x67	HSS203x203x13	W360x162	0.06
5	700	187.01	W360x72	HSS254x254x9.5	W360x237	0.06
4	700	157.39	W410x67	HSS254x254x9.5	W360x237	0.06
3	700	126.54	W460x68	HSS305x305x9.5	W360x237	0.05
2	700	94.51	W410x85	HSS305x305x13	W360x463	0.05
1	700	61.13	W460x89	HSS305x305x13	W360x463	0.04

Table 3.6 Selected Sections for 14-Storey EBF

Storey	Link length (mm)	Design Seismic forces	Beam	Brace	Column	Link rotation (rad)
14	700	251.72	W200x42	HSS178x178x9.5	W360x91	0.080
13	700	144.50	W200x59	HSS178x178x13	W360x91	0.080
12	700	142.00	W250x58	HSS203x203x9.5	W360x91	0.079
11	700	136.47	W310X52	HSS203x203x13	W360x196	0.076
10	700	129.41	W310x74	HSS254x254x9.5	W360x196	0.073
9	700	121.45	W360x79	HSS254x254x9.5	W360x196	0.071
8	700	112.87	W410x74	HSS305x305x9.5	W360x382	0.067
7	700	103.52	W460x68	HSS305x305x9.5	W360x382	0.064
6	700	92.51	W460x82	HSS305x305x9.5	W360x382	0.066
5	700	81.50	W460x89	HSS305x305x13	W360x634	0.063
4	700	70.49	W460x97	HSS305x305x13	W360x634	0.059
3	700	59.48	W530x85	HSS305x305x13	W360x634	0.056
2	700	48.48	W530x92	HSS305x305x13	W360x990	0.052
1	700	37.47	W530x101	HSS305x305x13	W360x990	0.049

3.7.3. Finite Element Modeling of 4-Storey, 8-Storey and 14-Storey EBFs

The same finite element modeling technique is used to model the three designed 4-, 8- and 14-storey EBFs. Figure 3.10 presents FE mesh for 14-storey EBF, where only bottom six storeys are shown. Three types of analyses including pushover, frequency and seismic analyses were performed in ABAQUS on the created FE models. To perform seismic analysis, a leaning column was added to the FE model to account for P-delta effects. The leaning column was modeled by ABAQUS T3D2, two node three dimensional truss elements, connected to the frame at every floor using pin-ended rigid links. It was designed to carry half of the floor masses and gravity loads which were not taken by EBFs directly, without adding any lateral stiffness to the system. The lumped masses and gravity loads were exerted to the column nodes at their corresponding levels. A 5% Rayleigh proportional damping ratio was used for the seismic analysis. The supports of all columns including the dummy column are considered as pin supported at the base. The yield strength of all the components was considered as 350 MPa. The mass of the components were also taken into account by adding the density of the steel to the material model.

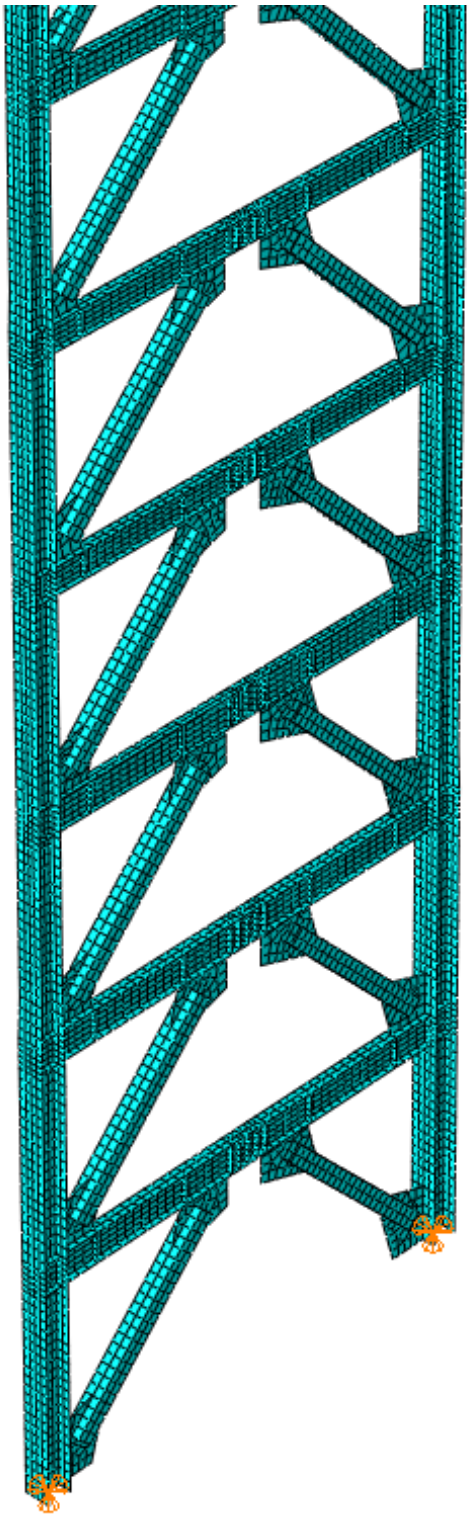

Figure 3.10. Finite element model of 14-storey EBF (only bottom 6-storeys are shown)

3.8. Summary

In this research, non-linear finite element models were used to study the behavior of eccentrically braced frames. This chapter explained the details and considerations for developing the finite element models for EBFs. In order to have reliable FE models, the first model was built using an available test specimen data. The results obtained from finite element simulation were compared to the corresponding experimental responses. The validation curve showed a good agreement between the FE model and the selected test specimen in terms of the initial stiffness and post-yield responses with a small difference of 3%. The validated modeling technique was then used to develop finite element models for three designed EBFs with 4, 8 and 14 storeys to study the seismic performance of the eccentric braced frames. These three EBFs were designed based on the capacity design approach presented by CAN/CSA S16-09. The design procedure for designing EBFs was also explained in detail in this chapter.

Chapter 4. Seismic Performance of Eccentric Braced Frames

4.1. Introduction

In this chapter, the three designed 4-, 8- and 14-storey EBFs, explained in the chapter 3, were employed to study the seismic performance of eccentrically braced frames using nonlinear dynamic analysis. For seismic analysis, the FE models of the designed EBFs were subjected to eight selected ground motion records. The response spectra of the selected ground motions were scaled to match the design spectra of Vancouver. The criteria for selecting the ground motion records are explained in this chapter. Then, non-linear dynamic analyses results are compared against the criteria suggested by NBCC (2010) and CAN/CSA S16-09 (2009).

4.2. Nonlinear Dynamic Analysis of EBFs

4.2.1. Frequency Analysis

Prior to the seismic analysis, frequency analyses were performed on EBF models to determine the fundamental periods and mode shapes corresponding to each eccentrically braced frame. The finite element model used for frequency analysis consists of the gravity column. Finding the fundamental period is useful for scaling the ground motion records to make it suitable for seismic analysis of the designed EBFs. Also, the material model which was used for seismic analysis required the Raleigh proportional damping coefficients α and β. Knowing the fundamental frequencies of EBFs, these damping coefficients can be calculated using equation 4.1. The Raleigh proportional damping ratio (ξ) was considered as 5%.

$$\alpha = \xi \frac{2\omega_i \omega_j}{\omega_i + \omega_j} \qquad \beta = \xi \frac{2}{\omega_i + \omega_j} \qquad 4.1$$

where ω_i and ω_j are the circular frequencies corresponding to i^{th} and j^{th} fundamental periods.

The fundamental periods and mode shapes were also used for modal pushover analysis which is discussed in chapter 5. Comparing the fundamental period determined from frequency analyses with the period that suggested by NBCC 2010 for EBFs shows that the code estimation of the periods of EBFs is very conservative.

4.2.2. Ground Motion Records

According to NBCC 2010, the ground motion histories used in the dynamic analysis should be spectrum compatible. The uniform hazard spectrum for each region is provided by NBCC 2010. For this study, the design spectrum of Vancouver was used as it is the location of the office buildings considered in this research. As per ASCE7-10, when peak maximum responses are considered to investigate seismic response of structure, at least three ground motions must be utilized; and when the median value of maximum responses are used, a minimum of seven earthquakes are required.

For this research, eight earthquake records were employed, five of which were selected from the strong ground motion database of Pacific Earthquake Engineering Research Center (PEER 2010), and the other three records were chosen from Engineering Seismology toolbox website (Atkinson et al. 2009). All the records, including five real ground motion and three synthesized are presented in Table 4.1 and Table 4.2.

Since the magnitudes of most recorded seismic activities in British Columbia were measured between 6 and 7, for a range of 400 years (Lamontagne et al. 2008), the real earthquake records were selected to have a magnitude in this range. The simulated ground motions were chosen for site class C with the magnitude of 6.5 and 7.5, including both near fault and far fault records. To select the real ground motion records, the ratio of the peak acceleration (PGA) to the peak velocity (PGV) was taken into account. This ratio should be close to 1 for Vancouver (between 0.8 and 1.2) (Naumoski et al. 2004)

The response spectrum of unscaled ground motions and the design spectrum of Vancouver; corresponding to 5% of critically damped SDOF system in soil class C, were employed for scaling the earthquake records, using the partial area method of scaling. In this method, the area under the response spectrum of the selected ground motion must be determined for a range between $0.2T_1$ and $1.5T_1$, where T_1 is the fundamental period of the structure. The area under the design spectrum of Vancouver must be also obtained for the same range of period. The ratio of the first and second areas gives the scaling factor, using which the accelerograms were scaled to have the same area under the design and earthquake response spectrum within the specified period range. The lower bound $0.2T_1$ was selected to account for the effects of higher modes on seismic response; the upper bound $1.5T_1$ was chosen to consider the increase of fundamental period of structure in the plastic range. Figure 4.1, Figure 4.2, and Figure 4.3 present acceleration spectra for selected ground motions and Vancouver design spectra for 4-, 8-, and 14 storey EBFs respectively. The scaled accelerograms are also presented in Figure 4.4 to Figure 4.6.

Table 4.1 Real Ground Motion Records

Event	Magnitude	PGA (g)	PGV (m/s)	A/V	Scaling factor 4-storey	Scaling factor 8-storey	Scaling factor 14-storey
San Fernando, 1972	6.6	0.188	0.179	1.05	1.52	1.67	1.45
Kobe, 1995	6.9	0.143	0.147	0.973	1.65	1.7	2.2
Loma Prieta	6.93	0.233	0.221	1.05	1.35	1.46	1.97
Imperial Valley 2	6.53	0.525	0.502	1.04	0.98	1.01	0.827
Northridge	6.69	0.51	0.483	1.055	0.61	0.66	0.83

Table 4.2 Simulated Ground Motion Records

Event	Magnitude	Distance (km)	Scaling factor 4-storey	Scaling factor 8-storey	Scaling factor 14-storey
6C1	6.5	8.4	0.758	0.84	1.05
6C2	6.5	13.2	1.147	1.268	1.49
7C2	7.5	45.7	1.494	1.373	1.335

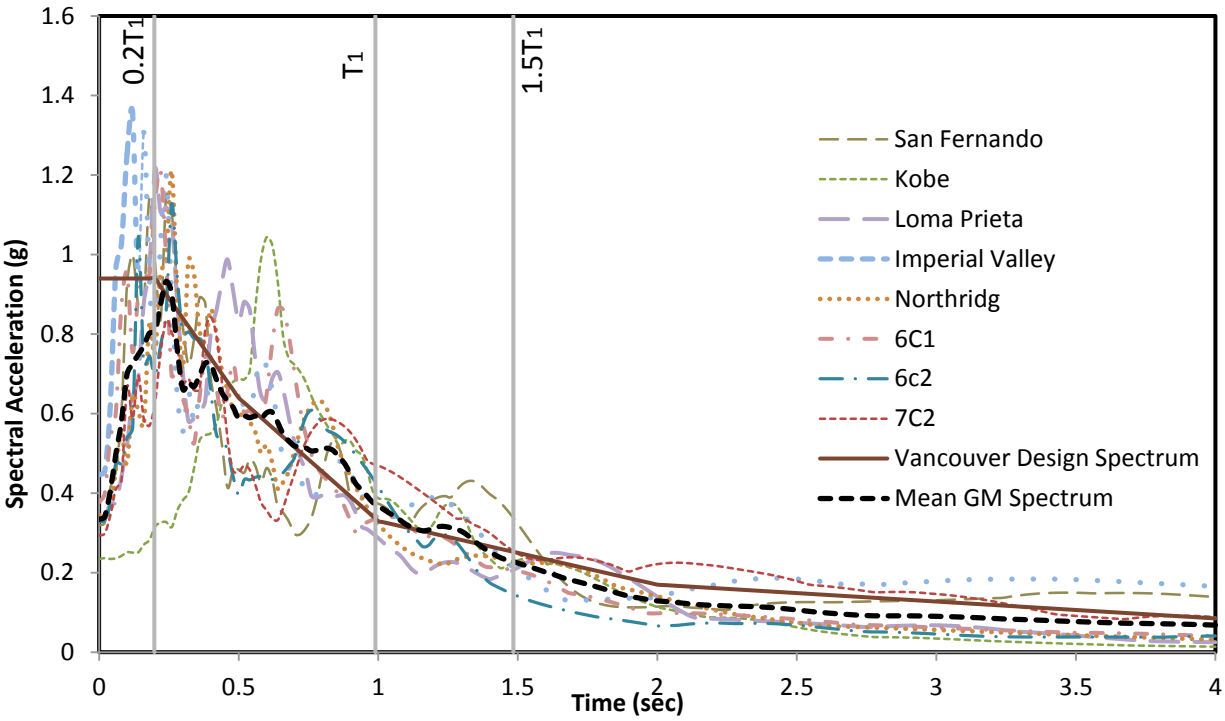

Figure 4.1. Acceleration spectra for selected ground motions and Vancouver design spectra for 4-storey

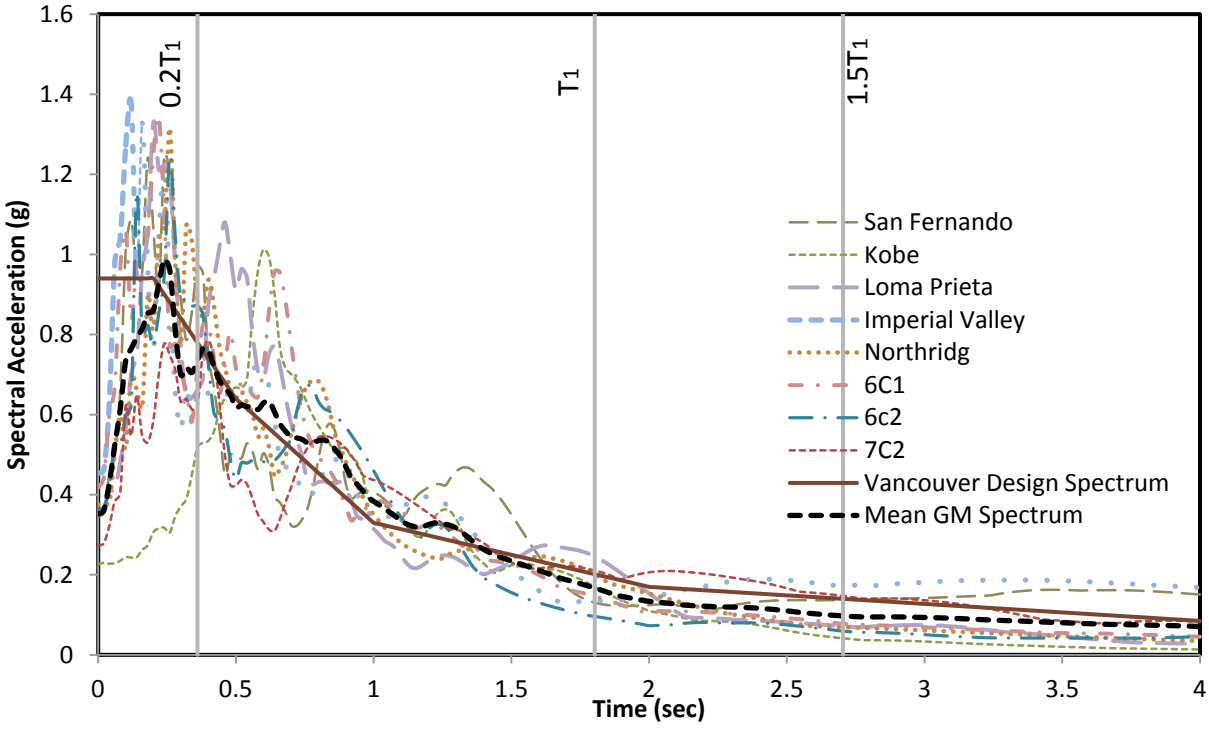

Figure 4.2. Acceleration spectra for selected ground motions and Vancouver design spectra for 8-storey

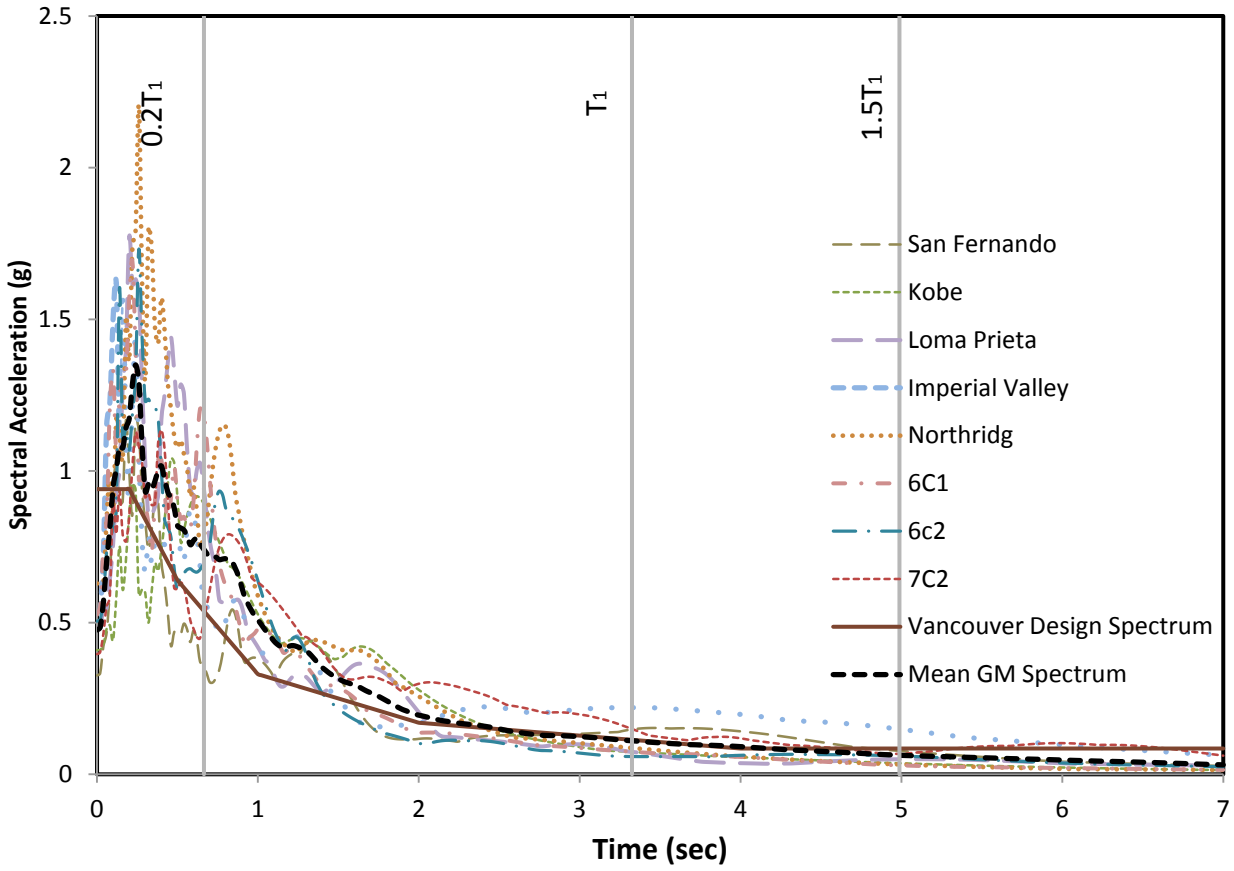

Figure 4.3. Acceleration spectra for selected ground motions and Vancouver design spectra for 14-storey

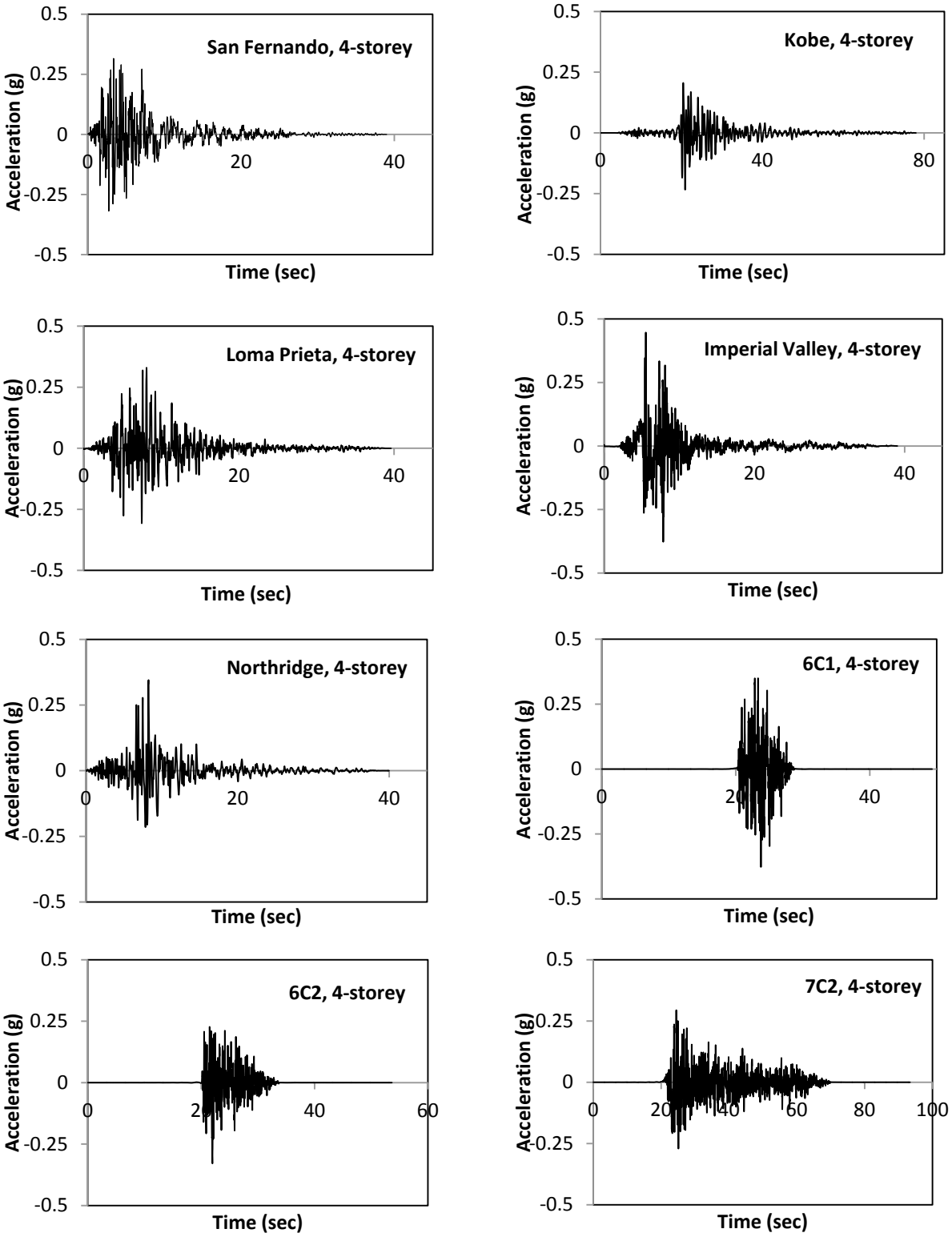

Figure 4.4. Scaled Earthquake records for 4-storey EBF

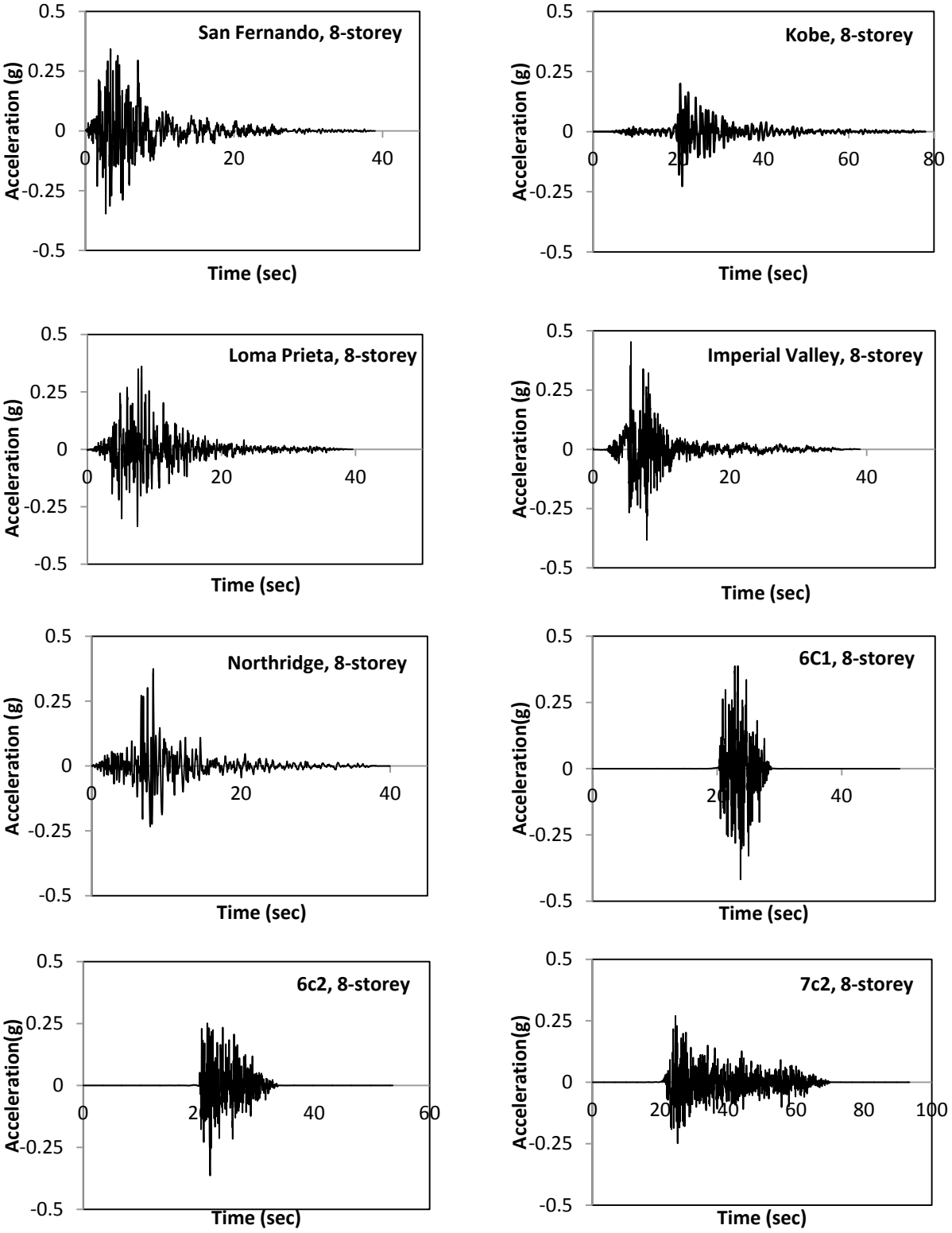

Figure 4.5. Scaled Earthquake records for 8-storey EBF

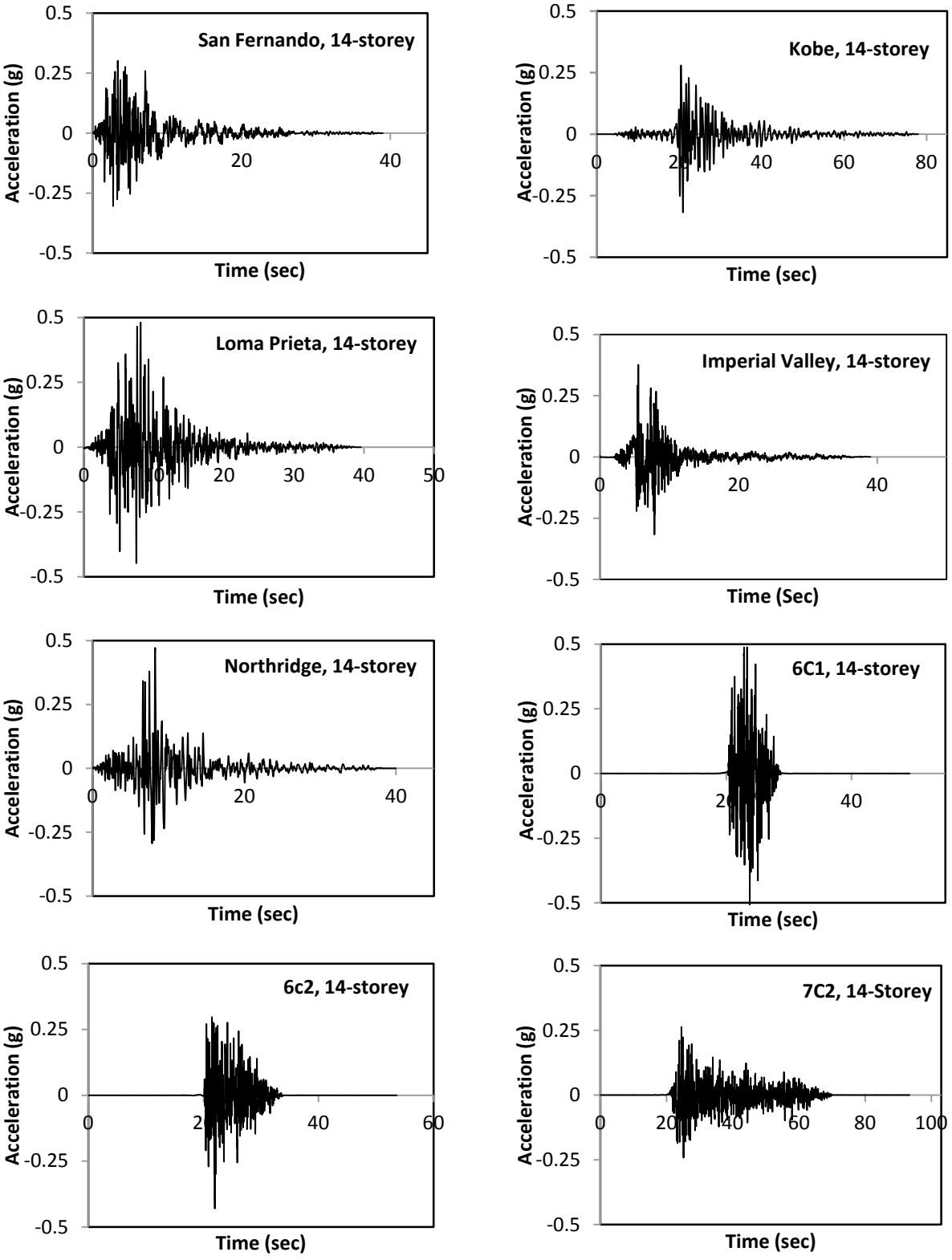

Figure 4.6. Scaled Earthquake records for 14-storey EBF

4.3. EBF Seismic Response

Nonlinear dynamic analyses were performed on 4-, 8- and 14-storey EBFs using the ground motions introduced in the previous section. Since the link is the most important element in EBFs, the responses of the link are the main concentration of this study. The critical response parameters for the links are the inelastic link rotations and the maximum normalized shear forces in the link. The maximum inelastic link rotations extracted from ABAQUS were compared with the code limit of 0.08 rad. To normalize the shear forces in the link, the obtained values from ABAQUS were divided by the probable shear resistance $R_y V_P$ and were checked with 1.3, the amplification factor provided by S16-09 (CSA 2009). The inter-storey drifts were also determined and evaluated with 2.5% of the storey height. The results provided in this research are the peak values of responses obtained for each earthquake. Then, the average was taken between the peak responses of 8 earthquake records to present the EBF seismic behavior. According to ASCE7-10, taking average of the maximum responses is allowed if at least seven earthquake records are used for time history analyses.

4.3.1. Link Responses

Link Rotation

The results of maximum link rotations and its median values between 8 earthquakes are presented in Figure 4.7, Figure 4.9, and Figure 4.11 for three EBFs under study.

For 4-storey EBF, for all the records, the link rotations were less than the limit of 0.08 specified in CSA S16-09. For most records, the largest deformation occurred at the first and third stories,

the same level as the highest link shear forces were observed. Figure 4.7 shows that the average values of link rotations are about 0.05 rad.

For 8-storey structure, as shown in Figure 4.9, most ground motions indicated the maximum link rotation at first and sixth level, where the maximum link shear forces were also developed. The link rotations varied from 0.02 to 0.05, which were lower than the limit.

For 14-storey structure, as shown in Figure 4.11, the average link rotations were between 0.02 and 0.06 for all the floors, except for the eleven and twelve levels where link rotations exceeded the 0.08 limit. These values were 0.085 and 0.09 for 11^{th} and 12^{th} floor respectively. A concentration of link rotation was also observed at the first floor; however, the median value for the first floor was well below the limit.

Link Normalized Shear Force

The results of normalized shear forces in the links are illustrated in Figure 4.7, Figure 4.9, and Figure 4.11. The limit of strain hardening factor suggested by CSA S16-09 is 1.3. As the results show this limit was exceeded for all EBFs; however, these values are still within the range of experimental results which showed the average overstrength factor of 1.5 for the short links (OkazakiArce et al. 2005) (Arce 2002). Past tests also showed the link overstrength factor of more than 1.5 (Hjelmstad and Popov 1983, Engelhardt and Popov, behavior of long links in eccentrically braced frames 1989). There are also some recent tests that reported the overstrength factor close to 2 for built-up shear links used in bridge (McDaniel et al. 2002). The limit of 1.3 presented by CSA S16-09 accounts for strain hardening developed in the links; however, the reported experimental results and also the observations made in this study showed that the link

overstrength factor can also be due to the participation of the flanges in resisting shears. Based on these observations, the suggested overstrength factor of the link provided by current Canadian seismic provision may be un-conservative.

For 4-storey EBF, all the floors; except for the 4th level, slightly exceeded (maximum of 7%) the code limit of 1.3. For 8-storey structure, the second, third and the last floors exhibited overstrength values lower than 1.3. All other floors went beyond the code bound. For 14-storey EBF, the links over-strength was below 1.3 for most floors. Only the first and top floors (11-13th) showed higher magnitudes. The maximum strain hardening factor of 1.48 occurred at 11th floor which was 14% higher than CSA S16-09 requirement.

4.3.2. Other Responses

Inter-Storey Drift

Figure 4.8, Figure 4.10, and Figure 4.12 present the inter-storey drifts for the three designed EBFs. As shown in Figure 4.8, the inter-storey drifts for 4-storey EBF vary between 0.68 to 0.79%. Comparing the obtained values from ABAQUS with NBCC 2010 drift limit, it was observed that inelastic inter-storey drifts in all the floors were within the NBCC drift limit.

Similar findings were also observed for 8-storey EBF, where the magnitudes of inter-storey drifts were reported between 0.4 to 0.8% of the storey height, which are 67% to 80% lower than the $0.025h_s$ limit suggested by NBCC 2010.

For 14-storey EBF, as shown in Figure 4.12, the values were between 0.6% and 1.29% which were higher than the other two EBFs. However, they were still 50% lower than the limit. In all EBFs, the results trend for the inter-storey drift was the same as the link rotations.

Base Shear

Table 4.3 and Figure 4.13 present the base shear forces obtained from nonlinear dynamic analyses on each EBF. As it can be seen, Imperial Valley earthquake imposes the maximum shear at the base for all the EBFs. The average values of all records for each EBF were also compared to the design value. As it can be seen in the Table 4.3, the average base shear obtained from non-linear dynamic analysis is higher than the design base shear. This is due to the overstrength of the selected members. In the current design of EBFs suggested by CSA S16-09, the link and the outer beam have the same section. The link should be designed to yield, while the outer beam with the same section should resist forces by the strain-hardened link. Meeting these two requirements is an iterative procedure which may lead into over-sizing link element, and consequently over-sizing all other members of the frame which should be designed for the capacity of the link. This also results in larger force demands in EBF members.

Table 4.3 Non-Linear Dynamic Base Shear (kN)

EBF	SF	KOBE	LP	IV	Northridge	6C1	6C2	7C2	Average	Design
4	2342	2020	2238	2502	2337	2265	2236	2192	2304	1030.63
8	2695	2744	2783	3332	3283	2967	2439	3035	2910	1321.84
14	3485	4104	3876	4358	4219	4255	3926	3945	4145	1531.87

Yielding Pattern

To study the yielding pattern of 4-, 8- and 14 storey EBFs, the results obtained for the Imperial Valley were utilized. This earthquake was chosen because it had the maximum PGA and also the maximum base shear was found for this earthquake record.

For 4-storey EBF, the first yielding was observed at the link web of the first floor, then it continued to the second to forth floor. The simultaneous yielding of all links was observed during the ground motion. At the time that maximum base shear occurred, the links of all storeys were yielded. Some minor yielding was also observed at the end of some outer beams where tehy connected to the links. This yielding took place because of high axial forces in the beam and high moments at the end of the link which transferred to the beam. It is acceptable provided that enough lateral supports are supplied (Engelhardt and Popov, behavior of long links in eccentrically braced frames 1989). All other members behaved elastically during the analysis.

For 8-storey frame, the initial yielding was reported at the first to sixth floor, then it continued to the 7^{th} and 8^{th} floor. The simultaneous yielding of the links of all the floors was observed at the time 7.7 sec where the peak acceleration occurs. At the instance of maximum base shear, only the links at first to fourth floors were yielded. In all cases no inelastic activity was reported by the other members except for at the outer beam immediately after link ends.

For 14-storey EBF, the first yielding occurred at the link web of 11^{th} to 13^{th} storeys. Then it continued to the first floor, middle floors 5 and 6 and upper floors 12 and 13. Although the links at all floors were yielded, but their yielding did not happen at the same time in spite of selecting

the links of all floor to have the same link strength factor α at design phase. The most simultaneous yielding was observed when 2-7 and 10-14 floors were yielded at the same time.

For all frames, all the links were fully yielded. Also some yielding was observed at the flanges of the outer beam where it was connected to the link. No yielding was detected in other members meaning that they remained elastic during nonlinear dynamic analyses. Figure 4.14 to Figure 4.16 present yielding pattern for 4-, 8- and 14-storey EBFs when maximum simultaneous yielding happened.

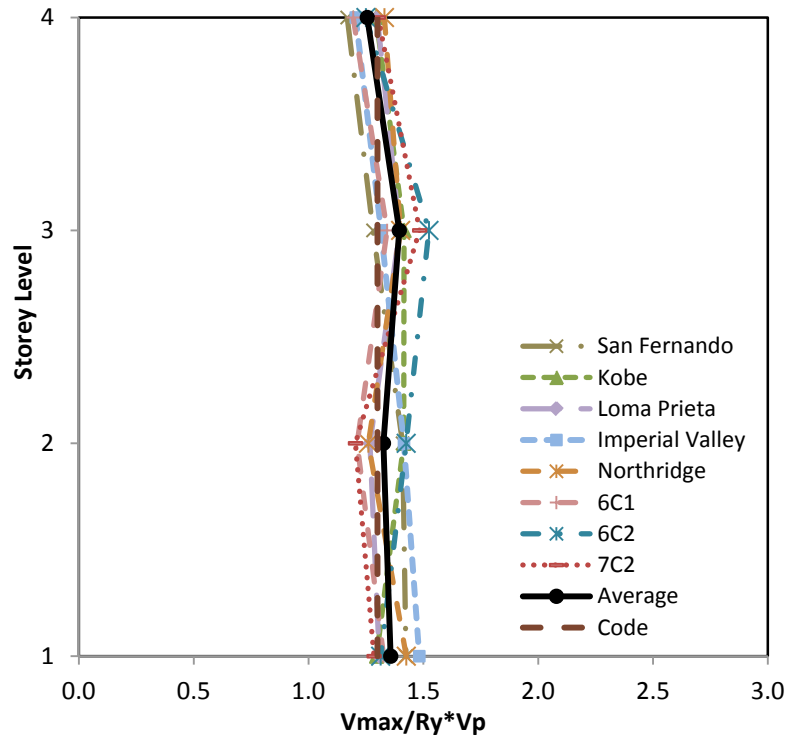

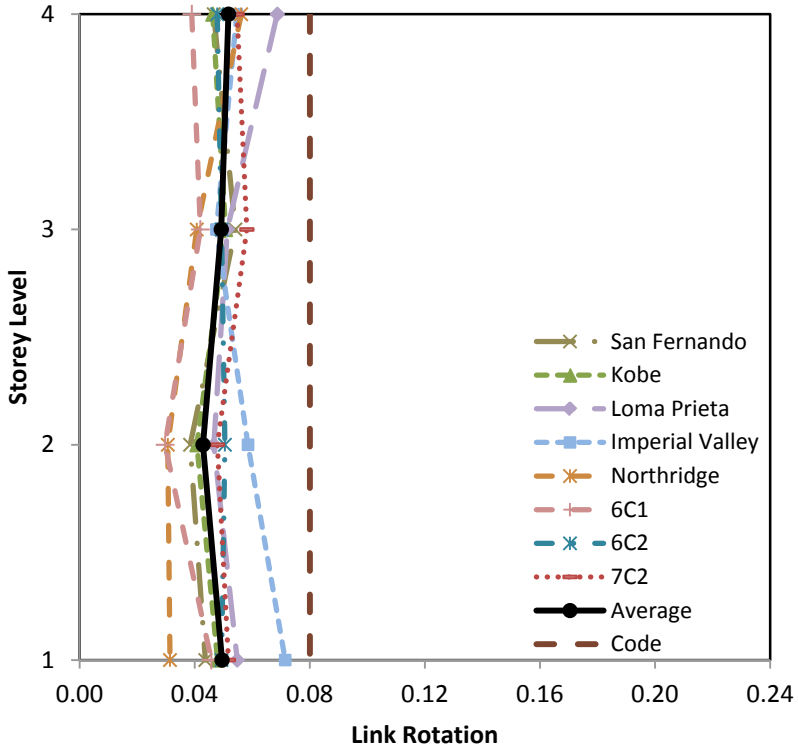

Figure 4.7. Normalized Maximum Link Shear Forces and Link Rotations for 4-storey EBF

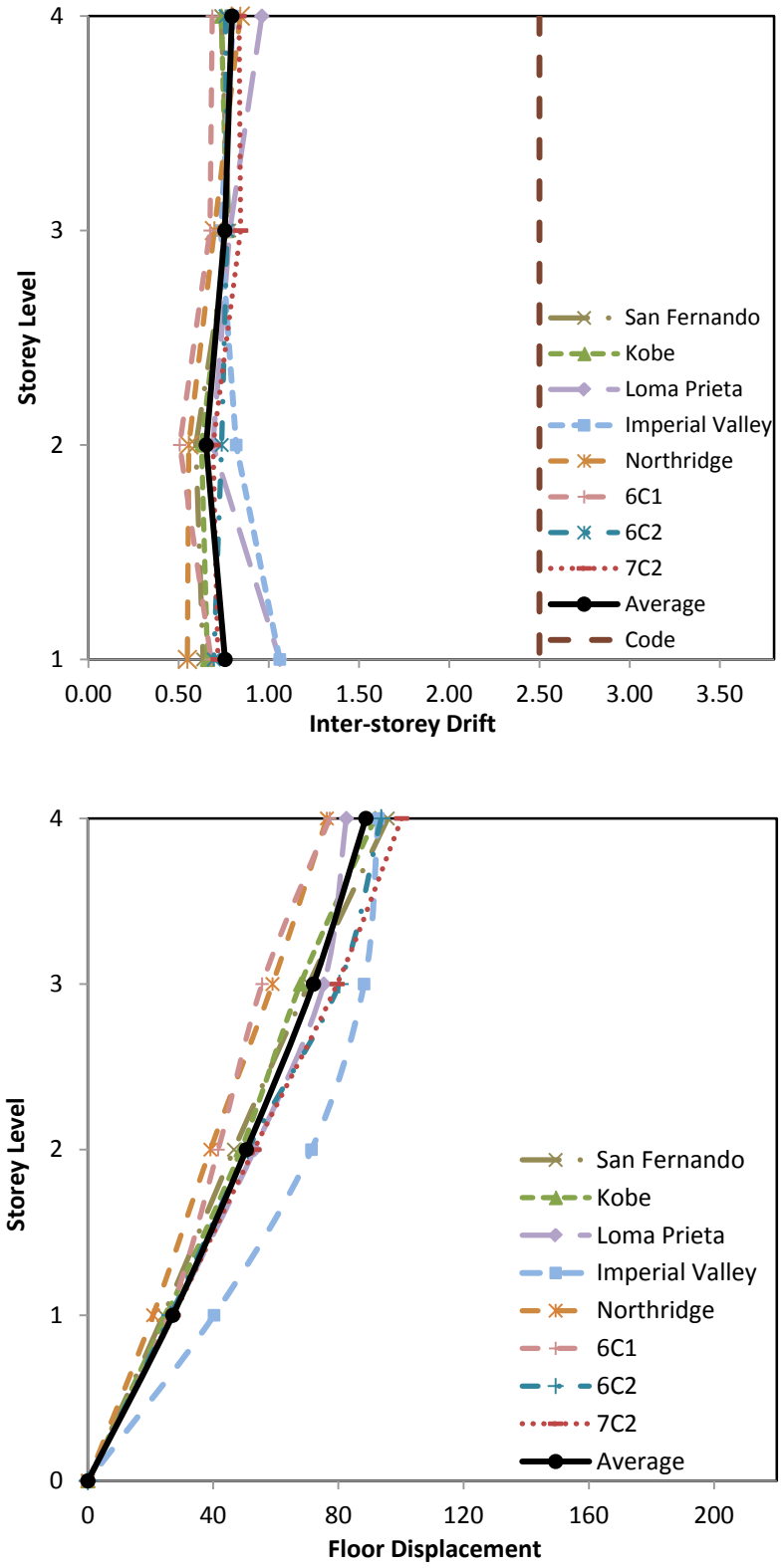

Figure 4.8. Inter-storey Drift and Floor Displacement for 4-storey EBF

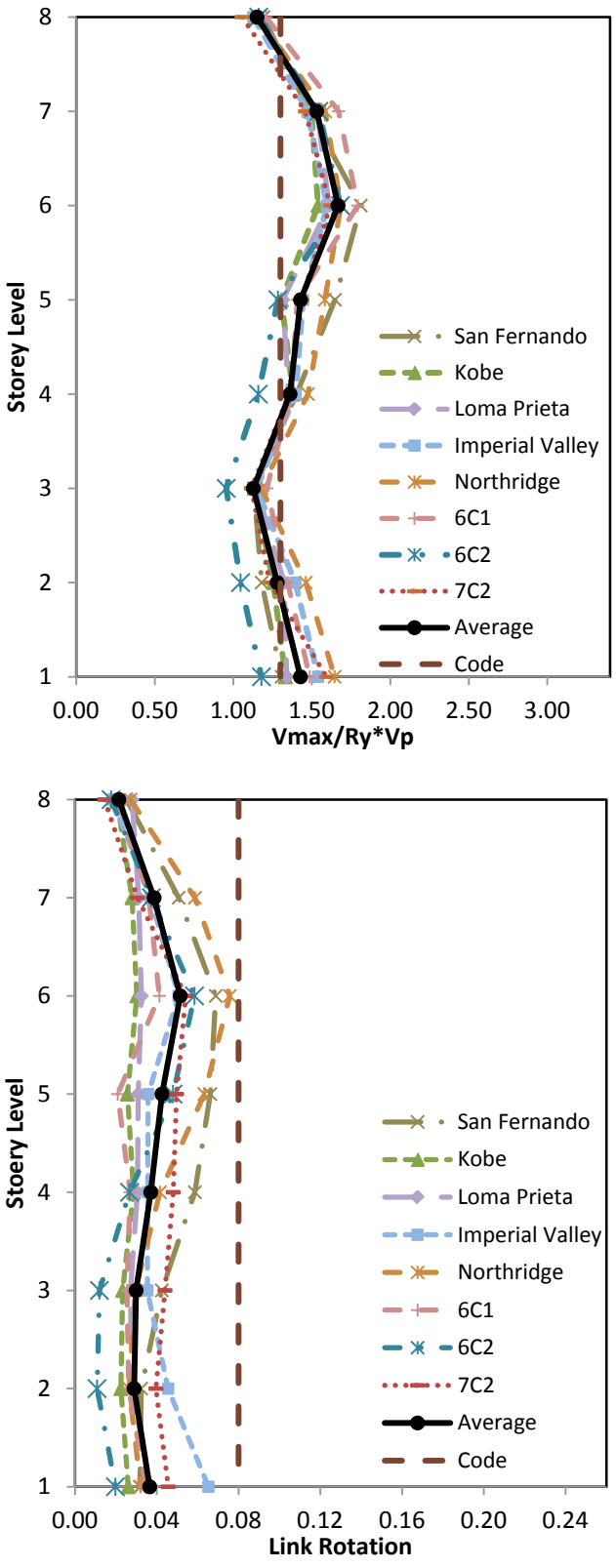

Figure 4.9. Normalized Maximum Link Shear Forces and Link Rotations for 8-storey EBF

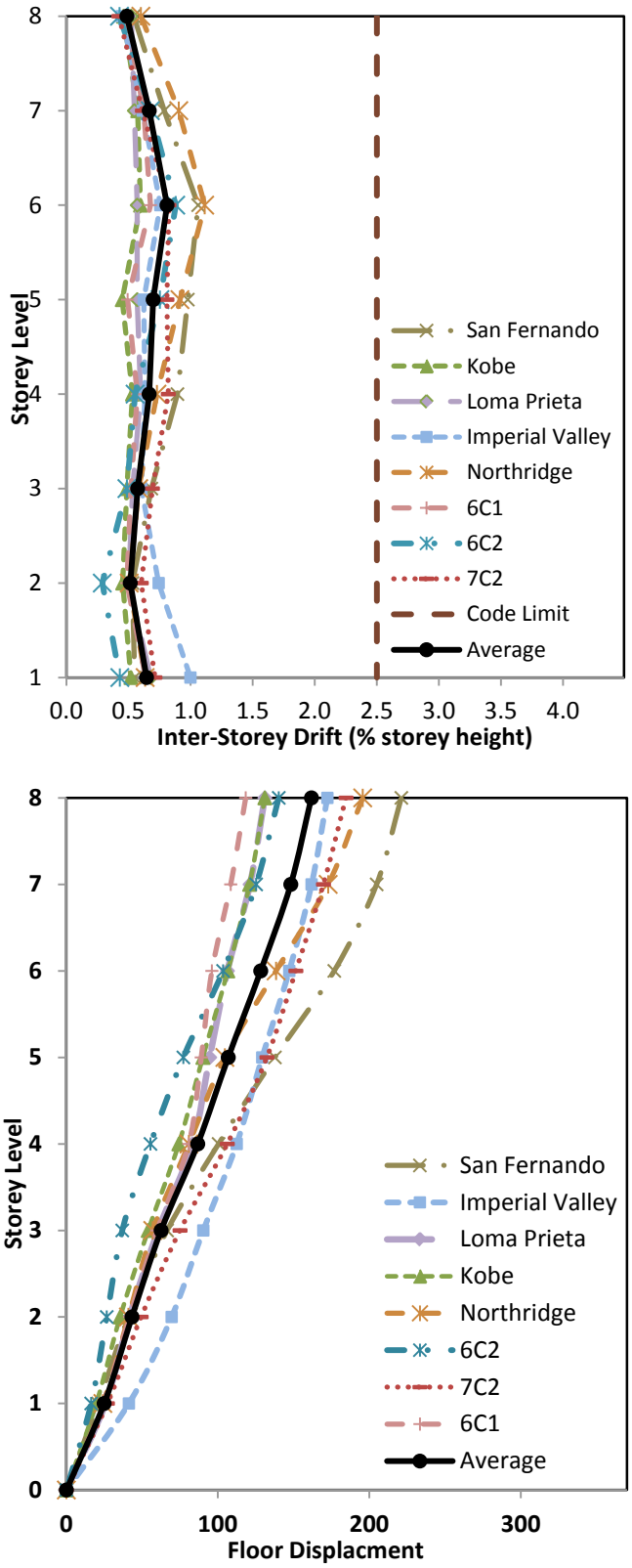

Figure 4.10. Inter-storey Drift and Floor Displacement for 8-storey EBF

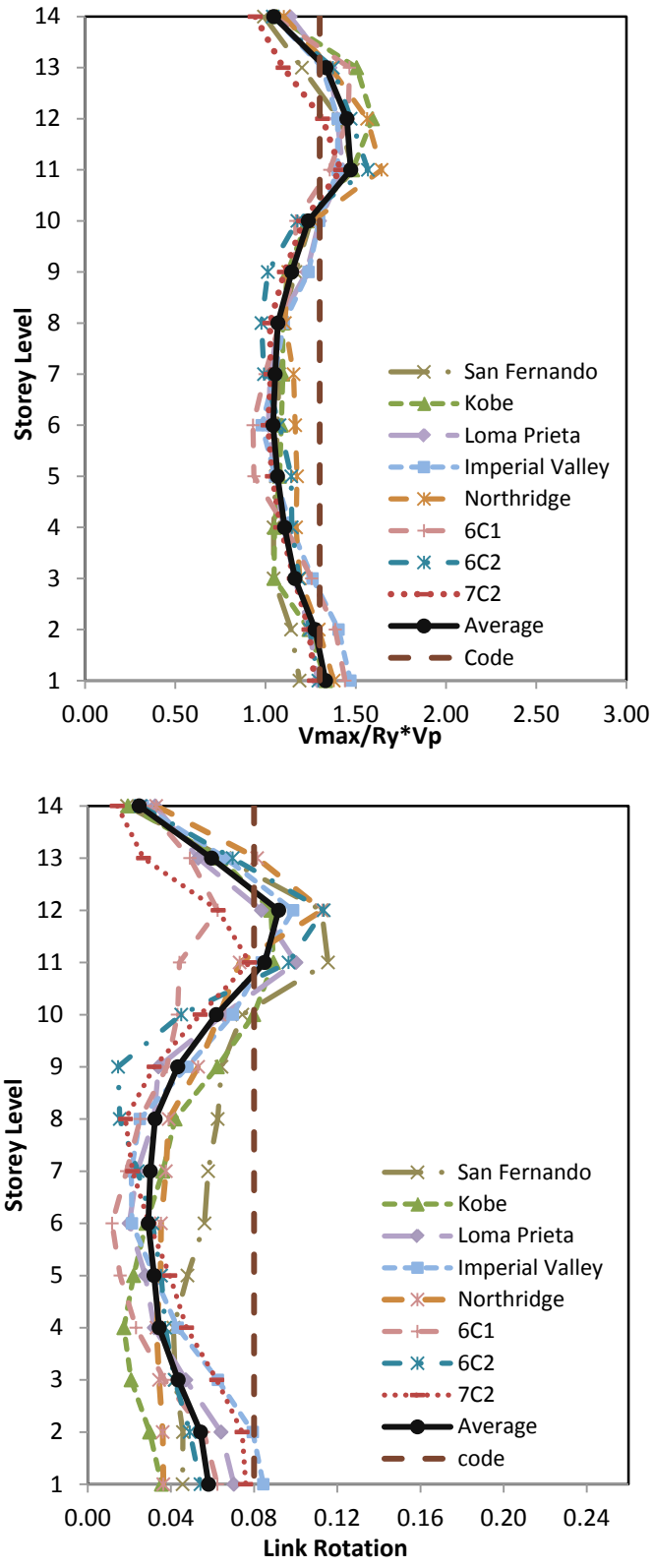

Figure 4.11. Normalized Maximum Link Shear Forces and Link Rotations for 14-storey EBF

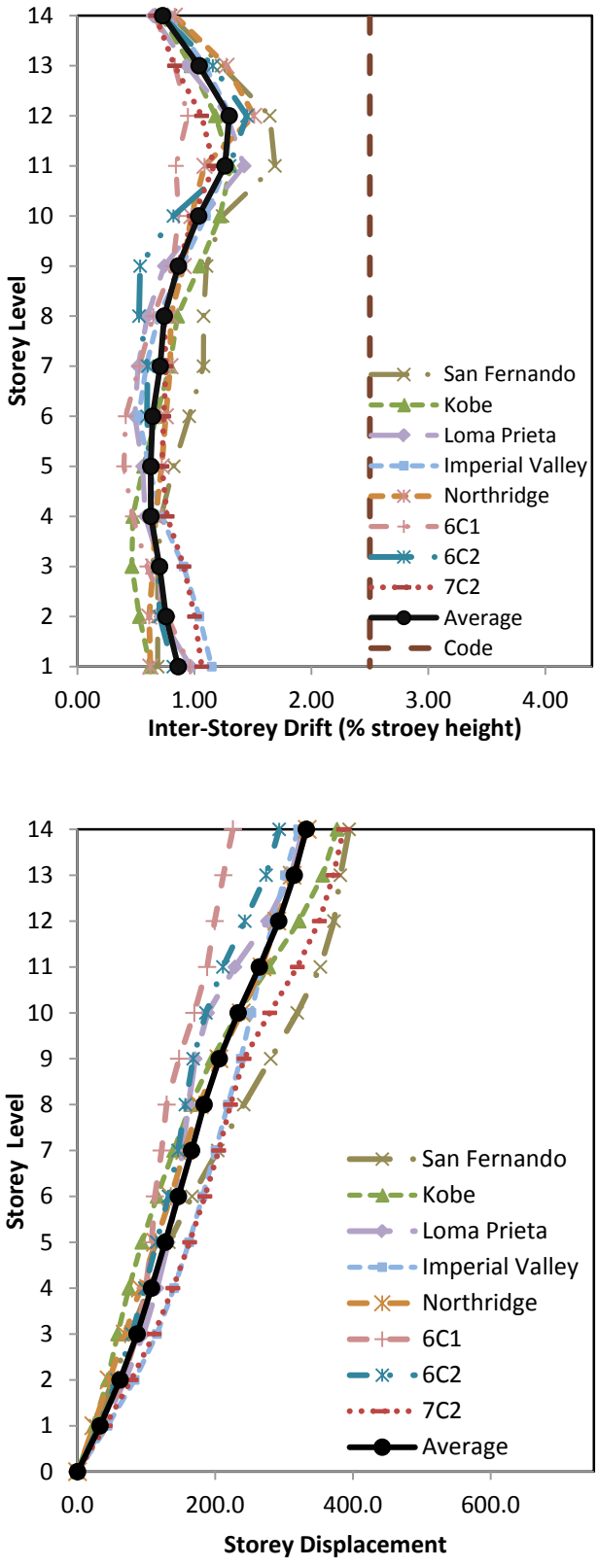

Figure 4.12. Inter-storey Drift and Floor Displacement for 14-storey EBF

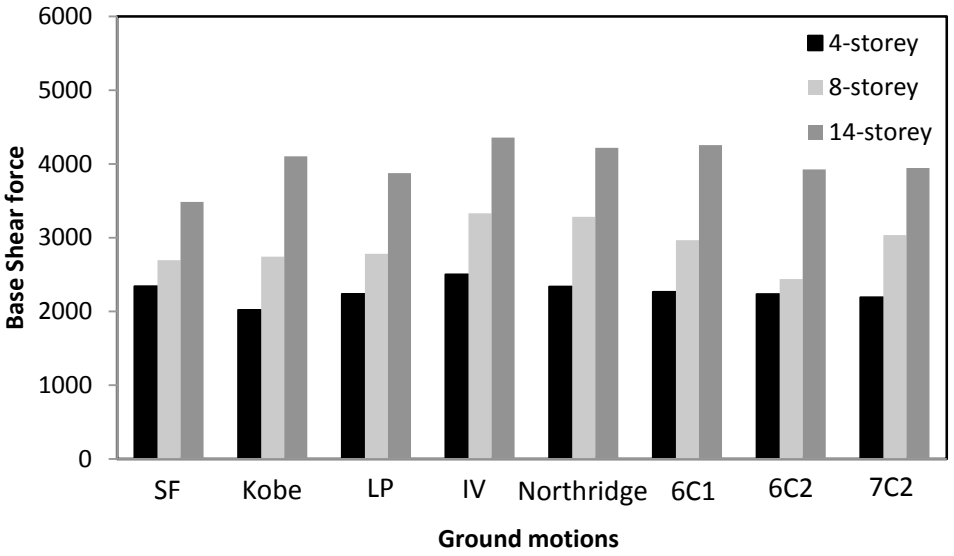

Figure 4.13. Dynamic Base shear forces for 8 Earthquake records

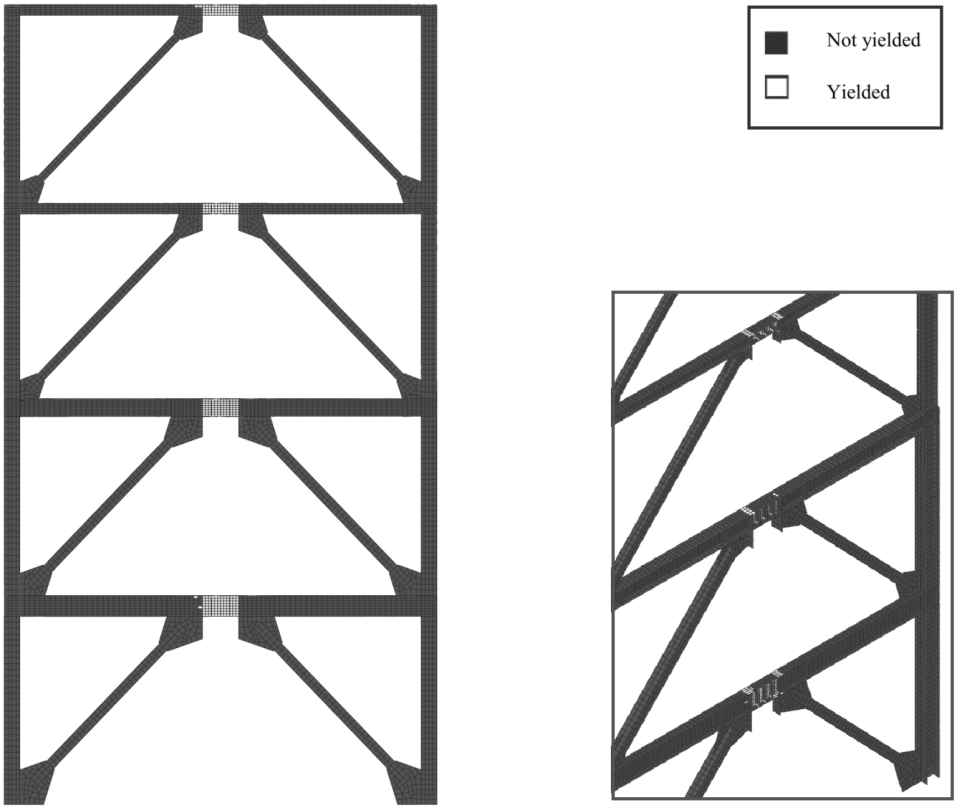

Figure 4.14. a) Yield pattern for 4-storey at the time most links are yielded, b) Yield pattern for 14-storey at the time maximum base shear occurred

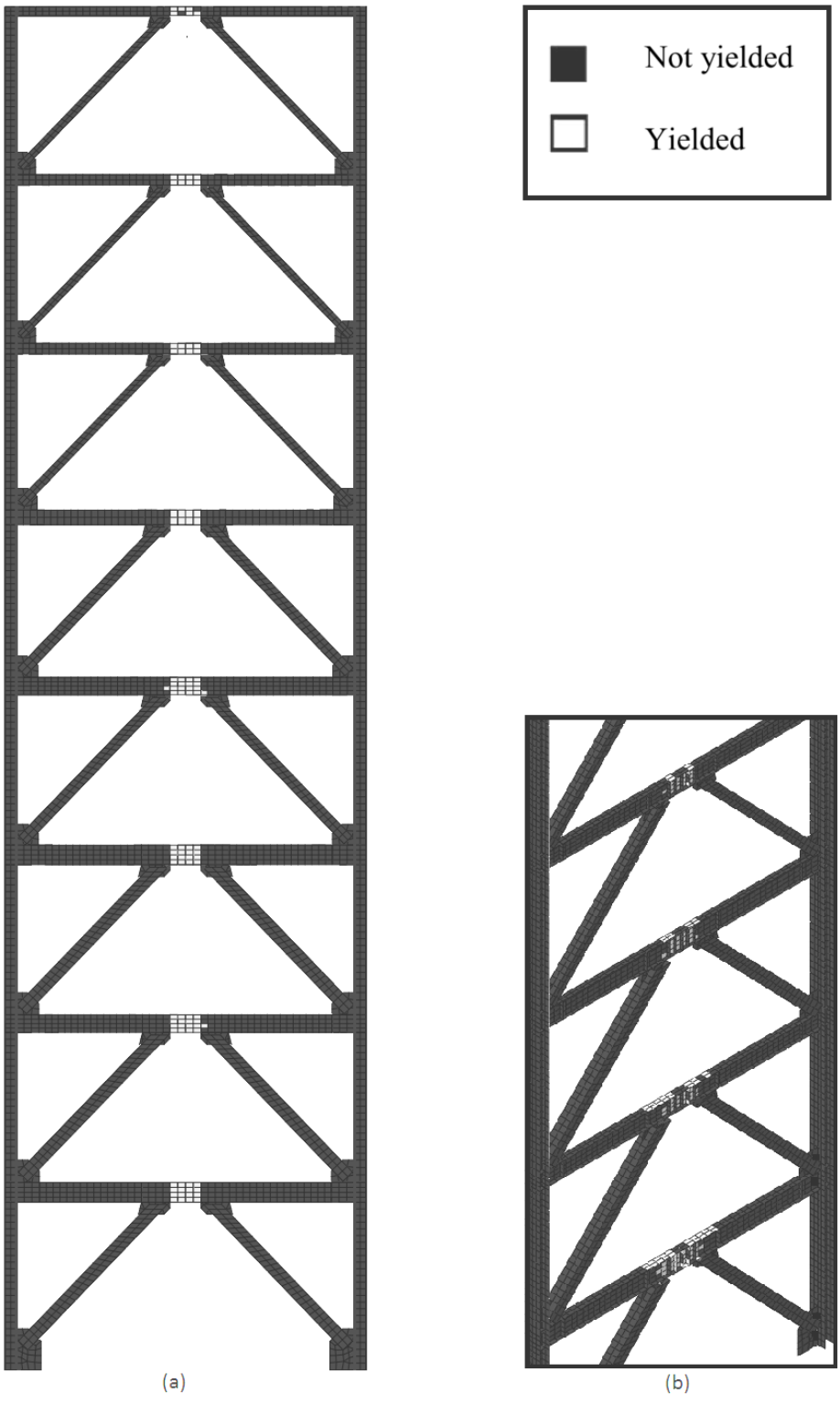

Figure 4.15. a) Yield pattern for 8-storey at the time most links are yielded, b) Yield pattern for 14-storey at the time maximum base shear occurred

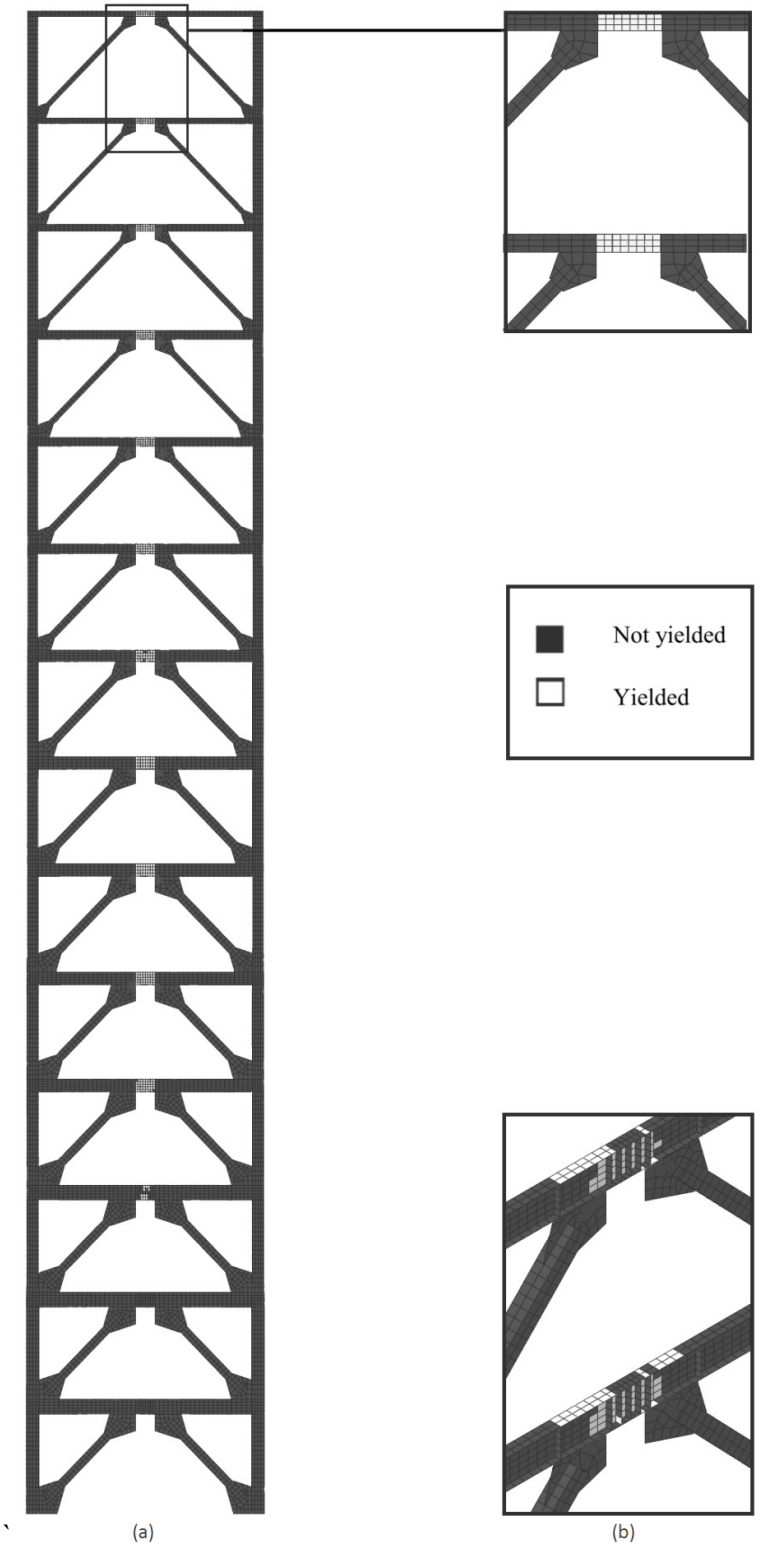

Figure 4.16. a) Yield pattern for 14-storey at the time most links are yielded, b) Yield pattern for 14-storey at the time maximum base shear occurred

4.4. Summary

In this chapter, the results of nonlinear dynamic analyses of three EBFs with 4-, 8- and 14 storeys modeled in ABAQUS were presented. The seismic responses were demonstrated in terms of link rotations, shear link overstrength and the inter-storey drifts. Also, the yielding sequence of three designed EBFs was studied. It showed that the EBFs didn't lose their load carrying capacity when all the links were yielded. After yielding of all the links, the outer beam participated in carrying the load as it was considered in the design. In general, the EBF behavior was found satisfactory. All the links showed the inelastic behavior and other member remained in their elastic state as it was assumed in the design.

For the maximum link rotation, 4 and 8 storey EBFs showed the average rotations under the code limit of 0.08 rad. However, for 14 storey structure, in the levels 11 and 12, the magnitude of median link rotations went beyond the code limit. Also a concentration of link rotation was observed at the first floor of 8 and 14 storeys but they are under the limit. For all EBFs, ratios of shear forces in the links to probable shear strength were higher than the limit of 1.3 in some floors, which is still under the values presented by some experimental studies. The limit of 1.3 presented by CSA S16-09 accounts for strain hardening developed in the links. The experimental results showed that the link overstrength is mainly due to strain hardening; however, the shear resistance of the flanges may also increase the link overstrength. The inter-storey drift results show the values 50 to 70% lower than the limit of $0.025\,h_s$ presented by NBCC 2010. It was observed that all the designed EBFs met the code inter-storey drift limit.

For all EBFs, maximum base reactions obtained from non-linear dynamic analysis were higher than the design base shear. This primarily stems from the overstrength of the selected members

due to design considerations. The yielding pattern of EBFs under the Imperial Valley ground motion, which has the maximum peak acceleration and induces the largest shear force at the base of all frames, were also described. It showed most inelastic activities of the EBFS were confined to the shear link while the other members behaved elastically. Some minor yielding was also observed in the outer beam close to its connection to the link.

Chapter 5. Evaluation of Modal Pushover Method for Eccentrically Braced Frames

5.1. Introduction

The modal pushover analysis (MPA) is a pushover analysis procedure based on structural dynamics theory and consistent with the response spectrum analysis (RSA). In this chapter, first the structural dynamics theory underlying the modal pushover analysis is briefly discussed. Then, the steps for implementing the modal pushover method are explained in detail. Finally, the application of modal pushover analysis on EBFs is investigated by applying MPA on three selected EBFs (low, medium and high-rise) through comparing the different response quantities of MPA with the results of nonlinear time history analysis (NLTHA).

5.2. Modal Pushover Analysis

The governing equation of motion of a multi-storey structure subjected to horizontal ground motion $\ddot{u}_g(t)$ can be expressed by equation 5.1.

$$m\ddot{u} + c\dot{u} + ku = -m\iota\ddot{u}_g(t) = P_{eff}(t) \qquad 5.1$$

Where the vector u represents n lateral floor displacements relative to ground, the matrices m, c, k are the mass, damping and lateral stiffness matrices of the system, the vector ι represents the displacements of masses resulting from static application of a unit ground displacement, $P_{eff}(t)$ is the effective lateral earthquake force. The spatial distribution of $P_{eff}(t)$ over the height of the building is defined by the vector $s = m\iota$ which can be expanded as a summation of modal inertia force distribution $\mathbf{s}_n$.

$$m\iota = \sum_{n=1}^{N} s_n = \sum_{n=1}^{N} \Gamma_n m\phi_n \qquad 5.2$$

where ϕ_n is the n^{th} natural vibration mode of the structure and Γ_n is modal participation factor which can be calculated using equations below:

$$\Gamma_n = \frac{L_n}{M_n}, \quad L_n = \phi_n^T m\iota, \quad M_n = \phi_n^T m\phi_n; \qquad 5.3$$

The free vibration of an undamped system in one of its natural vibration mode (r^{th} mode) can be expressed as:

$$u_r(t) = \phi_r q_r(t) \qquad 5.4$$

Considering equation 5.4 and5.2, equation 5.1 can be written for the r^{th} mode as:

$$m\phi_r \ddot{q}_r(t) + c\phi_r \dot{q}_r(t) + k\phi_r q_r(t) = -\Gamma_r m\phi_r \ddot{u}_g(t) \qquad 5.5$$

Using the orthogonality of the modes presented in equation 5.6, it can be shown that only the n^{th} mode contributes to the response.

$$\begin{gathered} \phi_n^T m\phi_r = 0, \quad \phi_n^T k\phi_r = 0, \quad \phi_n^T c\phi_r = 0 \\ \phi_n^T m\phi_n = M_n, \quad \phi_n^T k\phi_n = K_n, \quad \phi_n^T c\phi_n = C_n \end{gathered} \qquad 5.6$$

To show this, both sides of the equation 5.5 are multiplied by ϕ_n^T, resulting in the equation 5.7 in which just the n^{th} mode gives the non-zero terms.

$$M_n \ddot{q}_n(t) + C_n \dot{q}_n(t) + K_n q_n(t) = -M_n \Gamma_n \ddot{u}_g(t) \qquad 5.7$$

Dividing both sides by M_n gives:

$$\ddot{q}_n(t) + 2\xi_n\omega_n\dot{q}_n(t) + \omega_n^2 q_n(t) = -\Gamma_n\ddot{u}_g(t) \qquad 5.8$$

where ω_n is the natural vibration frequency and ξ_n is the damping of n^{th} mode.

The equation of motion of the nth-mode elastic SDOF system is:

$$\ddot{D}_n + 2\xi_n\omega_n\dot{D}_n + \omega_n^2 D_n = -\ddot{u}_g(t) \qquad 5.9$$

Therefore, $q_n(t)$ can be formulated by comparing equations 5.8 and 5.9.

$$q_n(t) = \Gamma_n D_n(t) \qquad 5.10$$

Utilizing equation 5.10, equation 5.4 can be rewritten for the n^{th} mode as:

$$u_n(t) = \Gamma_n\phi_n D_n(t) \qquad 5.11$$

For an inelastic multi-storey structure, the relations between lateral forces f_s and lateral displacements u depend on the history of the displacement. Thus, the equation of motion 5.1 changes into equation 5.12 for inelastic systems.

$$m\ddot{u} + c\dot{u} + f_s(u, \text{sign}\dot{u}) = m\iota\ddot{u}_g(t) = P_{eff}(t) \qquad 5.12$$

Employing the modal orthogonality, equation 5.12 changes into equation 5.13.

$$\ddot{q}_n(t) + 2\xi_n\omega_n\dot{q}_n(t) + \frac{F_{sn}}{M_n} = -\Gamma_n\ddot{u}_g(t) \qquad 5.13$$

Also, the equation of motion of the nth-mode inelastic SDOF system is:

$$\ddot{D}_n + 2\xi_n \omega_n \dot{D}_n + \frac{F_{sn}}{L_n} = -\ddot{u}_g(t) \qquad 5.14$$

Solving equation 5.14 gives the deformation of the inelastic SDOF system corresponding to the n^{th} mode. Using the peak value of $D_n(t)$, the maximum roof displacement (u_{rno}) of MDOF system related to the n^{th} mode can be found by equation 5.11 . To implement a pushover analysis consistent with the response spectrum analysis, the structure is pushed under the lateral forces S_n^* to reach u_{rno}. All response parameters of interest can be found using u_{rno} for each mode and they can be combined with any desired modal combination rule to give the total responses.

$$S_n^* = m\phi_n \qquad 5.15$$

The equations explained above are the underlying equations forming MPA procedure to find the responses of MDOF system from the equivalent SDOF systems using the following steps (Chopra and Goel 2001):

1. Determine the natural frequencies, and the modal vectors.
2. Perform pushover analysis on the multistory structure subjected to the force distribution $S_n^* = m\phi_n$ and idealize the obtained pushover curves.
3. Transform the idealized pushover curve of the MDOF system to the F_{sn}/L_n-D_n curve of the nth mode SDOF system.

$$\frac{F_{sny}}{L_n} = \frac{V_{bny}}{M_n^*}, \quad D_{ny} = \frac{u_{rny}}{\Gamma_n \phi_{rn}} \qquad 5.16$$
$$M_n^* = L_n \times \Gamma_n,\ L_n = \varphi_n^T m \iota,\ \Gamma_n = L_n / M_n$$

4. The elastic vibration period is

$$T_n = 2\pi\left(\frac{L_n D_{ny}}{F_{sny}}\right)^{1/2} \qquad 5.17$$

5. Determine the maximum deformation D_n of the SDOF system.

Knowing the period of the SDOF system and the damping ratio ξ_n, the equation of motion 5.18 can be solved with any applicable numerical method to find the peak deformation of SDOF system.

$$\ddot{D}_n + 2\xi_n\omega_n\dot{D}_n + \frac{F_{sn}}{L_n} = -\ddot{u}_g(t) \qquad 5.18$$

where F_{sn}/L_n relation is defined in Figure 4.13.

As indicated in Figure 4.13-right, the initial slope of the idealized curve is ω_n^2, and second slope is equal to $\alpha_n\omega_n^2$, where α_n can be found from equation 5.22.

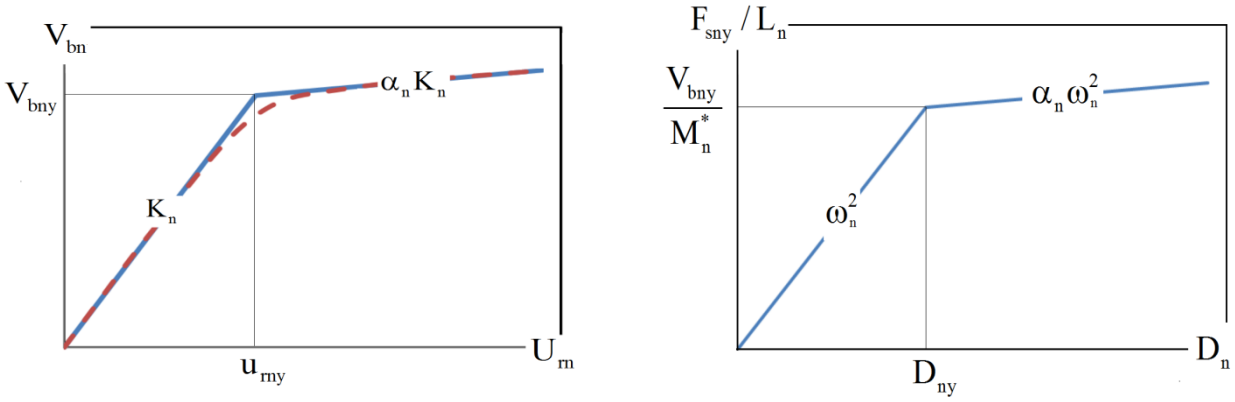

Figure 5.1. Idealized pushover curve of MDOF, and properties of nth-mode inelastic SDOF system

6. Obtain the peak roof displacement u_{rno} corresponding to Peak deformation D_n

$$u_{rno} = \Gamma_n\phi_{rn}D_n \qquad 5.19$$

7. Find other responses of interest from pushover curve using the maximum displacement of the roof obtained in step 5.

8. Estimate total responses by a preferred combination rule. SRSS rule was used in this paper.

$$u_{rno} = \sqrt{\sum_{n=1}^{N} u_{rno}^2} \ , \qquad r_o = \sqrt{\sum_{n=1}^{N} r_{no}^2} \qquad 5.20$$

5.3. Application of Modal Pushover Analysis for EBFs

In order to evaluate the capability of MPA procedure on predicting seismic demands of EBFs, the procedure discussed above was implemented on the three designed EBFs with 4, 8 and 14 storeys. From the eight scaled ground motions employed for non-linear time history analyses in the chapter 4, four earthquake records, consisting of two real and two simulated, were selected arbitrarily for implementing the MPA analysis. The earthquake records include Imperial Valley, Loma Prieta, 6C1 and 6C2. The results were compared with the average responses of interest obtained from non-linear time history analyses under the same four earthquakes. In the following, performing the MPA procedure on the three designed EBFs is explained in detail.

The MPA procedure starts with finding the natural frequencies and the modal vectors of the system. Thus, the frequency analyses were conducted for the three selected EBFs in ABAQUS, through which the modal properties (Table 3.3) and the mode shapes (Figure 5.2) were recognized for the three frames. The number of modes was determined based on the summation of their participating masses which must be larger than 90% of the total effective mass of the building. Based on that the first 3 fundamental modes were found sufficient to be used in MPA.

Table 5.1 Modal periods of three EBFs

Frames	**4-Storey EBF**			**8-Storey EBF**			**14-Storey EBF**		
Modes	**Mode 1**	**Mode 2**	**Mode 3**	**Mode 1**	**Mode 2**	**Mode 3**	**Mode 1**	**Mode 2**	**Mode 3**
Period (sec)	0.98	0.431	0.31	1.80	0.66	0.40	3.33	1.15	0.64

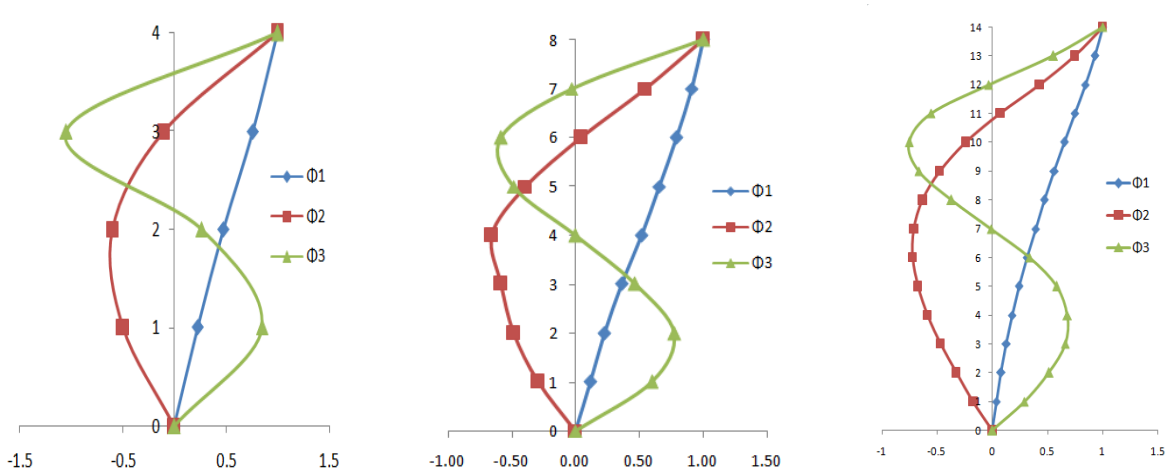

Figure 5.2. Mode shapes of 4, 8, and 14 Storey EBF

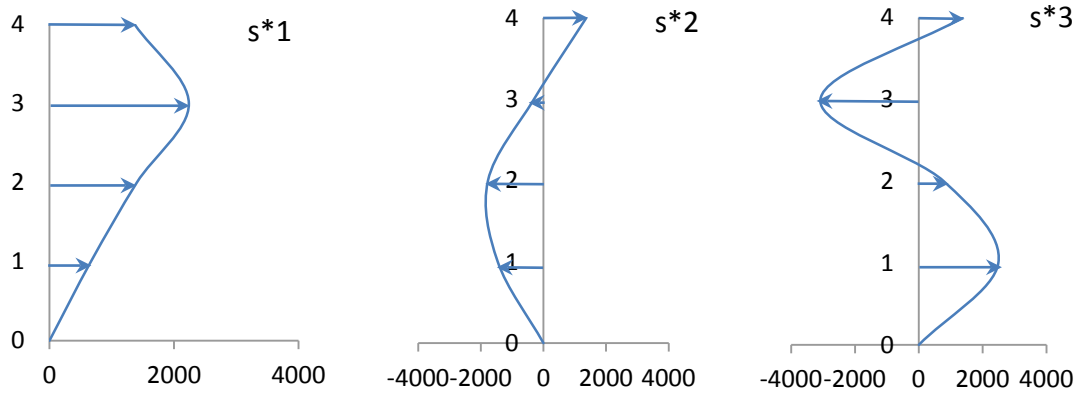

Figure 5.3. 4- Storey Force Distribution $S_n^* = m\phi_n$

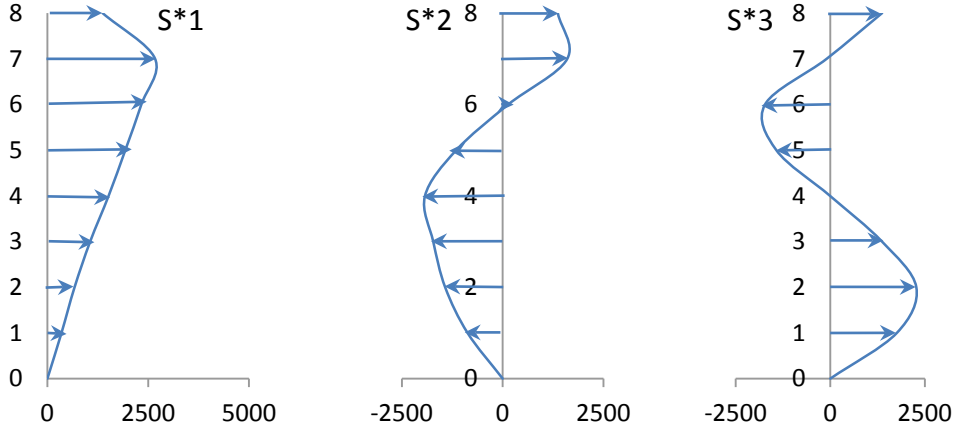

Figure 5.4. 8-Storey Force Distribution $S_n^* = m\phi_n$

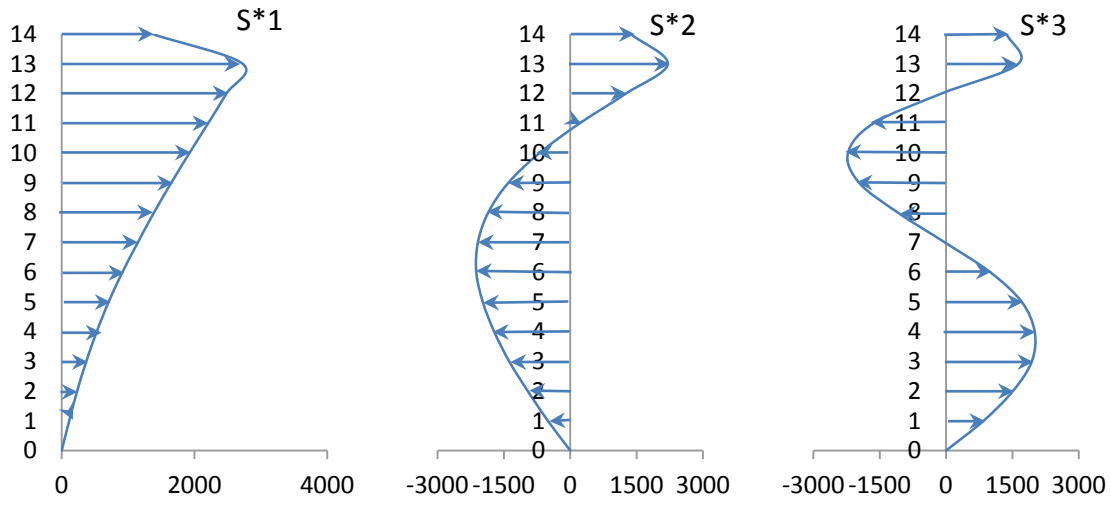

Figure 5.5. 14-Storey Force Distribution $S_n^* = m\phi_n$

The EBFs were pushed by the force distribution S_n^* to obtain the pushover curves corresponding to each mode. Multiplying the modal vectors of each mode (Figure 5.2) by the mass of each floor gives the force distribution S_n^* (Figure 5.3-Figure 5.5), which was applied increasingly to each structure to provide the pushover curves $V_{bn} - U_{rn}$ of each mode. The gravity loads were considered in the pushover analyses. The resulting pushover curves were idealized to present a bilinear curve using the following procedure (FEMA-273) using determined target roof displacement U_{rno} and the corresponding base shear V_{bno} .

1. The yield base shear V_{bny} was selected based on judging the actual pushover curve. Then it was changed iteratively to make the area under idealized and actual curve equal.
2. The slope of the elastic part of the curve was obtained by calculating slope of a line between the origin and a point on the actual pushover curve with the base shear equal to $0.6 * V_{bny}$.

3. Knowing the initial slope and the yield base shear, the yield displacement can be calculated.

$$u_{rny} = \frac{V_{bny}}{K_n} \qquad 5.21$$

4. The area under the actual pushover curve was calculated by trapezoidal rule. The area under the idealized bilinear curve was also calculated. The iterative procedure was repeated to make the difference between two areas as small as possible.

5. The strain-hardening ratio was determined by

$$\alpha_n = \left(\left(\frac{V_{bno}}{V_{bny}}\right) - 1\right) / \left(\left(\frac{u_{rno}}{u_{bny}}\right) - 1\right) \qquad 5.22$$

The actual and idealized pushover curves for three modes of the three EBFs are presented in Figure 5.12 to Figure 5.8.

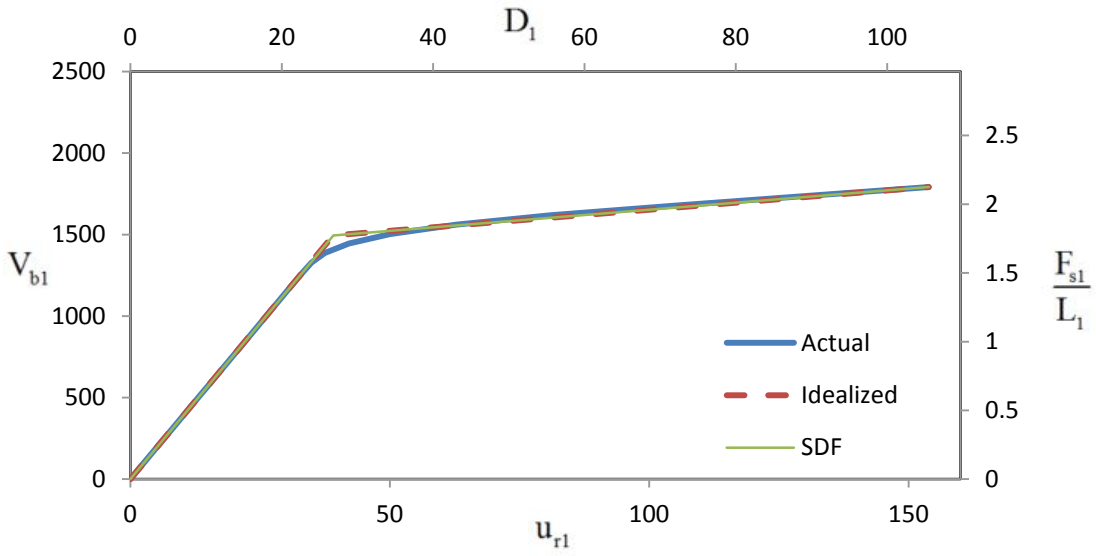

Figure 5.6. 4-Storey Mode 1, Actual, Idealized ($V_{b1} - U_{r1}$) and SDOF ($F_{s1} / L_1 - D_1$) Pushover Curves

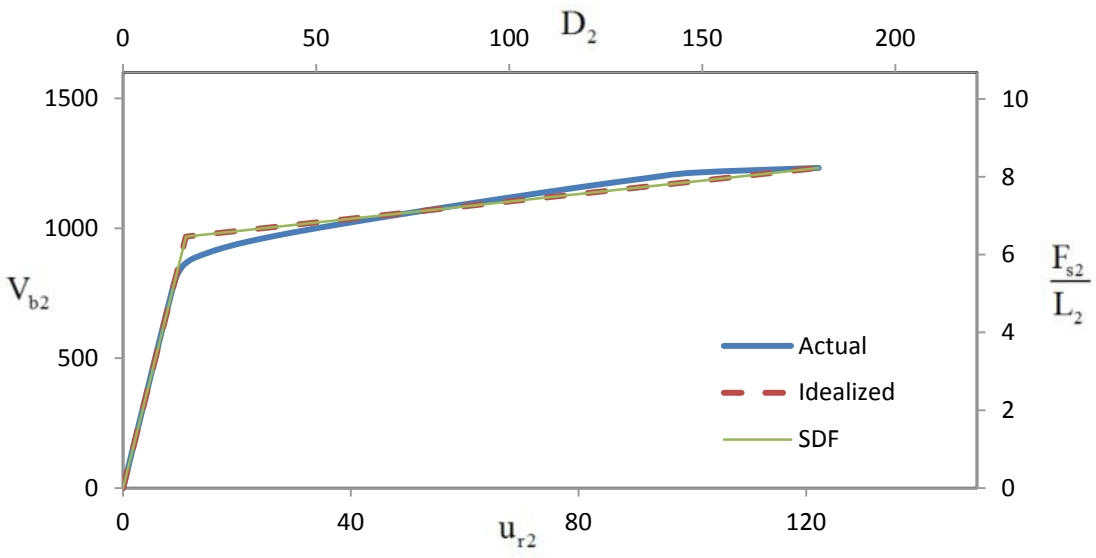

Figure 5.7. 4-Storey Mode 2, Actual, Idealized ($V_{b2} - U_{r2}$) and SDOF ($F_{s2} / L_2 - D_2$) Pushover Curves

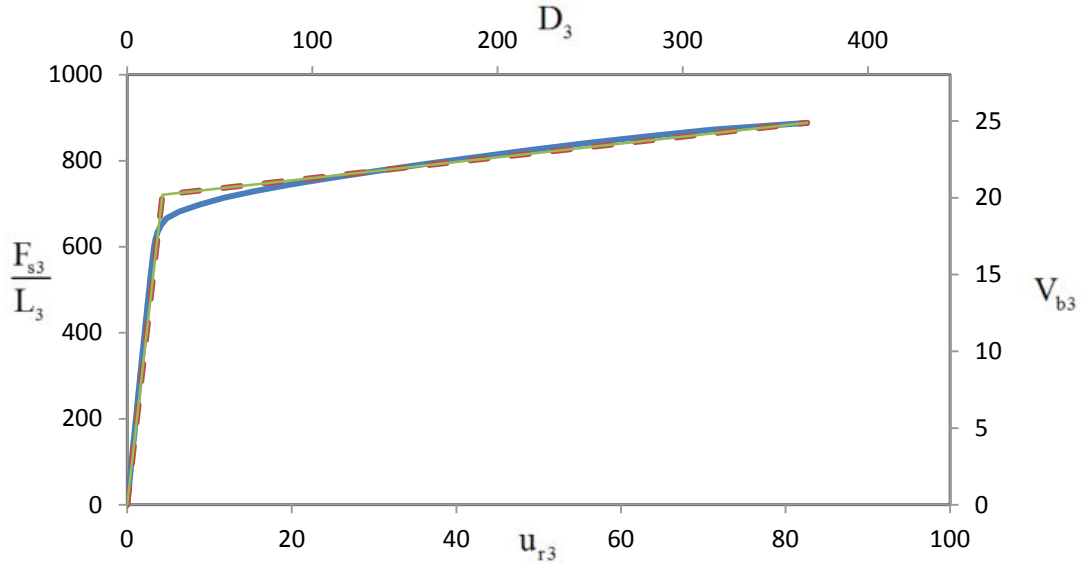

Figure 5.8. 4-Storey Mode 3, Actual, Idealized ($V_{b3} - U_{r3}$) and SDOF ($F_{s3} / L_3 - D_3$) Pushover Curves

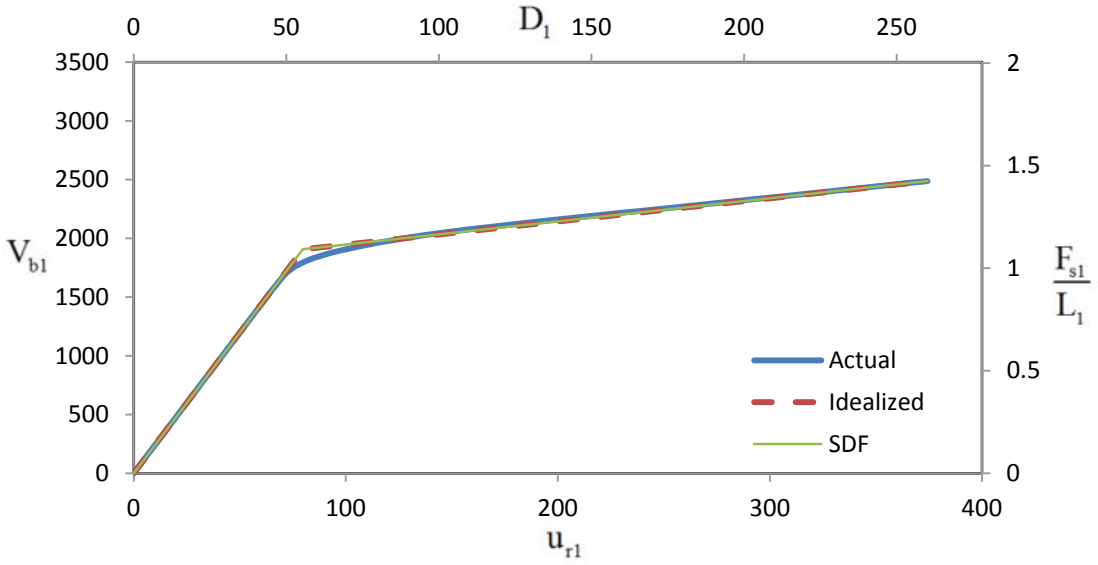

Figure 5.9. 8-Storey Mode 1, Actual, Idealized ($V_{b1} - U_{r1}$) and SDOF ($F_{s1} / L_1 - D_1$) Pushover Curves

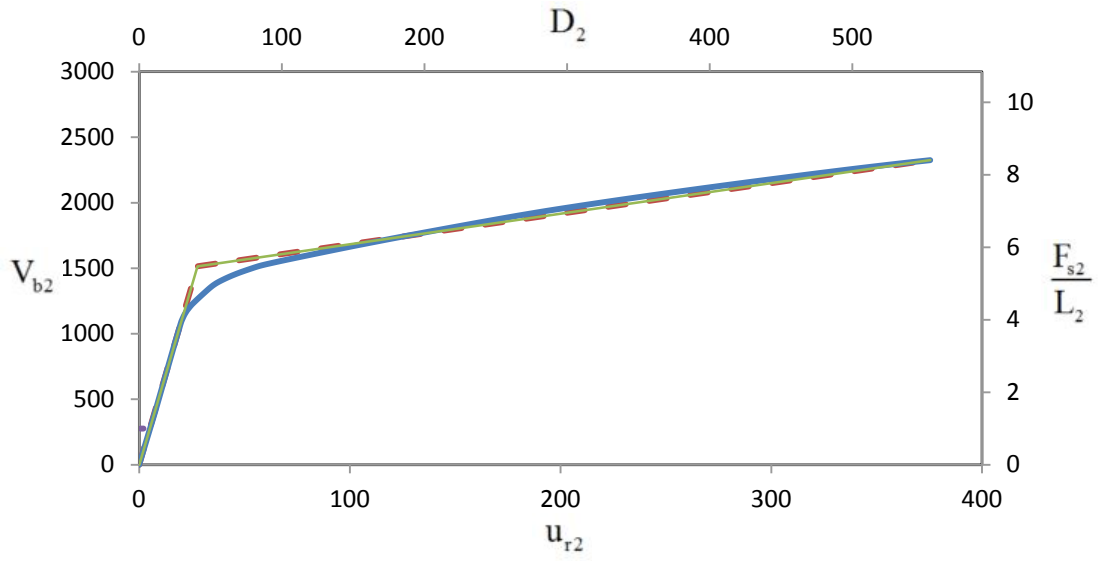

Figure 5.10. 8-Storey Mode 2, Actual, Idealized ($V_{b2} - U_{r2}$) and SDOF ($F_{s2} / L_2 - D_2$) Pushover Curves

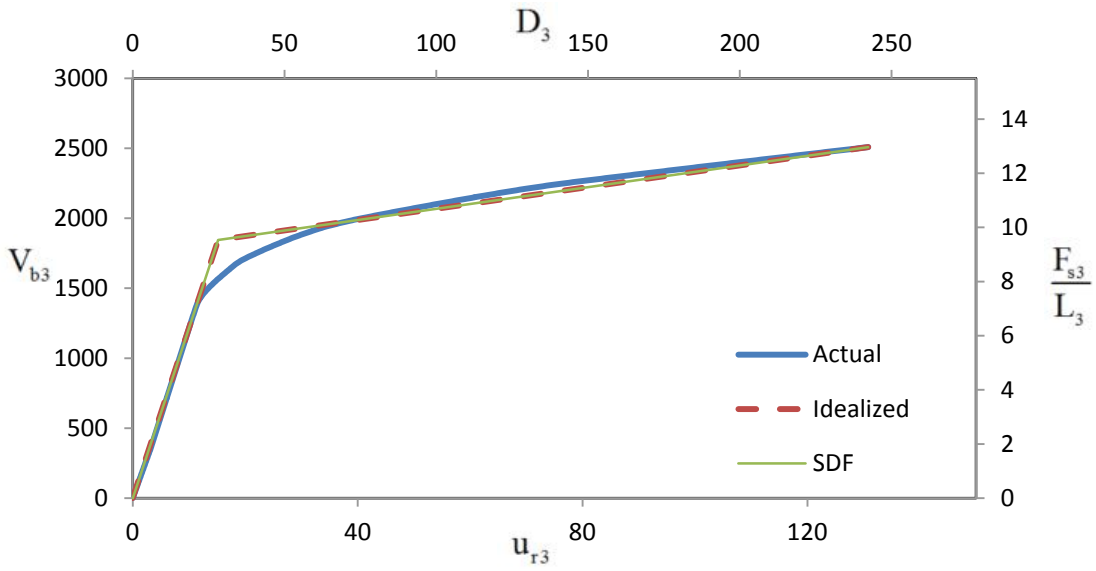

Figure 5.11. 8-Storey Mode 3, Actual, Idealized ($V_{b3} - U_{r3}$) and SDOF ($F_{s3} / L_3 - D_3$) Pushover Curves

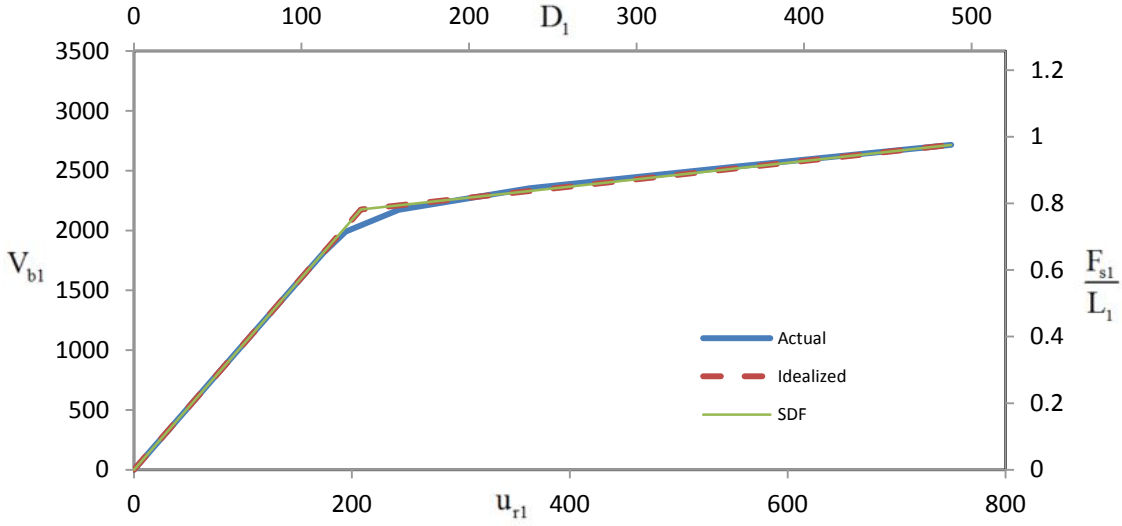

Figure 5.12. 14-Storey Mode 1, Actual, Idealized ($V_{b1} - U_{r1}$) and SDOF ($F_{s1} / L_1 - D_1$) Pushover Curves

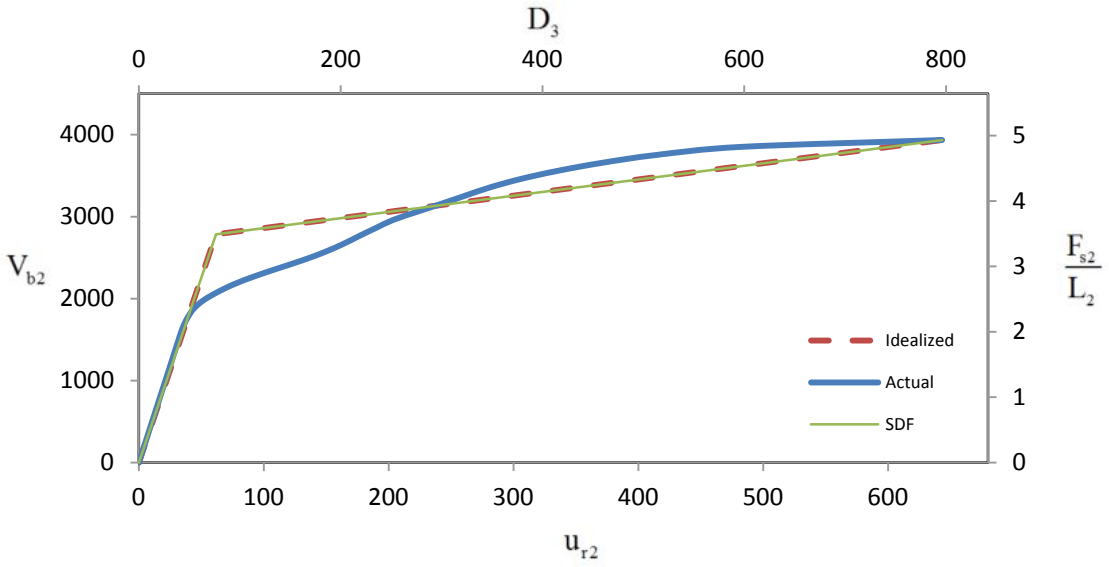

Figure 5.13. 14-Storey Mode 2, Actual, Idealized ($V_{b2} - U_{r2}$) and SDOF ($F_{s2} / L_2 - D_2$) Pushover Curves

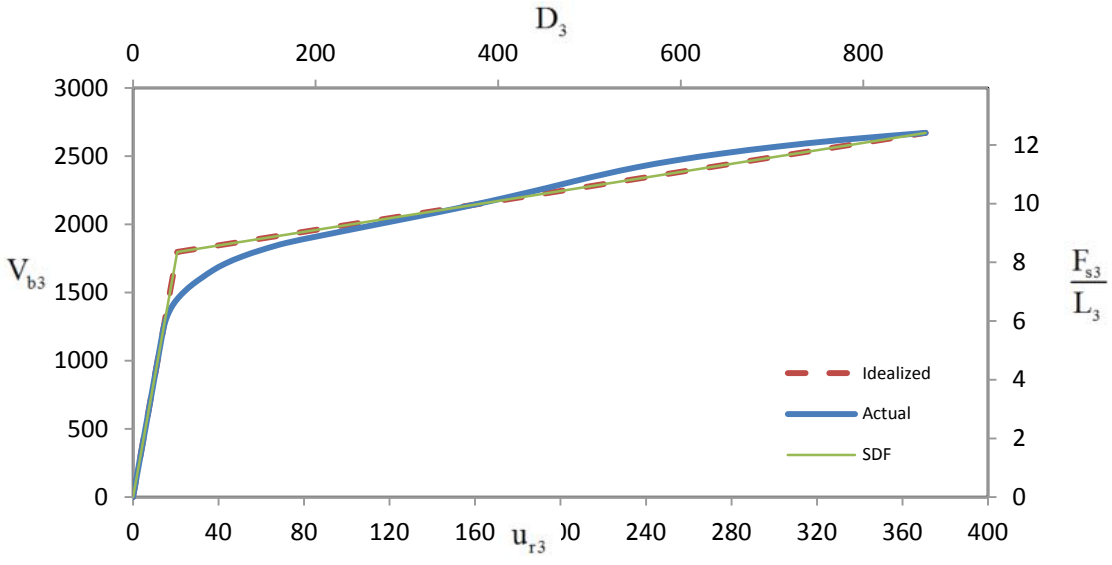

Figure 5.14. 14-Storey Mode 3, Actual, Idealized ($V_{b3} - U_{r3}$) and SDOF ($F_{s3} / L_3 - D_3$) Pushover Curves

The idealized pushover curves of the MDOF systems were used to find the relation between force F_{sn} and deformation D_n. To do this the points $\left(D_{ny}, \frac{F_{sny}}{L_n}\right)$ and $\left(D_{no}, \frac{F_{sno}}{L_n}\right)$ were determined using equation 5.16. The elastic vibration period was obtained by equation 5.17. The properties of SDOF systems corresponding to each EBF are presented in Table 5.2.

Table 5.2 Structural Properties of Equivalent SDOF System

Frames	**Mode**	$\mathbf{L_n}$ (kg)	$\mathbf{\Gamma_n}$	$\mathbf{M_n^*}$ (kg)	$\mathbf{F_{sny}/L_n}$ (m/s2)	$\mathbf{D_{ny}}$ (mm)	$\mathbf{F_{sno}/L_n}$ (m/s2)	$\mathbf{D_{no}}$ (mm)	$\mathbf{T_n}$ (sec)
4 Storey EBF	1	578134.8	1.46	843359.71	1.77	26.81	2.13	105.49	0.77
	2	-20824.6	-0.68	149787.31	6.46	16.27	8.23	180.14	0.32
	3	158640.8	0.22	35701.49	20.195	19.02	24.88	367.19	0.19
8 Storey EBF	1	1213613.1	1.44	1746314.9	1.092	55.40	1.42	260.09	1.42
	2	-408681.7	-0.68	276649.9	5.476	40.89	8.41	554.56	0.543
	3	358373.14	0.54	193474.63	9.536	28.14	12.97	242.29	0.341
14 Storey EBF	1	1810436.8	1.54	2783860.2	0.782	135.48	0.98	487.79	2.62
	2	987363.77	-0.80	797724.26	3.491	76.339	4.93	796.19	0.93
	3	503985.4	0.427	215241.40	8.595	35.71	11.65	306.28	0.405

Knowing $F_{sn}/L_n - D_n$ relation, the equation of motion of the nth-mode inelastic SDOF system (equation 5.18) can be solved by any numerical method to determine the peak elastic response. Then, the peak roof displacement of each EBF was calculated using equation 5.19. Applying SRSS rule, the peak modal responses were combined to obtain the total response of interests using equation 5.20. In this research, the displacement at each floor and the inter-storey drifts were obtained and compared with the results of NLTHA.

5.4. Evaluation of MPA procedure

The applicability of MPA procedure on EBFs was evaluated by comparing the floor displacements and inter-storey drifts and the base shear obtained from MPA and NLTHA procedures performed on 4, 8, and 14-storey EBFs. Table 5.3 to Table 5.8 present the average peak floor displacements and inter-storey drifts for four selected earthquake records for modal pushover method. The corresponding responses obtained by NLTHA procedure are also presented for comparison. These results are also illustrated in Figure 5.15 to Figure 5.20.

As it can be observed in the Figure 5.15, for 4-storey EBF, the fourth floor displacement was predicted well with the MPA procedure with just a few percent errors with respect to the displacement obtained from non-linear seismic analysis. However, higher differences were detected at the intermediate floors. Figure 5.18 shows the inter-storey drift of 4-storey EBF. The results showed that, the inter-storey drift of the third floor was well predicted with considering the first mode response with just 1 percent error from NLTHA. The inter-storey drift of other floors showed higher differences with respect to NLTHA results. The results of both displacements and inter-storey drifts showed that considering the first mode is enough in predicting seismic responses of low-rise (4-storey) EBF; and adding the higher modes did not increase the accuracy of the results considerably.

For 8-storey EBF, Figure 5.16 indicates that the first mode predicted the displacements of the lower floors very well, adding the second mode increased the accuracy of the displacement responses at the top stories from 5% error to 1% error. However, including the third mode raised the differences at first and second floors by 6 to 7%, while decreased the errors in the other floors. For inter-storey drift, the positive effect of adding the responses of the second mode is

more apparent as it is shown in Figure 5.19. Including the inter-storey drift related to the second mode could improve the accuracy of the results by a maximum of 20% for the top floor. No considerable improvement was observed by including the third mode responses.

For 14-storey EBF, as it can be seen in the Figure 5.17, the highest differences from NLTHA displacements were found at the intermediate floors, and the top two floors. These differences were reduced by about five times by considering the second mode responses. Including the third mode improved the results by just a few percent. For inter-story drift, the difference between MPA and NLTHA results are more significant in 14-storey EBF as it is shown in Figure 5.20. Adding the inter-storey drifts corresponding to the second mode improved the modal pushover results greatly.

Table 5.3 Comparison of MPA and NLTHA peak values of floor displacements for 4-Storey EBF

Floor	Modal Response			Modal Combination			NLTHA	Percentage Error (%)		
	Mode 1	Mode 2	Mode 3	1 Mode	2 Modes	3 Modes		1 Mode	2 Modes	3 Modes
1	18.783	-5.888	1.515	18.783	19.684	19.743	24.170	-22.29	-18.56	-18.32
2	39.596	-7.141	0.475	39.596	40.235	40.238	49.361	-19.78	-18.49	-18.48
3	63.216	-1.217	-1.876	63.216	63.228	63.255	72.717	-13.07	-13.05	-13.01
4	83.117	11.852	1.790	83.117	83.957	83.976	86.560	-3.98	-3.01	-2.99

Table 5.4 Comparison of MPA and NLTHA peak values of floor displacements for 8-Storey EBF

Floor	Modal Response			Modal Combination			NLTHA	Percentage Error (%)		
	Mode 1	Mode 2	Mode 3	1 Mode	2 Modes	3 Modes		1 Mode	2 Modes	3 Modes
1	16.00	-10.05	6.00	16.00	18.90	19.83	17.841	-10.29	5.94	11.16
2	30.86	-16.48	7.76	30.86	34.98	35.83	32.467	-4.95	7.75	10.37
3	48.58	-19.89	4.66	48.58	52.49	52.70	48.959	-0.78	7.22	7.64
4	69.54	-22.27	-0.02	69.54	73.02	73.02	69.521	0.03	5.04	5.04
5	88.49	-13.37	-4.87	88.49	89.49	89.62	90.718	-2.46	-1.35	-1.21
6	106.74	1.50	-5.89	106.74	106.75	106.92	112.110	-4.79	-4.78	-4.63
7	122.31	18.46	-0.32	122.31	123.70	123.70	128.634	-4.91	-3.84	-3.84
8	134.68	33.96	10.05	134.68	138.90	139.26	140.464	-4.11	-1.11	-0.85

Table 5.5 Comparison of MPA and NLTHA peak values of floor displacements for 14-Storey EBF

Floor	Modal Response			Modal Combination			NLTHA	Percentage Error (%)		
	Mode 1	Mode 2	Mode 3	1 Mode	2 Modes	3 Modes		1 Mode	2 Modes	3 Modes
1	10.46	-16.17	5.29	10.46	19.25	19.97	22.020	-52.51	-12.56	-9.31
2	21.54	-30.70	9.45	21.54	37.50	38.67	43.591	-50.58	-13.97	-11.28
3	34.31	-44.13	12.13	34.31	55.90	57.20	63.431	-45.91	-11.87	-9.82
4	48.86	-54.96	12.52	48.86	73.54	74.59	78.745	-37.96	-6.61	-5.27
5	65.48	-63.20	10.68	65.48	91.00	91.63	92.505	-29.22	-1.63	-0.95
6	84.66	-67.86	6.21	84.66	108.50	108.68	106.819	-20.74	1.57	1.74
7	106.13	-66.68	-0.20	106.13	125.34	125.34	123.342	-13.96	1.62	1.62
8	128.55	-59.25	-6.83	128.55	141.55	141.71	140.991	-8.82	0.40	0.51
9	152.58	-44.71	-12.29	152.58	159.00	159.47	162.514	-6.11	-2.16	-1.87
10	177.88	-22.30	-13.88	177.88	179.28	179.81	187.319	-5.04	-4.29	-4.01
11	203.91	6.74	-10.26	203.91	204.02	204.28	215.044	-5.18	-5.13	-5.01
12	229.40	40.11	-0.67	229.40	232.88	232.88	244.337	-6.11	-4.69	-4.69
13	252.21	70.27	10.19	252.21	261.81	262.01	271.413	-7.08	-3.54	-3.46
14	272.00	93.87	18.39	272.00	287.74	288.33	291.667	-6.74	-1.35	-1.14

Table 5.6 Comparison of MPA and NLTHA Inter-Storey Drift (% of floor height) for 4-Storey EBF

Floor	Modal Response			Modal Combination			NLTHA
	Mode 1	Mode 2	Mode 3	1 Mode	2 Modes	3 Modes	
1	0.494	-0.155	0.040	0.494	0.518	0.520	0.636
2	0.548	-0.033	-0.027	0.548	0.549	0.549	0.663
3	0.622	0.156	-0.062	0.622	0.641	0.644	0.615
4	0.524	0.344	0.096	0.524	0.627	0.634	0.364

Table 5.7 Comparison of MPA and NLTHA Inter-Storey Drift (% of floor height) for 8-Storey EBF

Floor	Modal Response			Modal Combination			NLTHA
	Mode 1	Mode 2	Mode 3	1 Mode	2 Modes	3 Modes	
1	0.421	-0.265	0.158	0.421	0.497	0.522	0.708
2	0.391	-0.169	0.046	0.391	0.426	0.428	0.505
3	0.466	-0.090	-0.082	0.466	0.475	0.482	0.536
4	0.552	-0.063	-0.123	0.552	0.555	0.569	0.589
5	0.499	0.234	-0.127	0.499	0.551	0.565	0.610
6	0.480	0.391	-0.027	0.480	0.620	0.620	0.721
7	0.410	0.446	0.146	0.410	0.606	0.623	0.615
8	0.326	0.408	0.273	0.326	0.522	0.589	0.469

Table 5.8 Comparison of MPA and NLTHA Inter-Storey Drift (% of floor height) for 14-Storey EBF

Floor	Modal Response			Modal Combination			NLTHA
	Mode 1	Mode 2	Mode 3	1 Mode	2 Modes	3 Modes	
1	0.275	-0.425	0.139	0.275	0.507	0.526	0.974
2	0.292	-0.382	0.109	0.292	0.481	0.493	0.806
3	0.336	-0.354	0.070	0.336	0.488	0.493	0.725
4	0.383	-0.285	0.010	0.383	0.477	0.477	0.599
5	0.437	-0.217	-0.048	0.437	0.488	0.491	0.545
6	0.505	-0.123	-0.118	0.505	0.520	0.533	0.504
7	0.565	0.031	-0.169	0.565	0.566	0.590	0.558
8	0.590	0.195	-0.174	0.590	0.622	0.646	0.616
9	0.632	0.383	-0.144	0.632	0.739	0.753	0.745
10	0.666	0.590	-0.042	0.666	0.889	0.890	0.964
11	0.685	0.764	0.095	0.685	1.026	1.031	1.189
12	0.671	0.878	0.252	0.671	1.105	1.134	1.245
13	0.600	0.794	0.286	0.600	0.995	1.035	1.003
14	0.521	0.621	0.216	0.521	0.811	0.839	0.704

The base shear related to the average of peak top floor displacements of each mode were extracted from the corresponding pushover curves and were combined to estimate the base shear of each EBF subjected to earthquake ground motions. As shown in Table 5.9, MPA method could reasonably predict the base shear of three selected EBFs with a few percentage of error comparing to the results of NLTHA.

Table 5.9 Comparison of the base shear obtained from MPA and NLTHA

EBFs	Base shear			Combination	Base Shear NLTHA	Percentage Error (%)
	Mode 1	Mode 2	Mode 3	3 Modes		
4-storey EBF	1623.81	877.28	339.32	1876.57	2304	-18.55
8-Storey EBF	2020.89	1355.48	1219.18	2721.71	2910	-6.47
14-Storey EBF	2216.26	2278.32	1674.20	3592.42	4145	-13.33

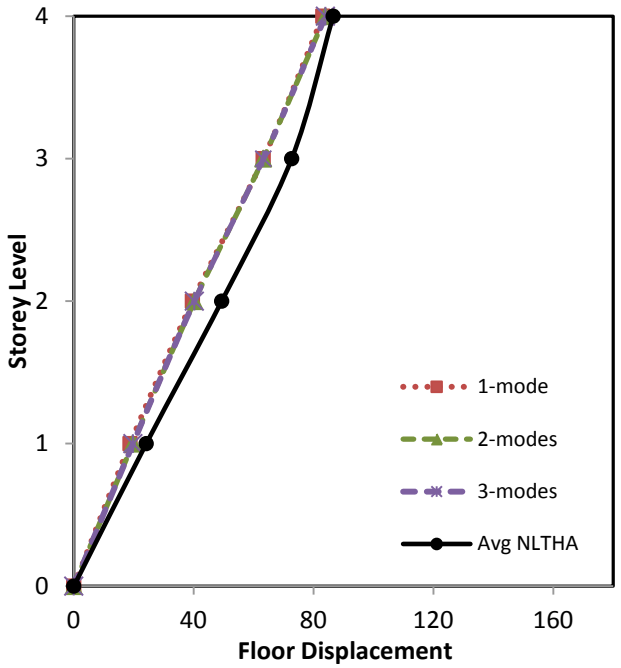

Figure 5.15. 4-Storey EBF Floor Displacements (MPA and NLTHA)

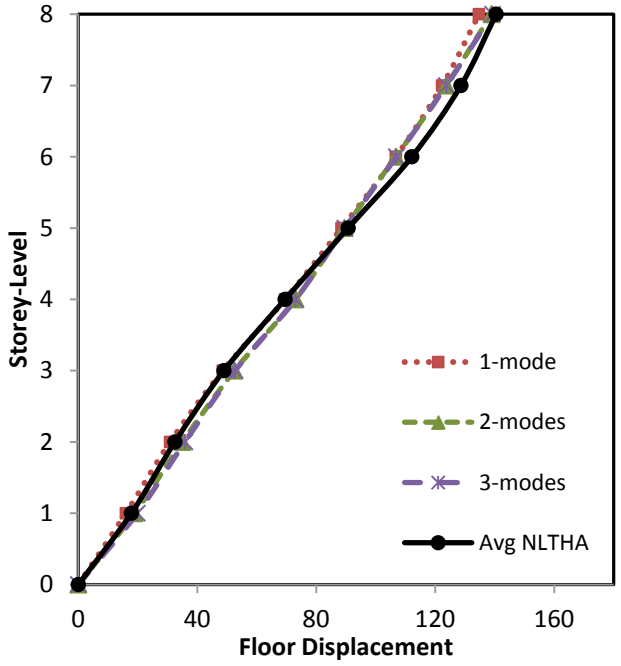

Figure 5.16. 8-Storey EBF Floor Displacements (MPA and NLTHA)

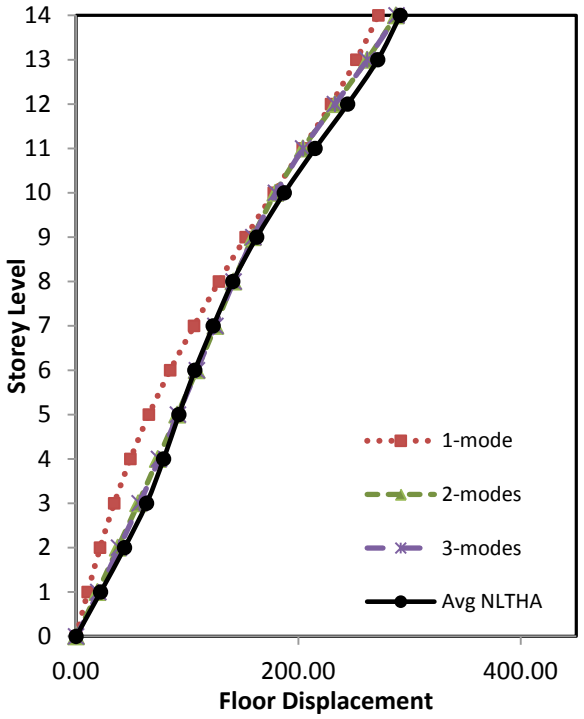

Figure 5.17. 14-Storey EBF Floor Displacements (MPA and NLTHA)

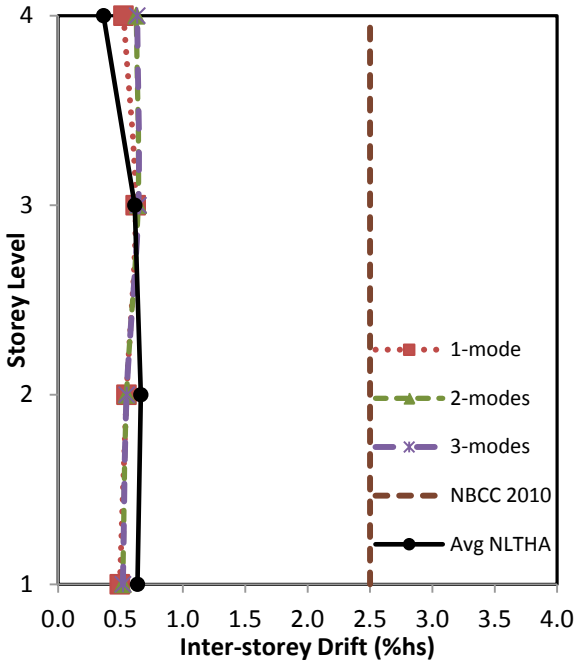

Figure 5.18. 4-Storey EBF Inter-Storey Drift (MPA and NLTHA)

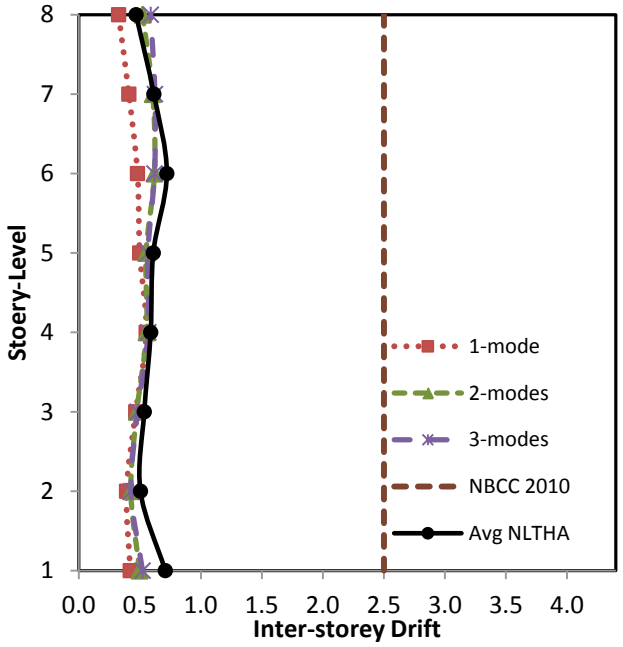

Figure 5.19. 8-Storey EBF Inter-Storey Drift (MPA and NLTHA)

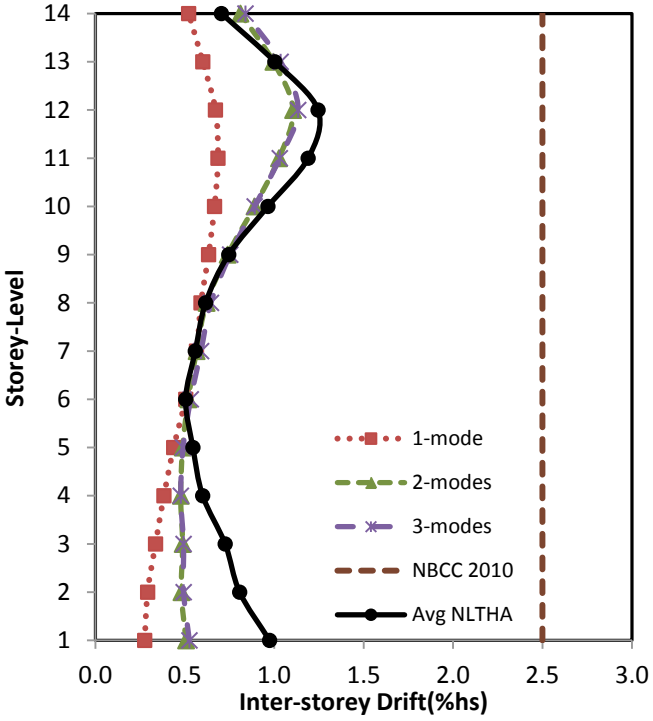

Figure 5.20. 14-Storey EBF Inter-Storey Drift (MPA and NLTHA)

5.5. Summary

This chapter evaluated the accuracy of modal pushover analysis in predicting seismic demands for eccentrically braced frames. The results of modal pushover analysis were compared with the results of non-linear time history analysis for 4-, 8- and 14-storey EBFs for four selected earthquake records. The major findings of this study are summarized as follows:

For 4-storey EBF, which is representing low-rise EBFs, the roof displacement was well predicted by considering the first mode. Adding the higher mode effects did not improve the displacement and inter-storey drift responses considerably.

For 8-storey EBF, which is considered as a medium-rise EBF, the first mode was able to predict the displacements of lower floors accurately; however, adding the contribution of the 2nd mode improved the displacements of upper floors. The contribution of the 2nd mode in the inter-storey drift was found more significant. Thus, for this EBF, including the effect of second mode was found helpful in improving MPA responses. The effect of the 3rd mode was not considerable.

For 14-storey EBF, which represents a high-rise EBF, considering just the first mode could not lead to very accurate displacement and inter-storey drift responses. Adding the 2nd mode had more considerable influence on the improvement of both responses comparing to the 8-storey EBF. The third mode could also improve the responses by a few percent but that improvement was not found significant. For the three EBFs, the displacements of the roof were precisely predicted by MPA.

The base shear related to the average of peak top floor displacements of each mode were obtained from the associated pushover curve and were combined and compared with the non-linear dynamic base shear. The results showed that MPA method could reasonably predict the base shear of three selected EBFs. In conclusion, based on the study on 4-, 8- and 14-storey EBFs, adding the higher mode effects in MPA method was found un-required for low-rise, helpful for medium-rise and necessary for high-rise EBFs.

Chapter 6. Evaluation of Capacity Spectrum Method for Eccentrically Braced Frames

6.1. Introduction

The Capacity Spectrum Method (CSM) is a nonlinear static analysis procedure which can be used to estimate seismic demands of buildings. The capacity curve is described by roof displacement and base shear. The demand curve is obtained from the selected design response spectrum. The initial stiffness, yield strength and ductility demands of structures are calculated from the superposition of the capacity curves and demand curves. To account for inelastic behavior of the buildings, CSM uses inelastic response spectra or equivalent damped spectra. Appropriateness of both response spectra have been evaluated for framed structures in previous studies (Chopra and Goel 1999). Fajfar (1999) introduced a relatively simple and easy to use CSM procedure with a constant ductility demand spectra developed by Vidic et al. (1994). This capacity spectrum method is known as N2 method (P. Fajfar 1999) and has been implemented in Eurocode 8. This chapter evaluates the capacity spectrum method proposed by Fajfar (1999) for EBFs. Critical seismic response parameters roof displacement, ductility demand of 4-, 8- and 14-storey EBFs are estimated by CSM. Design acceleration response spectrum of Vancouver has been transformed into the constant ductility demand spectra. The pushover (base shear versus roof displacement) curves of the EBFs are converted into the capacity spectrum of the equivalent single-degree-of-freedom (equivalent SDOF) systems. Finally, the applicability of CSM in estimating seismic demands of low-rise, medium-rise and high-rise EBF is investigated by comparing the results from CSM with the results from more accurate non-linear seismic analysis.

6.2. Capacity Spectrum Method by Fajfar (1999)

The steps of capacity spectrum method proposed by Fajfar (1999) are as follows:

Development of Seismic Demand Curve:

Seismic demand is usually defined as the elastic (pseudo)-acceleration spectrum where spectral accelerations (S_{ae}) are given as a function of the natural period of the structure T. Site specific design spectrum can be used to develop of a seismic demand curve. The first step for developing a seismic demand curve is to convert a traditional response spectrum in acceleration-displacement format.

Step 1. Seismic Demand in Acceleration Displacement Response Spectrum format (ADRS):

Acceleration response spectrum can be converted in to acceleration-displacement response spectrum (ADRS) by utilizing following relation between Pseudo-acceleration and displacement for the Single-Degree-of-Freedom (SDOF) system,

$$S_{de} = \frac{T^2}{4\pi^2} S_{ae} \qquad 6.1$$

where S_{de} and S_{ae} are the spectral displacement and pseudo acceleration of elastic response spectrum respectively corresponding to the period *T* and a fixed viscous damping ratio.

Inelastic ADRS can be obtained indirectly from elastic ADRS. The acceleration spectra S_a and displacement spectra S_d for an inelastic SDOF system can be obtained by using strength reduction factor R_μ proposed by Vidic et al. (1994). As given in equation 6.2, force reduction factor is the ratio of elastic strength demand to inelastic strength demand of an SDOF system for

a specified ductility ratio. Reduction factor (R_μ) mainly depends on the ductility and on the period of the system.

$$S_a = \frac{S_{ae}}{R_\mu} \qquad 6.2$$

From Equation 5.2and 6.2

$$S_d = \mu \frac{T}{4\pi^2} S_a \qquad 6.3$$

where μ is the ductility factor defined as the ratio between the maximum displacement and the yield displacement.

Several studies (Miranda and Bertero 1994, Vidic et al. 1994) have been done to determine force reduction factor. In this research, the formulae proposed by Vidic et al. (1994) in slightly modified form will be used.

$$R_\mu = (\mu - 1)\frac{T}{T_o} + 1 \quad \text{when } T \le T_o \qquad 6.4$$

$$R_\mu = \mu \quad \text{when } T \ge T_o \qquad 6.5$$

$$T_o = 0.65\mu^{0.3} T_c \le T_c \qquad 6.6$$

where T_c is the characteristics period which refers the transition period where constant acceleration region intersect the constant velocity region and this is the period when largest forces are applied to the structure; T_o is the transition period which depends on structural ductility and it should not be greater than T_c.

The values of characteristics period and the transition period can be considered equal. Thus, in the simple version of the capacity spectrum method Fajfar (1999) considered

$$T_o = T_c \qquad 6.7$$

Once the ductility and force reduction factors are known constant ductility seismic demand spectrum can be obtained for different ductility. Figure 6.1 presents schematic figure of such seismic demand spectrum.

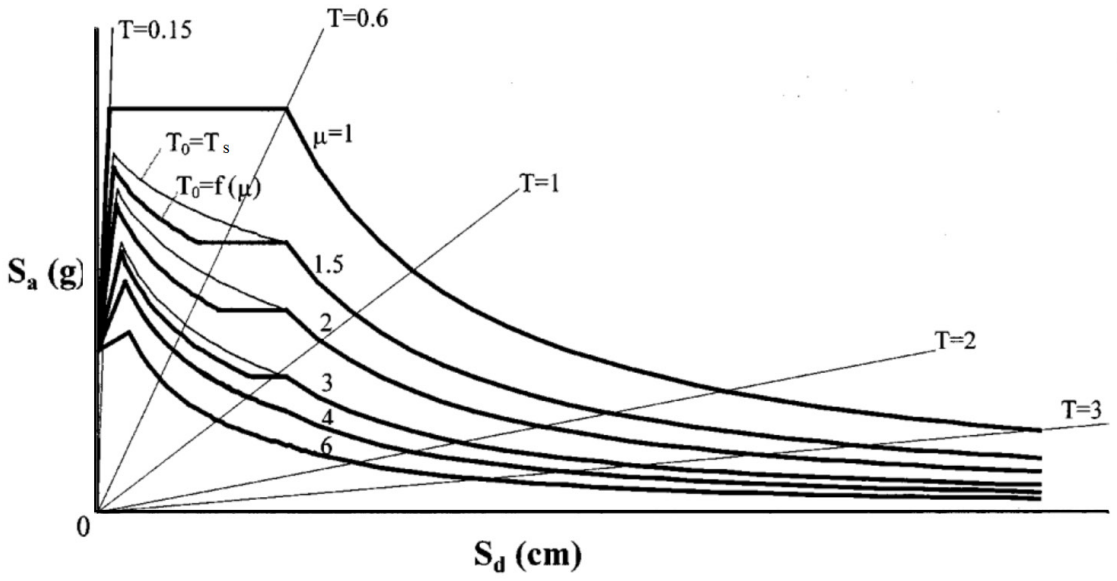

Figure 6.1. Schematic figure of an seismic demand spectrum (constant ductility response spectrum in ADRS format) by Fajfar (1999)

Developement of Capacity Curve of Equivalent Single Degree of Freedom system:

Step 1. Pushover curve of MDOF system: Estimate the first natural frequency of vibration ω_n, and associated normalized elastic vibration mode shape, ϕ of a multi-storey building (MDOF). Base shear-roof-displacement relation (pushover curve) for MDOF system is developed by

pushing the structure with lateral force proportional to the assumed displacement shape (ϕ_i) multiplied by storey mass, m_i.

$$p_i = m_i \phi_i \qquad 6.8$$

where, p_i is the lateral force at any storey i.

Step 2. Determination of Capacity Spectrum for equivalent SDOF system: First, the MDOF system is transformed into equivalent SDOF system Top displacement (D_t) and base shear (V_b) of MDOF system are transformed into force (F^*) displacement (D_t^*) relationship of equivalent SDOF system by following relationship.

$$F^* = V_b / \Gamma \qquad D_t^* = D_t / \Gamma \qquad 6.9$$

where Γ is called modal participation factor and is given by:

$$\Gamma = \frac{m^*}{\sum m_i \phi_i^2} \qquad 6.10$$

where m^* is the mass of equivalent single degree of freedom system (SDOF) for the fundamental mode.

$$m^* = L_n = \sum m_i \phi_i \qquad 6.11$$

Step 3. Idealize the pushover curve of equivalent SDOF into an elastic-perfectly plastic form: At this step the force (F^*) - displacement (D_t^*) relation of equivalent SDOF system is idealized based on some engineering judgment. This can be done by the guidelines provided in FEMA-273. Finally, bilinear idealized force (F^*) - displacement (D_t^*) curve are transferred into

capacity curve by representing spectral acceleration to spectral displacement curve of equivalent SDOF system. Spectral acceleration at the yielding point is $S_{ay} = \frac{F_y^*}{m^*}$. Elastic period of the idealized bilinear system F^* can be determined by:

$$T^* = 2\pi\sqrt{\frac{m^* D_y^*}{F_y^*}} \qquad 6.12$$

where D_y^* and F_y^* are the yield displacement and yield strength of the equivalent SDOF system. Schematic figure of the development of capacity curve from pushover curve of MDOF to force-displacement curve for equivalent SDOF system is presented in Figure 6.2. In this figure, the bilinear force-displacement curve is the capacity curve for equivalent SDOF system.

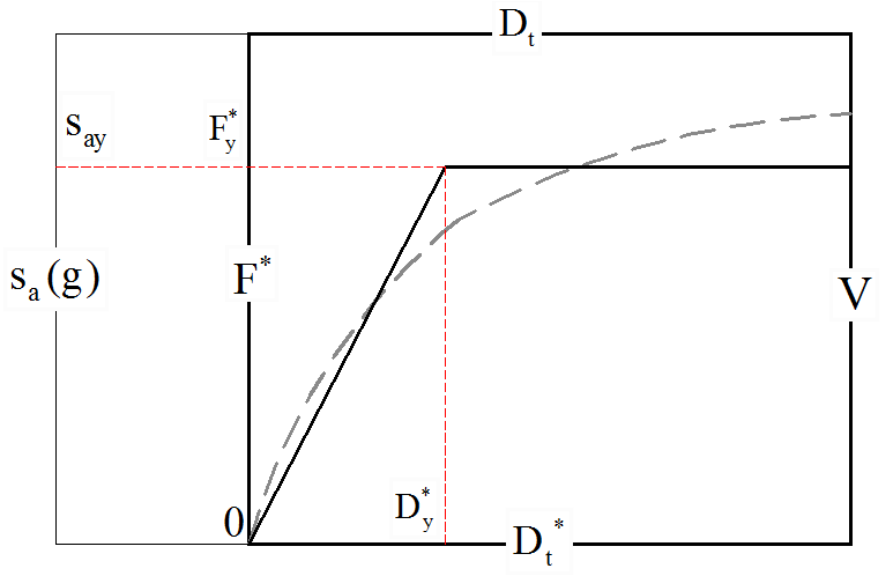

Figure 6.2. Development of the capacity spectrum of an equivalent SDOF system by Fajfar (1999)

Determination of Seismic Demand and Performance of Equivalent SDOF system:

Once the demand spectra and capacity spectra for equivalent SDOF system are established, they are superimposed in the same plot. Intersection point of the redial line of the capacity curve corresponding to the elastic stiffness of the equivalent SDOF system and the elastic demand spectrum, gives the strength demand (S_{ae}) if the structure remains elastic. The yield spectral acceleration S_{ay} for the equivalent SDOF system refers to the acceleration where the inelastic behavior begins. Ratio of the elastic acceleration demand and yield spectral acceleration is the reduction factor R_{μ}. After that, ductility demand can be calculated from equations 6.4 and 6.5. Equations 6.4 and 6.5 suggest that, in the medium- and long-period ranges, the equal displacement rule applies. This means that the displacement of the inelastic system is equal to the displacement of the corresponding elastic system with the same period. Finally, the displacement demand for the structure is determined from the intersection point of the capacity curve and the demand curve corresponding to the ductility demand.

6.3. Application of Capacity Spectrum Method (CSM) for EBFs

The three selected eccentrically braced frames (4-, 8- and 14-storey EBFs) designed according to capacity design approach of CAN/CSA S16-09 and presented in Chapter 3 are considered in this chapter to evaluate the applicability of capacity spectrum method for EBFs.

Capacity curves for EBFs:

Frequency analysis was performed for the selected EBFs to estimate fundamental periods and associated mode shapes of the EBFs. With the load pattern associated with the fundamental mode shapes, as given by equation 6.8, the EBFs were pushed and pushover curves (Base shear -

roof displacement) were estimated. ABAQUS (K. a. Hibbitt 2011) was used to perform nonlinear pushover analysis with calculated lateral load pattern. The target displacement for the pushover analysis was taken as the displacement when the expected rigid plastic mechanism occurred. For EBFs, this occurs when all the links are yielded. Figure 6.3 presents the nonlinear pushover curves for the selected EBFs. The MDOF systems were transformed into equivalent SDOF systems by applying relations given in Equation 6.9. Masses of equivalent SDOF systems are 578 ton, 1214 ton and 1810 ton for 4-storey, 8-storey and 14-storey building respectively. Modal participation factors of MDOFs were calculated as 1.46 for 4-storey EBF, 1.44 for 8-storey EBF and 1.54 for 14-storey EBF. Roof displacement (D_t) and base shear (V_b) relation of MDOF systems have been transferred into force (F^*) - displacement (D_t^*) relationship of equivalent SDOF system. After that, force (F^*) to displacement (D_t^*) relationship of equivalent SDOF systems were idealized as bilinear curves where the post-yielding stiffness of equivalent SDOF systems were zero. This was done following the guidelines in FEMA-273 where area under the original pushover curve and bilinear curve were same and the two curves intersected at the 60% of the yield strength. Bilinear idealized force-displacement curves of SDOF systems were then converted into spectral acceleration versus spectral displacement curves. Properties of equivalent SDOF systems are presented in Table 6.1 and idealized SDOF curves are shown in Figure 6.4.

Table 6.1 Structural Properties of Equivalent SDOF System

Frames	**Effective mass m^*** (ton)	**Modal Participation Factor Γ**	**Yield Strength F_y^*** (kN)	**Yield Displacement D_y^*** (mm)	**Elastic Period T^*** (sec)
4-Storey EBF	578.13	1.46	1299.05	34.00	0.77
8-Storey EBF	1213.61	1.44	1792.29	74.99	1.42
14-Storey EBF	1810.44	1.54	1782.24	170.72	2.62

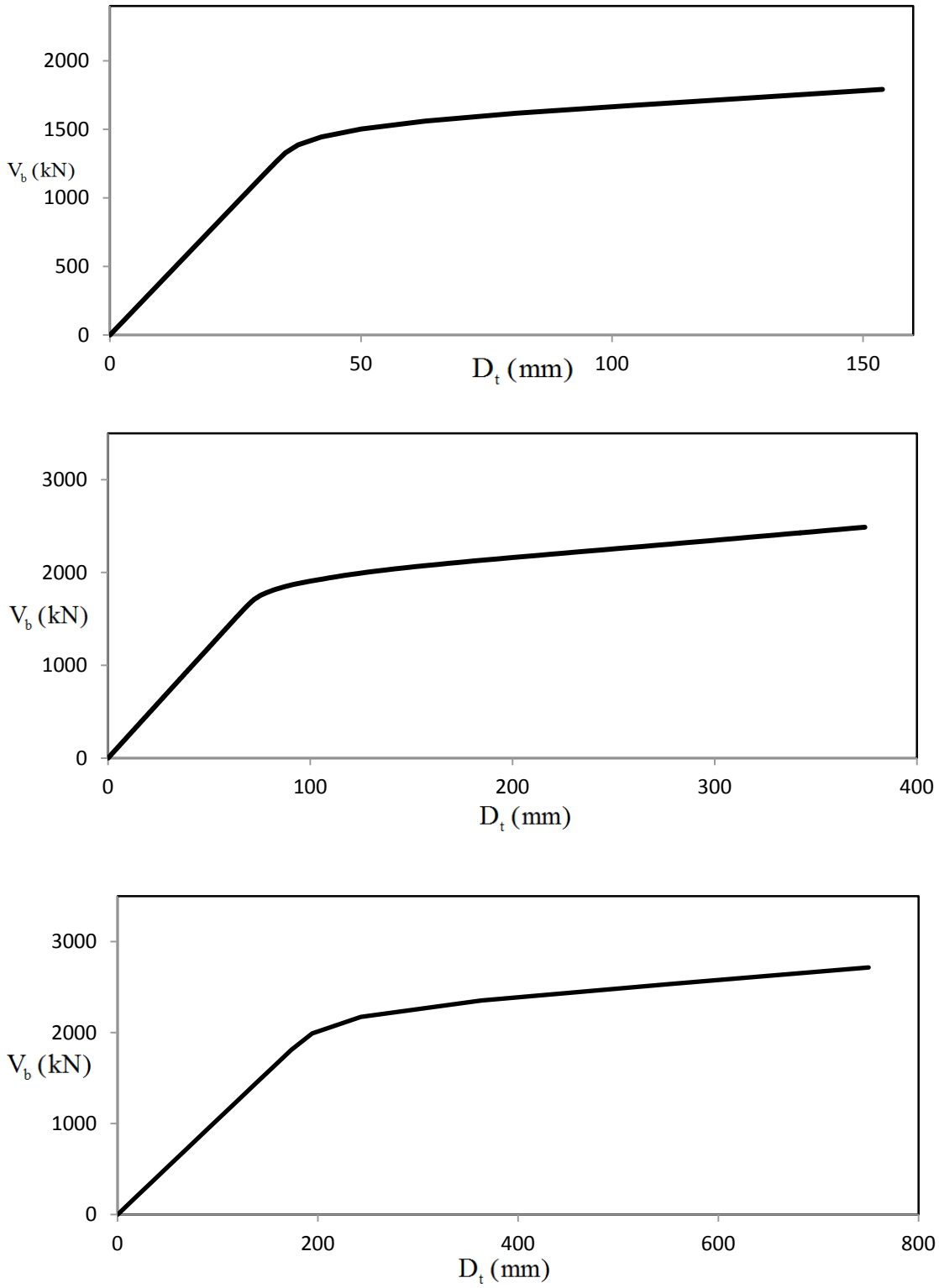

Figure 6.3. Base shear (V_b) - Roof Displacement (D_t) from Non-Linear Pushover Analysis of 4-Storey EBF (top), 8-Storey EBF (middle), 14-Storey EBF (bottom)

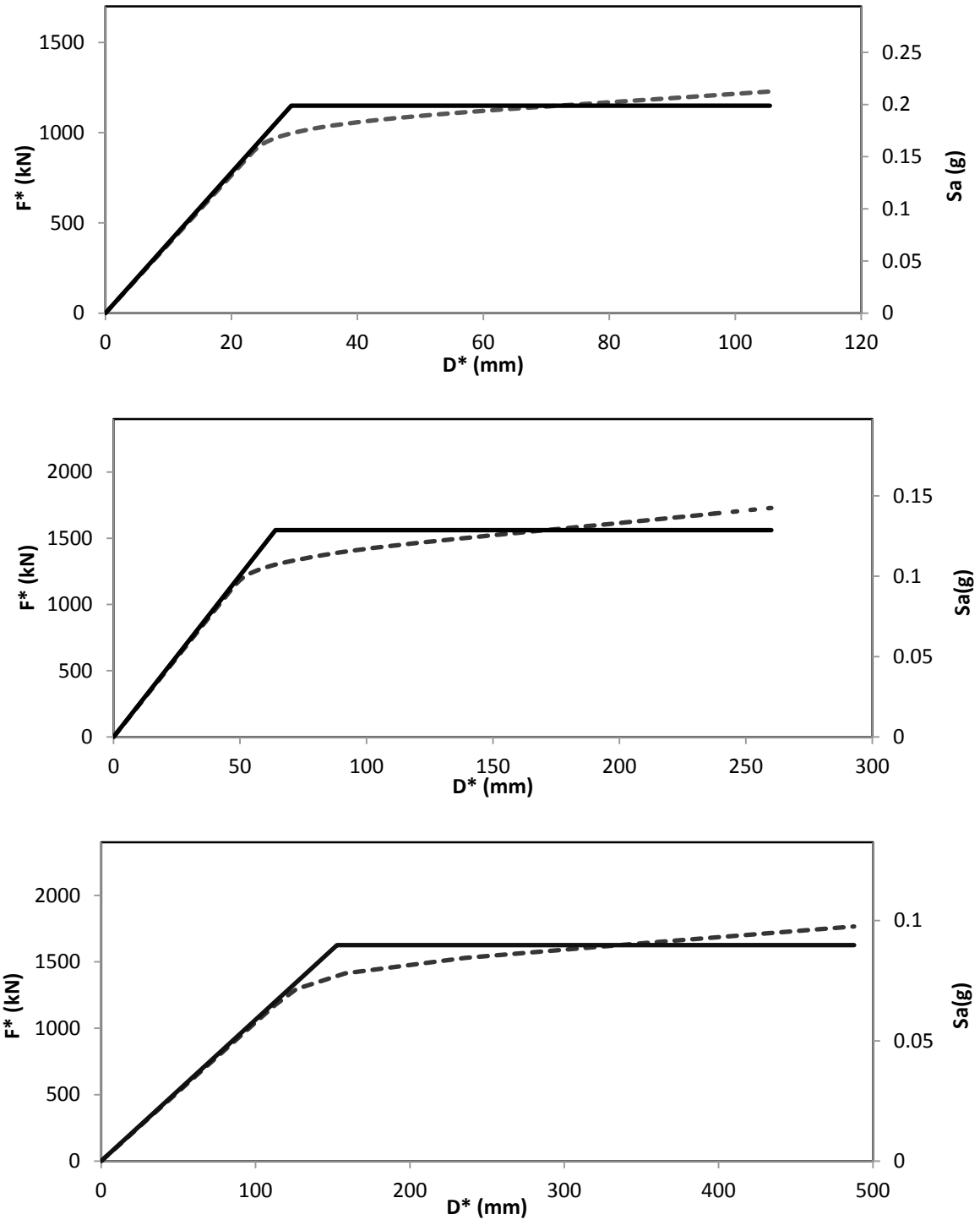

Figure 6.4. Force-Displacement and Idealized Curve as well as Spectral Acceleration vs. Spectral Displacement Curve of Equivalent SDOF System for 4-Storey EBF (top), 8-Storey EBF (middle), 14-Storey EBF (bottom)

Demand spectrum for EBFs:

Appendix J of National Building Code of Canada provides design spectral accelerations for different cities in Canada. Vancouver design spectral acceleration parameters (5% damped structure and for reference soil class C were used to obtain seismic demand curve. The design spectrum is presented in Figure 6.5. Displacement response spectrum was estimated from pseudo-acceleration using equation 5.2.

The demand curve constructed based on code spectral accelerations was for elastic response of the structure (e.g. ductility is equal to one). Acceleration spectrum (S_a) and displacement spectrum (S_d) for inelastic SDOF systems were determined from elastic ADRS by using expression of reduction factor by Vidic et al. (1994). From the Vancouver design spectrum, the characteristics period (T_c) is taken as 0.20 s.

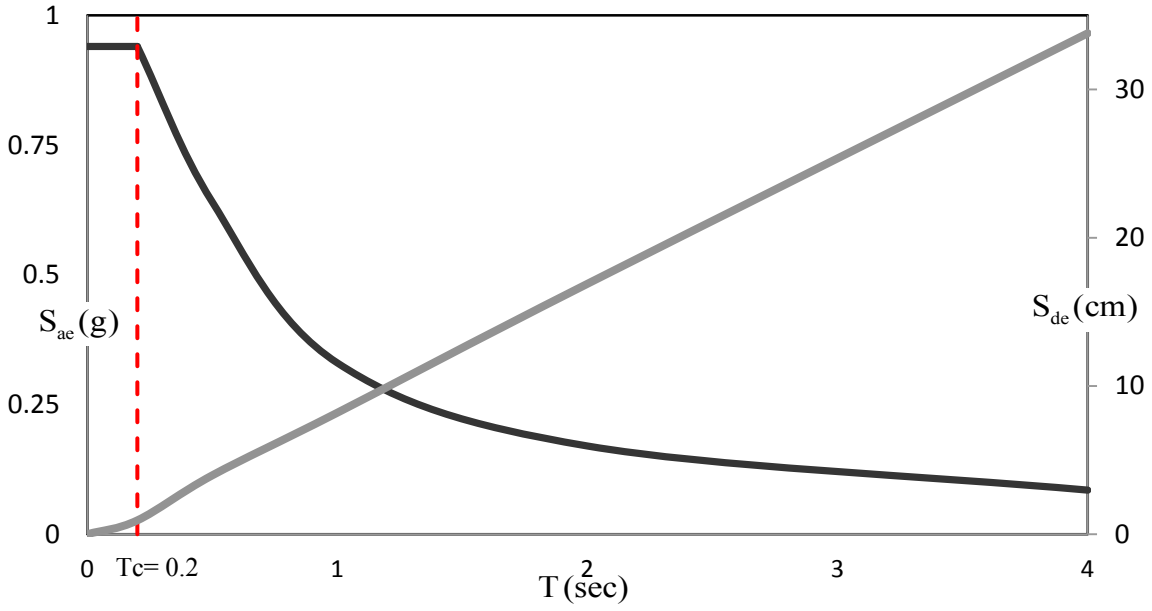

Figure 6.5. Elastic Design Acceleration Response Spectrum of Vancouver for 5% Damping Ratio and the Corresponding Displacement Spectrum

Seismic Demand estimation of EBFs using CSM:

Demand spectra and capacity spectra for equivalent SDOF system were drawn in the same plot. Radial line of the capacity curve corresponding to the elastic period of the equivalent SDOF system represents the elastic stiffness of the EBF system. Intersection of elastic demand spectrum and capacity spectra of equivalent SDOF system gives the strength demand (S_{ae}) when the response of the EBF is elastic. This intersection point is often referred as performance point. The yield spectral acceleration (S_{ay}) for the equivalent SDOF system refers to the spectral acceleration demands for the inelastic system. Ratio of the elastic spectral acceleration demand to the inelastic spectral acceleration demand is called force reduction factor, R_{μ}. Once the force reduction factor was calculated ductility demand was calculated by the reverse calculation of equations 6.4 and 6.5. Displacement demand of equivalent SDOF system was estimated from the same performance point. Figure 6.6, Figure 6.7 and Figure 6.8 present graphical representations of the application of capacity-spectrum method for 4-storey, 8-storey and 14-storey EBF respectively.

From the capacity curves of 4-, 8-, and 14-storey EBFs elastic periods were calculated. The elastic periods of equivalent SDOF systems were 0.77 s, 1.42 s, and 2.62 s. Since the elastic periods of all the selected EBFs are larger than T_c, " Equal Displacement Rule " applies here. Thus for all the selected cases, inelastic displacement demands are equal to the elastic displacement demands. Displacement demands of equivalent SDOFs were determined from the intersection points of the capacity curves and the demand curves corresponding to the ductility demands. The displacement demands for equivalent SDOF systems were determined as 63.5 mm, 117.5 mm and 219 mm for 4-storey, 8-storey and 14-storey EBFs respectively. The results

from equivalent SDOF systems were then transferred into displacement demands of MDOF systems by multiplying with the modal participations factors. The top displacement demands for 4-storey EBF, 8-storey EBF, and 14-storey EBF were determined as 92.63 mm, 169.08 mm, and 336.75 mm respectively. For the three selected EBFs, the displacement demands obtained from capacity spectrum method were compared with average top storey displacements from non-linear time history analysis. Table 3.3 presents the displacement demands of the selected EBFs. It is observed that that the displacement demands from CSM agree very well with the average maximum top storey displacements from nonlinear seismic analysis. The maximum difference between seismic analysis and CSM was 4.52% and was observed for 8-storey EBF.

According to the current design standard of Canada, ductility based reduction factor for EBF is 4.0 and over-strength related reduction factor is 1.5. In CSM, ductility demands of the selected EBFs were lower than the code suggested ductility. However, ductility demand calculations using CSM have some limitations. First of all, the elastic period calculated using CSM may not be constants after yielding of the structure. In addition, all the analysis approximations also have some influence on this lower ductility demand.

Table 6.2 Performance Evaluation of EBFs using CSM and NLTHA

Parameters	4-Storey EBF	8-Storey EBF	14-Storey EBF
Max Top Displacement (mm) (CSM)	92.63	169.08	336.75
Max Top Displacement (mm) (NLTHA)	88.78	161.77	332.28
Percentage Error (%) (CSM W.R.T NLTHA)	4.34	4.52	1.345

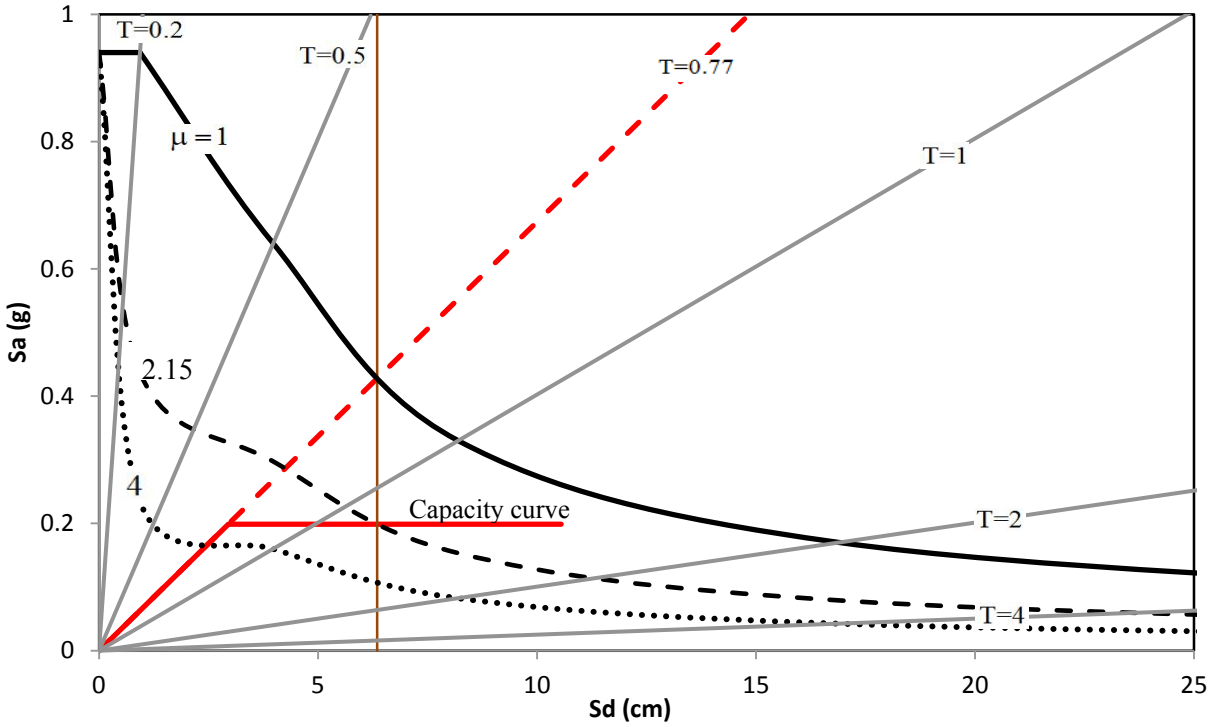

Figure 6.6. Graphical Representation of CSM on 4-Storey EBF in ADRS format

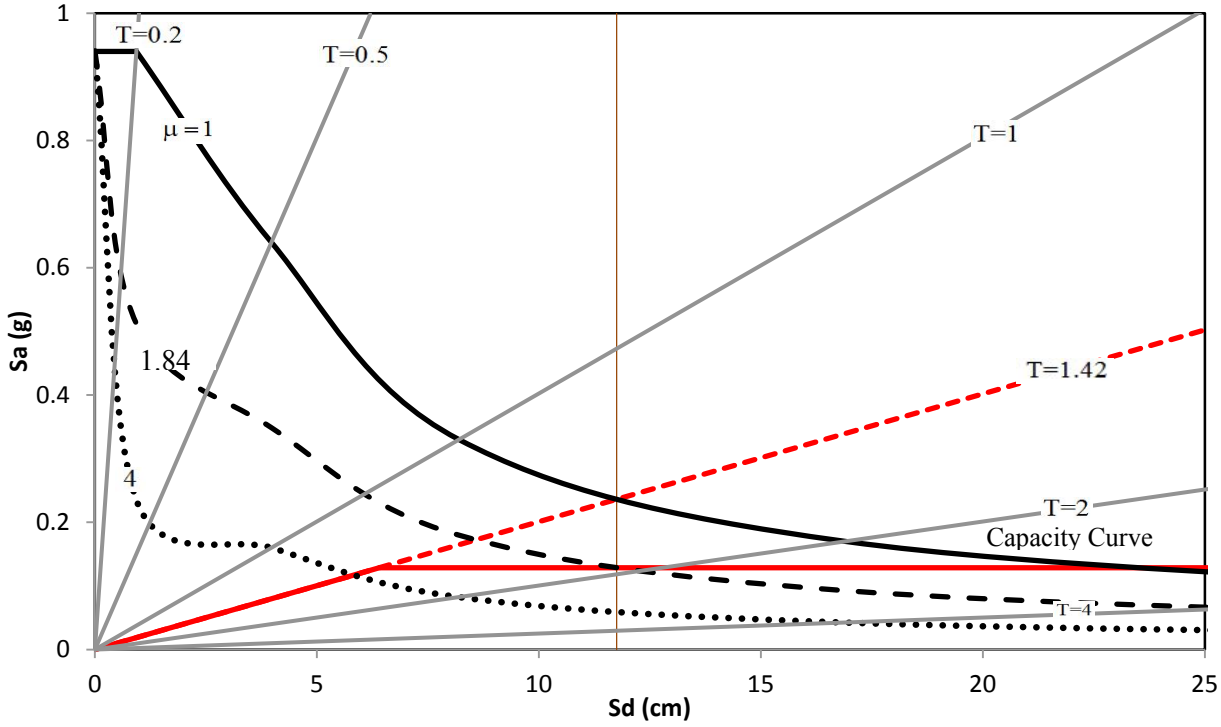

Figure 6.7. Graphical Representation of CSM on 8-Storey EBF in ADRS format

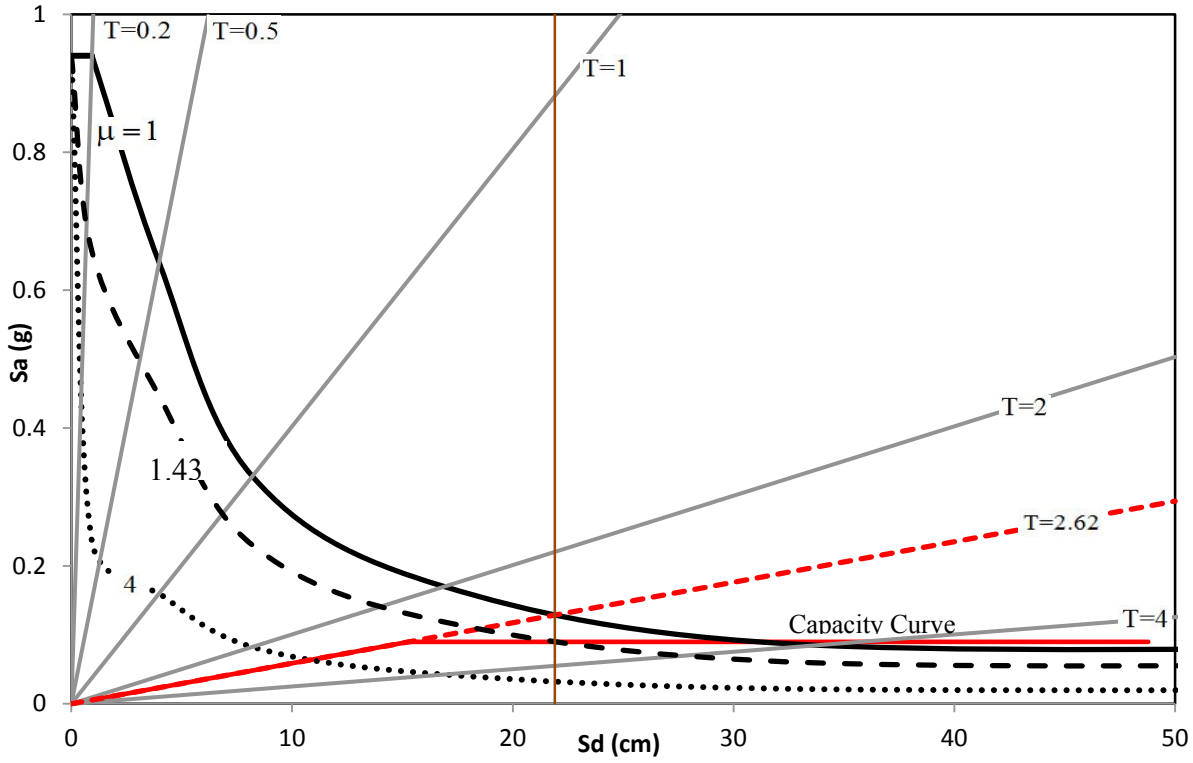

Figure 6.8. Graphical Representation of CSM on 14-Storey EBF in ADRS format

6.4. Summary

Seismic performance evaluation is one of the important steps in performance based design procedure. CSM has been used previously as a performance evaluation tool for framed structures. The applicability of CSM for estimation of seismic demands for three EBFs is investigated in this chapter. Non-linear pushover curves of MDOF have been converted into capacity curves of equivalent SDOF system. Vancouver design response spectrum was transferred into inelastic demand spectrum for different ductility factors. Displacement demand and ductility demand were calculated from the intersection point of the capacity curve and demand curve. For all the selected EBFs, the displacement demands were very close to the non-linear time history analysis results. On the other hand, estimated ductility demands of all EBFs

by CSM were lower than the designed ductility of EBF, which represents the satisfactory performance of these systems.

Finally, capacity-spectrum method can be used for estimation of performance parameters of EBFs. Capacity-spectrum method needs an assumed displacement shape and a lateral load pattern for nonlinear pushover analysis. In this method, first elastic vibration mode shape was used as an assumed mode shape. Therefore, this method cannot include higher mode contribution in the overall building performance. Therefore, this method is suitable for structure which is mainly dominated by its fundamental mode of vibration. For different hazard level, CSM can be performed with different response spectrum for corresponding hazard level. So the expected performance level for different level of ground motion can be analyzed by CSM as well.

Chapter 7. Summary and Conclusions

7.1. Summary

In this research, seismic performance of eccentrically braced frames designed according to NBCC 2010 and CSA S16-09 provisions was evaluated. A detailed finite element model with material and geometrical non-linearities was developed. The finite element model was validated using the results from one quasi-static experimental program. The same finite element modeling technique was then used to model a set of three eccentrically chevron braced frames with 4-, 8- and 14-storey designed according to current Canadian provisions. To determine the seismic responses of EBFs, non-linear time history analyses were conducted. A set of eight ground motions including real and simulated records compatible with design spectrum of Vancouver was selected for seismic analysis. The critical response parameters including inelastic link rotations and maximum shear forces in the links were investigated. Also, storey displacement and inter-storey drift results were provided. It is well accepted that the non-linear time history analysis provides very accurate results; however, seismic performance evaluation using NLTHA is very complex and time consuming and most importantly require expertise. Therefore, simple methods with enough accuracy in estimating seismic demands of EBFs are required by practicing engineers. Two such simple methods are modal pushover analysis and capacity spectrum method. MPA and CSM procedures are non-linear static methods that have been used previously for moment resisting frames. In this research, these two methods were evaluated for estimating seismic performance parameters of EBFs. The modal pushover method was selected because it incorporates the contributions of higher modes into the responses. This method was applied on the three EBFs to estimate the displacements and inter-storey drifts demands of all

floors as well as the base shear demands. The capacity spectrum method which graphically compares the capacity of the structure with seismic demands was employed as another non-linear static method. Critical seismic response parameters, such as top storey displacements and inter-storey drifts, from MPA and CSM were compared with the results obtained from non-linear seismic analysis.

7.2. Conclusions

The following observations were made from non-linear time history analysis of EBFs:

- The finite element model developed in this study was able to provide reasonably accurate predictions of the behavior of EBF. Excellent agreement was observed between results from FE analysis and results from experiment. The finite element model was capable to capture all essential features of the test specimens, such as initial stiffness, ultimate strength.

- Based on the results of non-linear time history analyses, it was observed that all EBFs behaved in compliance with the capacity design approach provided by Canadian seismic provisions. For all ground motions, all the links were yielded at all floors. Though some partial yielding of adjacent beams was observed for some ground motions, all other members remained elastic.

- During the design process, it was attempted to keep the ratio of the link shear resistance to the link shear forces uniform along the height of EBFs in order to avoid the concentration of link rotations at some specific floors as it was recommended in the

literature. However, the analysis results showed that the link rotations at all floor were not uniform especially in medium and high-rise EBFs.

- The average link rotation of all EBFs remained below the design limit of 0.08 rad, except for the two upper floors in 14-storey EBFs where the link rotation slightly exceeded the limit. The larger link rotation demands might be due to participation of higher modes. The modal pushover analysis also showed significant contribution of the second mode into the responses of 14-storey EBF. Thus, for design of taller EBF buildings higher mode contributions are important and shall be considered at the design phase.

- The link overstrength factors in all EBFs also follow the same trend as the link rotations with average values of 1.5, which exceeds the code limit of 1.3, but it is below of the available experimental results. The amount of overstrength developed by the link is because of strain hardening of the link and also due to development of shear resistance in the link flanges. Therefore, based on the results of this study, the current link overstrength factor of 1.3 suggested by CSA S16-09 underestimates the actual link overstrength factor. However, more analysis should be done on EBFs of different geometry before suggesting modifications of link overstrength factor.

The accuracy of MPA and CSM methods was also evaluated on the three EBFs. The following conclusions were made:

- In general, modal pushover analysis results showed sufficient accuracy in predicting seismic demands of all eccentric braced frames. For low-rise EBF, the top storey

displacement was accurately predicted by the first mode. Considering higher mode effects didn't improve the accuracy of the results considerably. For medium-rise EBF, the accuracy of the displacement and inter-storey drift results were improved by including higher modes contribution. For high-rise EBF, the most significant contributions of higher modes on both displacements and inter-storey drifts were observed leading into sufficiently precise results. For all EBFs, the results of storey displacements were more precise than inter-storey drifts. Also, the modal pushover method was able to predict the base shear demand with reasonable accuracy.

- The capacity spectrum method showed excellent accuracy in predicting the displacement demands and ductility demands of all EBFs. Based on the results of this study, CSM can be accepted as a simplified method for preliminary design of low to medium-rise EBFs. Although both CSM and MPA method was found precise in predicting top floor displacements of all EBFs, MPA is superior in providing more realistic measure of other floors displacements and inter-storey drifts.

7.3. Future Work

The non-linear time history analysis results provided in this thesis is limited to three eccentrically chevron braced frames. More research works are required on EBFs of different types, geometry and height to verify achievement of the desired frame behavior of EBFs designed according to current Canadian provisions. Also, based on the results of this study, the link overstrength factor suggested by CSA S16-09 is lower than the actual link overstrength. More studies are required on EBFs of different type and height before making more general conclusions and suggestions in this regard.

The applicability of modal pushover analysis method in this study was evaluated for eccentrically chevron braced frames with symmetrical plan. More studies are required for unsymmetrical plan with torsional effects.

The post-yielding behavior of the structure is neglected in capacity spectrum method. It is well-known that after yielding, stiffness of any lateral load resisting system changes. Thus, future research is required to incorporate post-yielding hardening in the capacity spectrum method.

References

ANSI/AISC. 2005. Seismic Provisions for Structural Steel Buildings. American Institute of Steel Construction Inc, Chicago, Illinois.

Arce, G. 2002. Impact Of Higher Strength Steels On Local Buckling And Overstrength Of Links In Eccentrically Braced Frames. Doctoral Dissertation, University Of Texas At Austin.

Atkinson, Gail, Karen Assatourians, and Bernie Dunn. 2009. Engineering Seismology Toolbox. http://www.seismotoolbox.ca/GMDatabases.html.

Balendra, T., Lam, K. Y., Liaw, C. Y., and Lee, S. L. 1987. Behavior of Eccentrically Braced Frame by Pseudo-Dynamic Test. Journal of Structural Engineering 113 (4): 673-688.

Chintanapakdee, C., and Chopra, A.K. 2003. Evaluation Of Modal Pushover Analysis Using Generic Frames. Earthquake Engineering and Structural Dynamics 32.

Chopra, A.K., and Goel, R.K. 2001. A Modal Pushover Analysis Procedure to Estimate Seismic Demans for Buildings: Theory and Preliminary Evaluation. Pacific Earthquake Engineering Research Center, California.

Chopra, A.K., and Goel, R.K. 1999. Capacity-Demand-Diagram Methods for Estimating Seismic Deformation of Inelastic Structures: SDOF Systems. Urban Earthquake Disaster Mitigation, University of California, Pacific Earthquake Engineering Research Center, California.

CSA. 2009. Limit states design of steel structures. Canadian Standards Association. Toronto, Ontario.

David, S.O. 2009. Seismic Analysis Design Of Taller Eccentrically Braced Frames. École Polytechnique de Montréal.

Della Corte, G., D'Aniello, M., and Landolfo, R. 2013. Analytical And Numerical Study Of Plastic Overstrength Of Shear Links. Journal of Constructional Steel Research 82: 19-32.

Dubina, D. 2014. Full-Scale Experimental Validation Of Dual Eccentrically Braced Frame With Removable Links (Duarem). Research Report, Politehnica University of Timisoara.

Engelhardt, M. D, and Popov, E. P. 1989. Behavior Of Long Links In Eccentrically Braced Frames. University of California, Berkeley 89 (1).

Fajfar, P., and Fischinger, M. 1988. N2—A Method For Nonlinear Seismic Analysis Of Regular Structures. In Proceedings of the Ninth World Conference in Earthquake Engineering: 111-116.

Fajfar, P. 1999. Capacity Spectrum Method Based on Inelastic Demand Spectra. Earthquake Engineering and Structural Dynamics 28 (9): 979-993.

FEMA. 1997. NEHRP Guidlines for the Seismic Rehabilitation of Buildings, FEMA-273. Applied Technology Council for the Building Seismic Safety Council, the Federal Emergency Management Agency, Washinton,D.C., USA.

FEMA. 2000. Prestandard and Commentary for the Seismic Rehabilitation of Buildings, FEMA-356. American Society of Civil Engineers. Federal Emergecy Management Agency, Washington, D.C., USA.

Ghobarah, A., and Ramadan, T. 1990. Effect Of Axial Forces On The Performance Of Links In Eccentrically Braced Frames. Engineering Structures 12 (2): 106-113.

Ghobarah, A., and Ramadan, T. 1991. Seismic Analysis Of Links Of Various Lengths In Eccentrically Braced Frames. Canadian Jounal of Civil Engineering.

Goel, R. K., and Chopra, A. K. 2004. Evaluation Of Modal And FEMA Pushover Analysis: SAC Buildings. Earthquake Spectra, 20 (1): 225-254.

Hibbitt, Karlsson, and Sorensen. 2011. ABAQUS/Standard User's Manual. Pawtucket: HKS Inc.

Hjelmstad, K. D., and Popov, E. P. 1983. Cyclic Behavior And Design Of Link Beams. Journal of Structural Engineering 109 (10): 2387-2403.

Jacob, C. C. 2010. Creating an Eccentrically Braced Frame Model for Application in Seismic Performance Assessments. Department of Civil Engineering, Tufts University.

Karr, A. 2002. RUAUMOKO Users Manual. University of Canterbury. New Zealand.

Kasai, K, and Popov, E. 1986. General Behavior of WF Steel Shear link Beams. Journal of Structural Engineering 112 (2): 362-382.

Koboevic. S. 2000. An Approach To Seismic Design Of Eccentrically Braced Frames. McGill University. Montreal, Canada

Koboevic, S., Rozon, J. and Tremblay, R. 2012. Seismic Performance Of Low-To-Moderate Height Eccentrically Braced Steel Frames Designed For North American Seismic Conditions. Journal of Structural Engineering, ASCE.

Korzekwa, A, and Tremblay, R. 2009, Numerical Simulation Of The Cyclic Inelastic Behavior Of Buckling Restrained Braces. Proceedings Of The Conference On Behavior Of Steel Structures In Seismic Areas, *STESSA.* Philadephia, Pennsylvania, USA, 635-658.

Krawinkler, H., and Seneviratna, G. D. P. K. 1998. Pros And Cons Of A Pushover Analysis Of Seismic Performance Evaluation. Engineering Structures 20 (4): 452-464.

Lamontagne, M., Halchuk, S., Cassidy, J. F., and Rogers, G. C. 2008. Significant Canadian Earthquakes Of The Period 1600–2006. Seismological Research Letters 79 (2): 211-223.

Mago, N.M. 2013. Finite Element Analysis of Eccentrically Braced Frames with Replaceable Link. HERA, Report R4-145, Heavy Engineering Research Association, Manukau.

Malley, J. O., and Popov. E. P. 1984. Shear Links In Eccentrically Braced Frames. Journal Of Structural Engineering 110 (9): 2275-2295.

Manheim, E.N. 1982. On The Design Of Eccentrically Braced Frames. Ph.D Thesis, Department of Civil Engineering,University of California, Berkeley.

Mansour, Nabil. 2010. Developement Of The Design Of Eccentrically Braced Frames With Replaceable Shear Links. Department Of Civil Engineering, University of Toronto.

Martini, K., Amin, N., Lee, P.L., and Bonowitz, D. 1990. The Potential Role Of Non-Linear Analysis In The Seismic Design Of Building Structures. In Proceedings of Fourth US National Conference on Earthquake Engineering, Palm Springs, Cal.

McDaniel, C. C. , Uang, C. M., and Seible, F. 2002. Cyclic Testing Of Suspension Tower Shear Links Of The San Francisco-Oakland Bay Bridge. Department of Structural Engineering, University of California, San Diego.

Miranda, E., and Bertero, V. V. 1994. Evaluation Of Strength Reduction Factors For Earthquake-Resistant Design. Earthquake spectra 10(2): 357-379.

Mondkar, D.P., and Powell, G.H. 1975. ANSR-I General Pwpose Computer Progrnm For Analysis Of Non-Linear Structural Response. Report No. UCB/EERC-75/37, University of California:, Berkeley.

Naumoski, N., Saatcioglu, M., and Amiri-Hormozaki, K. 2004. Effects Of Scaling Of Earthquake Excitations On The Dynamic Response Of Reinforced Concrete Frame Buildings. 13th World Conference on Earthquake Engineering 2917, no.15.

NBCC. 2010. National Building Code of Canada. Canadian Commission on Building and Fire Codes. National Research Council of Canada (NRCC), Ottawa, Onterio.

Ohsaki, M., and Nakajima, T. 2012. Optimization Of Link Member Of Eccentrically Braced Frames For Maximum Energy Dissipation. Journal of Constructional Steel Research 75(2):38-44.

Okazaki, T, and Engelhardt, M.D. 2007. Cyclic Loading Behavior Of EBF Links Constructed Of ASTM A992 Steel. Jornal Of Constructional Steel Research 63: 751–765.

Okazaki, T., Arce, G., Ryu, H. and Engelhardt, M. 2005. Experimental Study Of Local Buckling, Overstrength, And Fracture Of Links In Eccentrically Braced Frames. ASCE Journal Of Structural Engineering 131 (10): 1526-1535.

Parkash, V., Powell, G.H., and Filippou, F.C. 1992. Drain-2DX: Base Program User Guide. Report No. UCB/SEMM-1992/29, University of California, Berkeley.

PEER. 2010. Next Generation Attenuation of Ground Motions Project (NGA) Database. Pacific Earthquake Engineering Research Center, Berkely, California. http://ngawest2.berkeley.edu/.

Popov, E. P., and Engelhardt, M. D. 1988. Seismic Eccentrically Braced Frames. Journal of Constructional Steel Research 10: 321-354.

Popov, E. P., Ricles, J. M. and Kasai, K. 1992. "Methodology for optimum EBF link design." Tenth World Conference Of Earthquake Engineering 7: 3983-3988.

Popov, E. P., Ricles J. M., and Kasai. K. 1992. Methodology For Optimum EBF Link Design. In Proceedings, Tenth World Conference of Earthquake Engineering 7: 3983-3988.

Popov, E. P., Kasai, K. and Engelhardt, M. D. 1987. Advances In Design Of Eccentrically Braced Frames. Earthquake spectra 3(1).

Ramadan, T., and Ghobarah, A. 1995. Analytical Model For Shear Link Behavior. Journal Of Structural Engineering 121: 1574-1580.

Richards, P. W. Cyclic Stability and Capacity Design of Steel Eccentrically Braced Frames. Doctoral dissertation, University of California: San Diego, 2004.

Ricles, J.M, and Popov, E.P. 1994. Inelastic Link Element For Ebf Seismic Analysis. Journal Of Structural Engineering, ASCE 120 (2): 441-463.

Ricles, J.M., and Popov, E.P. 1987. Dynamic Analysis Of Seimically Resistant Eccentrically Braced Frames. University of California Berkeley, California.

Ricles, J. M., and Popov, E.P. 1994. Inelastic Link Element For EBF Seismic Analysis. Journal Of Structural Engineering 120 (2): 441-463.

Roder, C.W., and Popov, E.P. 1977. Inelastic Behavior of Eccentrically Braced Steel Frame under Cyclic Loadings. University of California, Berkely.

Roeder, C.W., Foutch, D.A. and Goel, S. C., 1987. Seismic Testing Of Full-Scale Steel Building-Part II. Journal Of Structural Engineering 113(11): 2130-2145.

Saiidi, M., and Sozen, M.A. 1981. Simple Nonlinear Seismic Analysis Of R/C Structures. Journal Of The Structural Division 107 (5): 937-953.

Skokan, M.J. and Hart, G.C. 2000. Reliability Of Nonlinear Static Methods For The Seismic Performance Prediction Of Steel Frame Buildings. In Proceedings Of The 12th World Conference On Earthquake Engineering, Paper No. 1972.

Vidic, T., Fajfar, P., and Fischinger, M. 1994. Consistent Inelastic Design Spectra: Strength and Displacement. Earthquake Engineering and Structurea Dynamics 23 (5): 507-521.

Whittaker, A.S., Uang, C.M. and Bertero, V.V. 1987. Earthquake Simulation Tests And Associated Studies Of A 0.3-Scale Model Of A Six-Story Eccentrically Braced Steel Structure. Earthquake Engineering Research Center, College of Engineering, University of California.,.

Yang, M.S. 1982. Seismic Behavior Of An Eccentrically X-Braced Steel Structure. University of California, Earthquake Engineering Research Center.